A FUNDAMENTAL STUDY

OF THE SOLID STATE REDUCTION OF

VANADIUM PENTOXIDE

BY CARBON MONOXIDE AND HYDROGEN

Frances Stander

A Thesis submitted to the Faculty of Science,
University of Pretoria, in partial fulfilment
of the requirements for the degree of

Master of Science

Department of Chemistry
University of Pretoria
PRETORIA

August 1988

To Flip and my parents

ACKNOWLEDGEMENTS

The following people and institutions deserve my gratitude for their contributions to this study :

- Prof. C.P.J. van Vuuren for his assistance as supervisor during the course of this study.

- MINTEK for the bursary granted for this study.

- Dr. M.B. Mooiman for initiation of this project.

- Mrs. Sabine Verryn for running the X-ray powder diffraction patterns.

- Mr. Paul Botha for his assistance with the electron microscope.

- Prof. L.M.D. Stopforth for reading the manuscript.

- Neels Roos for his assistance with the preparation of this manuscript.

- My family and friends for their loving interest in my work.

- My husband Flip whose love, companionship and enthusiasm was an inspiration.

CONTENTS

SYNOPSIS

The reduction process of vanadium pentoxide by CO and H_2 was studied by means of thermal analysis techniques. X-ray powder diffraction analysis and electron microscopy were also used as complementary techniques.

It was found that the reduction of V_2O_5 to V_2O_3 occurs through the formation of the following intermediate vanadium oxides:

$$V_2O_5 \longrightarrow V_6O_{13} \longrightarrow VO_2(\text{rutile}) \longrightarrow V_nO_{2n-1}(4 \leq n \leq 8) \longrightarrow V_2O_3$$

The mechanism and kinetics of the reduction process were found to be sensitive to structure and to change with temperature. It is proposed that two mechanisms of solid-gas interaction contribute towards the overall reduction process, with the extent of contribution of each mechanism depending on the grain morphology and reduction temperature.

These complex processes that occur cause difficulties with the kinetic description of the reduction process, nevertheless, the Avrami-Erofe'ev model seems to offer a general description of the mechanism of reduction, describing a nucleation and growth process. However, the significance of the parameter n in the Avrami-Erofe'ev equation is still uncertain. Reduction by both CO and H_2 seems to start preferentially at defects such as steps, kinks and dislocations in the crystal surface. After coverage of the surface, the reaction interface advances inwards, resembling a contracting volume mechanism.

Throughout this study, higher reduction rates were achieved with H_2 than with CO. This is contrary to thermodynamic predictions and can probably be ascribed to kinetic favourability of the H_2 reduction reaction over the CO reaction.

The reduction of ammonium metavanadate (AMV) was also investigated and it was found that the in situ reduction of V_2O_5 (formed as decomposition intermediate) leads to higher reduction rates than the direct reduction of V_2O_5. This can probably be ascribed to the disorder and oxygen deficiency introduced into the V_2O_5 lattice during the decomposition of AMV in the absence of O_2. It is possible that the catalytic decomposition of ammonia (evolved during decomposition) on the V_2O_5 leads to the formation of an active boundary between V_2O_5 and lower oxides such as V_3O_7 and V_6O_{13} which enhances the reactivity.

OPSOMMING

Die reduksie van vanadium pentoksied deur CO en H_2 is bestudeer d.m.v. termiese analise tegnieke. X-straal poeierdiffraksie en elektron mikroskopie is ook gebruik as aanvullende tegnieke.

Daar is gevind dat die reduksie van V_2O_5 na V_2O_3 deur die vorming van die volgende intermediêre vanadium oksiede geskied:

$$V_2O_5 \longrightarrow V_6O_{13} \longrightarrow VO_2(\text{rutiel}) \longrightarrow V_nO_{2n-1}(4 \leq n \leq 8) \longrightarrow V_2O_3$$

Die meganisme en kinetika van die reduksie is as sensitief t.o.v. struktuur en temperatuursverandering bevind. Dit word voorgestel dat twee meganismes van vastestof-gas interaksie bydra tot die algehele reduksie proses, met die mate van bydrae van elke meganisme afhanklik van korrelmorfologie en reduksietemperatuur.

Hierdie komplekse prosesse wat plaasvind, veroorsaak probleme met die kinetiese beskrywing van die reduksieproses. Nietemin gee die Avrami-Erofe'ev model skynbaar 'n algemene beskrywing van die meganisme, nl. 'n proses van kernvorming en groei. Die betekenis van die parameter n in die vergelyking is egter steeds onseker. Reduksie deur byde CO an H_2 begin skynbaar by voorkeur by defekte in die oppervlak van die kristal. Na bedekking van die oppervlak beweeg die reaksie-tussenvlak na die middel van die kristal.

Deurentyd is hoër reduksietempo's met H_2 as met CO bereik. Dit is teenstrydig met termodinamiese voorspellings en kan moontlik toegeskryf word aan kinetiese bevoordeling van die H_2 reduksie reaksie bo die CO reaksie.

Die reduksie van ammonium metavanadaat (AMV) is ook ondersoek en dit is gevind dat die in situ reduksie van V_2O_5 (gevorm as ontbindings intermediêr) tot hoër reduksietempo's lei as die direkte reduksie van V_2O_5. Dit kan moontlik toegeskryf word aan die wanorde en tekort aan suurstof in die V_2O_5 rooster, wat veroorsaak word deur die ontbinding van AMV in die afwesigheid van O_2. Dit is moontlik dat die katalitiese ontbinding van ammoniak (vrygestel gedurende ontbinding van AMV) op V_2O_5, lei tot die vorming van 'n aktiewe grens tussen V_2O_5 en laer oksiede soos V_3O_7 en V_6O_{13}, wat die reaktiwiteit verhoog.

CHAPTER 1
INTRODUCTION

South Africa possesses the largest reserves of vanadium in the world. These reserves are present in the titaniferous magnetite deposits in the Bushveld complex and were estimated to be 32.6% of known world reserves in 1986 [1]. The main magnetite seam contains 1.6±0.2% V_2O_5 [2].

Approximately 85-90% of the total vanadium output is consumed by the steel industry with, the remainder being used as a catalyst in the manufacture of sulphuric acid, in chemicals and in the non-ferrous metals industry.

1.1. Vanadium in steel

Vanadium is an important alloying element added to a large variety of steels produced to fulfil highly specialized requirements. Small amounts impart valuable properties such as tensile and torsional strength, toughness and resistance to abrasion. These are indispensable characteristics of spring steels, tool steels, permanent magnets, wear-resistance cast irons and the important high-strength low-alloy (HSLA) steels which consume some 35% of all vanadium produced [1].

In the past, carbon was used to strengthen steel at the expense of other properties such as toughness, weldability and formability. Today, the carbon content of HSLA-steels is reduced to 0.05%, improving the toughness and weldability, while the yield strength is maintained by using suitable alloying additions such as aluminium, niobium, titanium or vanadium.

With the proper choice of carbon content and addition of alloying elements, steels can be made relatively soft and ductile, extremely hard to resist wear,

tough to withstand loads and shocks or resistant to corrosion.

1.2. The production of vanadium

1.2.1. The roast-leach process

In the RSA, vanadium is recovered by two companies, viz Highveld Steel and Vanadium Corporation and Transvaal alloys [1]. Both companies employ a roast-leach process to produce vanadium pentoxide or other vanadium compounds from the vanadium-bearing ore. A schematic representation of the roast-leach process is given in figure 1.1.

The principles of the roast leach-process can be outlined as follows : First, the vanadium in the vanadium-bearing ore or mineral is converted to sodium vanadates by roasting the ore together with a sodium salt at high temperatures in an oxidizing atmosphere. The following simplified reactions take place :

$$Na_2SO_4 + V_2O_5 \longrightarrow 2\,NaVO_3 + SO_2 + \tfrac{1}{2}O_2 \qquad \{R1.1\}$$

$$Na_2CO_3 + V_2O_5 \longrightarrow 2\,NaVO_3 + CO_2 \qquad \{R1.2\}$$

These processes are in actual fact much more complex, as was shown by Stander [3]. The sodium vanadates formed in these reactions are water-soluble and are consequently leached from the calcined ore. An excess of an ammonium salt, such as ammonium sulphate or chloride is then added to the leach liquor to precipitate ammonium metavanadate. After filtration, the ammonium metavanadate is decomposed to V_2O_5 which is melted at 850°C, tapped and cooled.

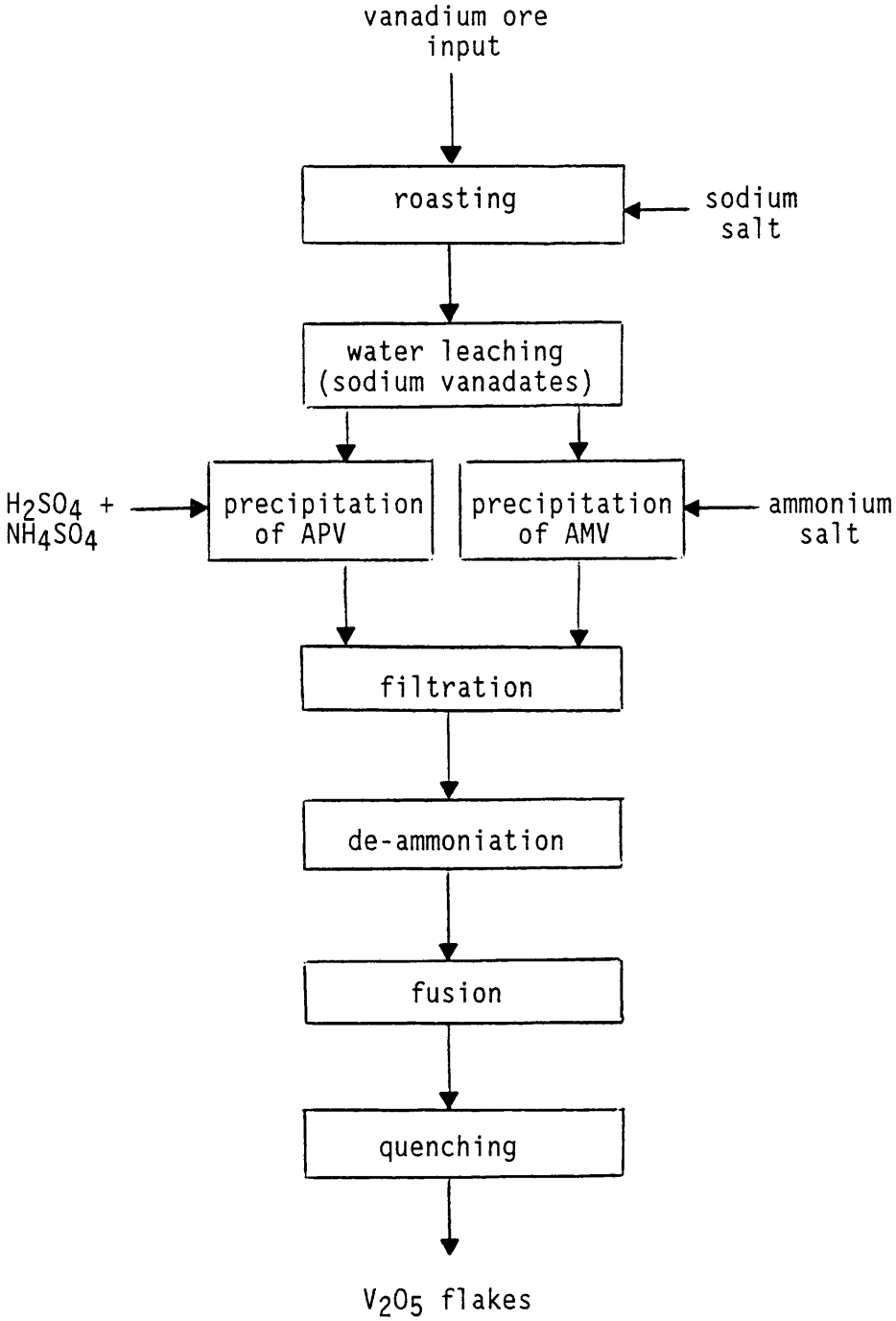

Figure 1.1. - Schematic representation of the principles of the roast-leach process

Instead of using an ammonium salt to precipitate ammonium metavanadate, ammonium sulphate is also added to an acidified pregnant solution to precipitate ammonium polyvanadates. The further processing of the polyvanadates to produce V_2O_5, is similar to the ammonium metavanadate route.

1.2.2. The reduction of V_2O_5

The vanadium pentoxide produced by the roast-leach process is converted to vanadium metal by employing an aluminothermic reduction technique [2], according to the following reaction :

$$3\ V_2O_5 + 10\ Al \longrightarrow 5\ Al_2O_3 + 6\ V \qquad \{R1.3\}$$

This reduction method is relatively expensive, and, in order to reduce the costs of vanadium recovery, alternative methods of reduction of V_2O_5 have been considered, such as a pre-reduction route by using hydrogen or carbon monoxide gas to reduce V_2O_5 to V_2O_3 according to :

$$V_2O_5 + 2H_2 \longrightarrow V_2O_3 + 2H_2O \qquad \{R1.4\}$$

$$V_2O_5 + 2CO \longrightarrow V_2O_3 + 2CO_2 \qquad \{R1.5\}$$

Consequently, the reduction of vanadium sesquoxide to vanadium metal, according to reaction 1.6, would imply a 40% decrease in aluminium consumption.

$$V_2O_3 + 2\ Al \longrightarrow 2\ V + Al_2O_3 \qquad \{R1.6\}$$

A project was undertaken by Mintek in 1984 [4] to investigate the possibility of the pre-reduction of V_2O_5, ammonium metavanadate, and vanadium slag

by CO and H_2, to produce V_2O_3. In all the tests carried out with V_2O_5 and vanadium slag, H_2 showed a higher reduction rate than CO. This is contradictory to thermodynamic predictions. Contrary to expectation, in all the tests carried out with ammonium metavanadate, the degree of conversion to V_2O_3 when H_2 was used, was lower than in similar experiments when CO was used. This finding required further investigation and initiated the present study.

1.3. Objectives of this study

In view of the unexpected findings of previous workers [4], the following objectives were set for this study :

(i) to study the fundamental aspects of the mechanism of reduction of V_2O_5 to obtain a better understanding of the processes that occur during reduction;

(ii) to compare CO and H_2 as reducing gases;

(iii) to investigate the processes that occur during conversion of ammonium metavanadate to V_2O_3 in CO and H_2 atmospheres.

CHAPTER 2
OXIDE TRANSITIONS DURING REDUCTION OF V_2O_5

2.1. INTRODUCTION

Extensive studies have been conducted in the past by several workers on the structures of vanadium oxides [5-11]. Several oxides are known to exist in the composition range V_2O_5 to V_2O_3 with stoichiometry VO_x and $1.5 \leq x \leq 2.5$.
In 1964 Stringer constructed a phase diagram of the vanadium-oxygen system after a critical review of the literature on vanadium oxides and suggested the existence of 12 oxide phases in the composition range V_2O_5 to V_2O_3 [11]. Kosuge constructed a slightly different phase diagram in 1966 with 10 oxide phases in the same range [12]. The phase diagram of Kosuge is given in figure 2.1. Since then, even more vanadium oxides have been reported to exist [13,14].

Structural changes that occur during vanadium oxide transitions have also been the subject of a large number of studies [15-18]. Some structural aspects of V_2O_5 and changes that occur during reduction which are of interest in this study will be discussed in section 2.4.

Vanadium oxides have wide industrial applications such as vanadium oxide based catalysts which are used in a number of oxidation processes [19-21]. In some cases, V_2O_5 is reduced to lower oxides during the course of the catalytic oxidation reaction. From this point of view, interest has originated in the reduction of V_2O_5.

Recently, Pospišil studied the reduction of $NiO\text{-}V_2O_5$ oxides with H_2 [22]. He found the oxides V_3O_7, V_6O_{13}, VO_2, V_7O_{13}, V_5O_9, V_4O_9 and V_2O_3

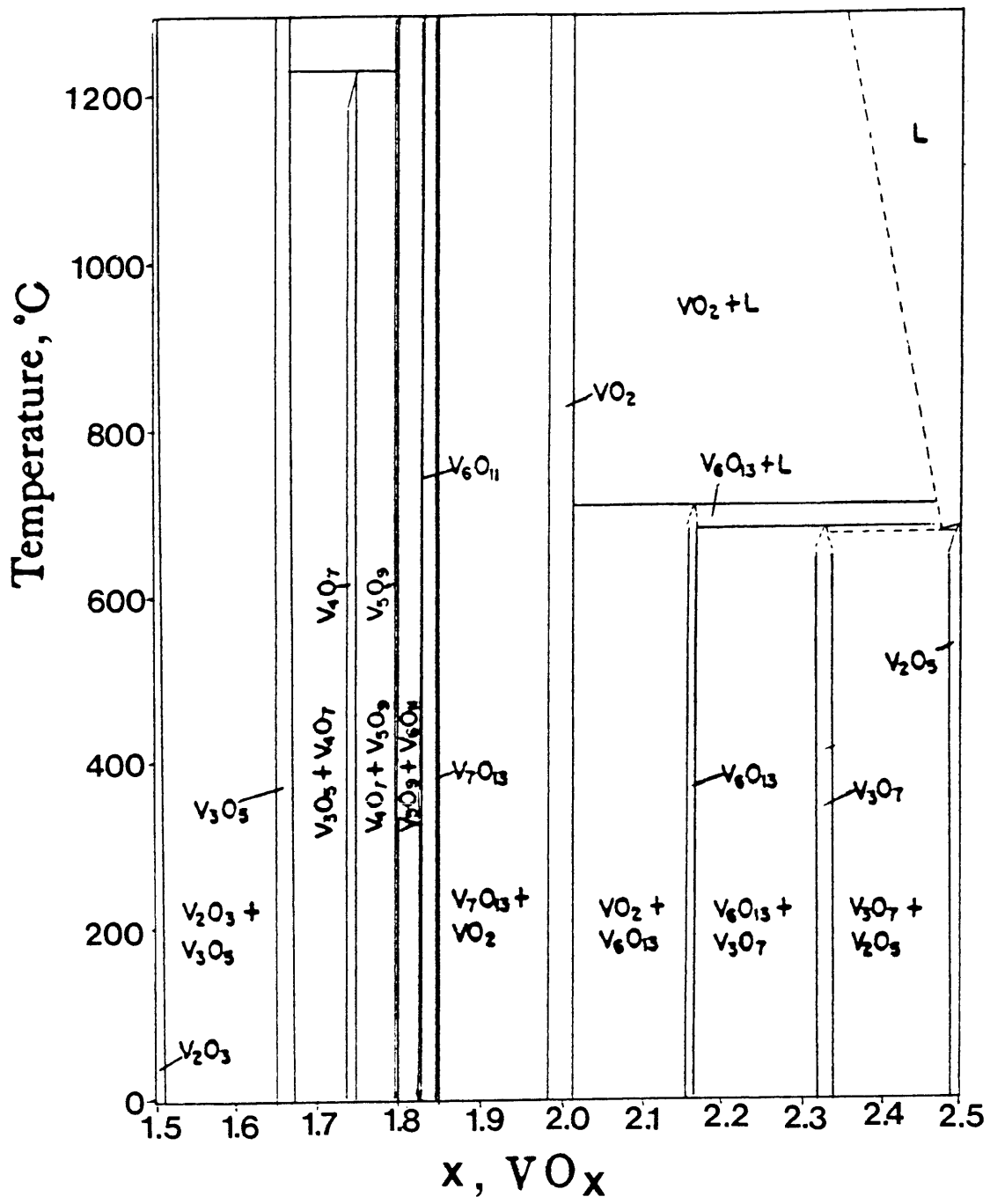

Figure 2.1 - Phase diagram proposed by Kosuge [12] for the V_2O_3-V_2O_5 system.

to form during the course of reduction. Bosch et al. [23] and Baiker et al. [24] studied the reduction of V_2O_5 by H_2 and found evidence of V_6O_{13}, VO_2, and V_2O_3 during reduction. They also mentioned the possibility that intermediate oxides such as V_6O_{11} could form, but found no evidence of such oxides. Baiker et al. also pointed out that the reduction is strongly influenced by the grain morphology of the oxide.

Although the kinetics of oxidation of CO on V_2O_5 have been studied by several workers [25-33], very little is mentioned about the formation of lower oxides during reduction of V_2O_5.

In view of these uncertainties surrounding the oxide transitions that occur, as well as the influence of different grain morphologies on the reduction, a study was conducted to determine the intermediate oxides that form during reduction of V_2O_5 by CO and H_2.

2.2. EXPERIMENTAL PROCEDURE

2.2.1. Materials and sample preparation

During this study, two types of V_2O_5 with different grain morphologies were used. The first type was supplied by the J. T. Baker Chemical Co. and was a fine, powderlike substance, consisting of minimum 99.6% V_2O_5. A similar type of V_2O_5 was obtained by the thermal decomposition of ammonium metavanadate at 400°C in air.

The second type was prepared by the decomposition of ammonium metavanadate in air at 700°C for two hours (the melting point of V_2O_5 is ±674°C). The V_2O_5 melt was subsequently left to cool slowly in the furnace. The crystals obtained consisted of orange platelets.

The reducing gases used were 99% carbon monoxide supplied by Fedgas and UHP hydrogen supplied by Afrox.

2.2.2. Thermal analysis studies

The reduction of V_2O_5 by CO and H_2 was studied by using mainly thermogravimetry (TG) and differential thermal analysis (DTA).

The reduction of V_2O_5 by CO was studied using a Stanton Redcroft STA 780 simultaneous thermal analyser which consists of an electronic microbalance connected to a microprocessor-based control unit, a Pt-Pt/13%Rh thermocouple system and platinum sample and reference containers (volume : 135mm^3, diameter : 6mm).

The reduction of V_2O_5 by H_2 was studied using a Du Pont 990 thermal analyser with a 951 TGA-module for the TG analyses. The DTA studies were performed on a Perkin-Elmer system 7/4 thermal analysis controller with a DTA 1700 differential thermal analyser and a 3700 Data Station. 60mm^3 platinum sample and reference cups (diameter : 4.7mm) were used.

The studies were carried out in dynamic atmospheres with gas flow rates of $\pm$50ml.min^{-1}. Sample masses varied between 20mg and 30mg.

2.2.3. X - ray powder diffraction analysis

In addition to thermal studies, XRPD analysis was used to identify intermediate and final products during the reduction process. A Seifert MZ IV instrument with Cu-K_α radiation was used. The ASTM Powder Diffraction Files of the Joint Committee on Powder Diffraction Standards

were used as reference for the characterization of the vanadium oxides. The XRPD data involved are given in Appendix A.

2.2.4. Surface-area measurements

Surface-area measurements were carried out on samples using a Micromeritics FlowSorb II 2300 instrument and the BET (Brunauer, Emmet and Teller) method of surface-area determination with nitrogen as the adsorbate.

2.2.5. Electron microscopy

The surface morphology of samples was studied with a Philips P500 scanning electron microscope, operating at 12kV. The samples were coated with a thin film of gold.

2.3. RESULTS

2.3.1. Sample characteristics

The electron micrographs in figure 2.2(a) and (b) show the different morphologies of the V_2O_5 powder and the V_2O_5 platelets respectively.

It can be seen from the electron micrographs that the V_2O_5 powder consists of agglomerates of poorly defined crystallites. The surface area of the V_2O_5 powder was found to be $2.87 \pm 0.02 m^2.g^{-1}$.

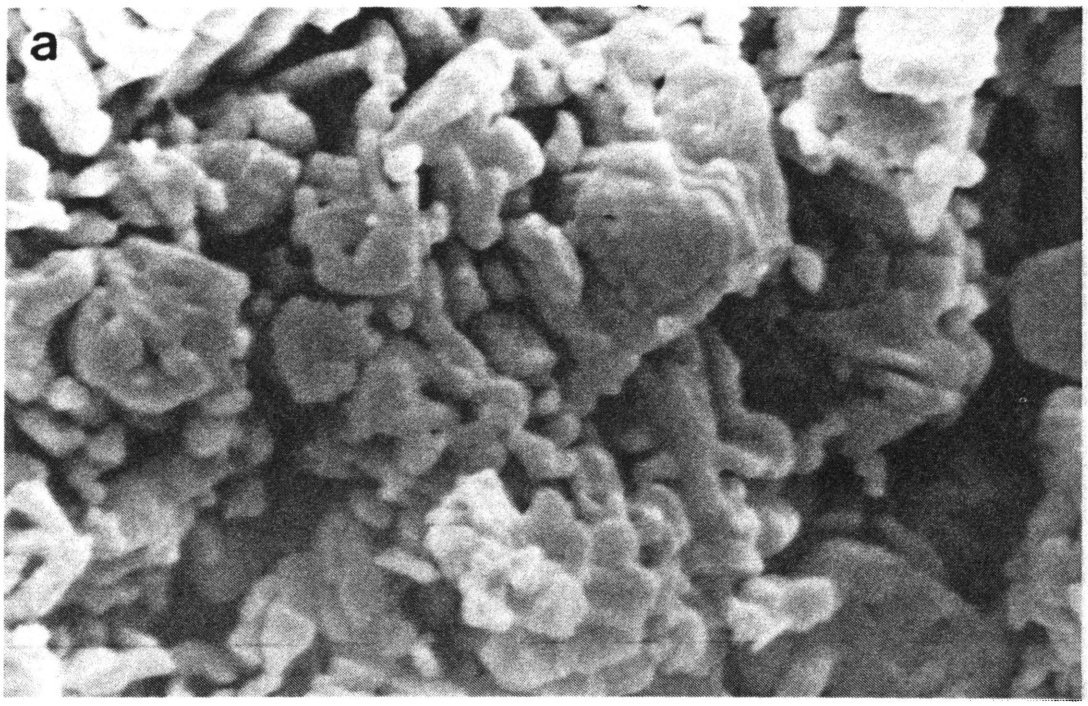

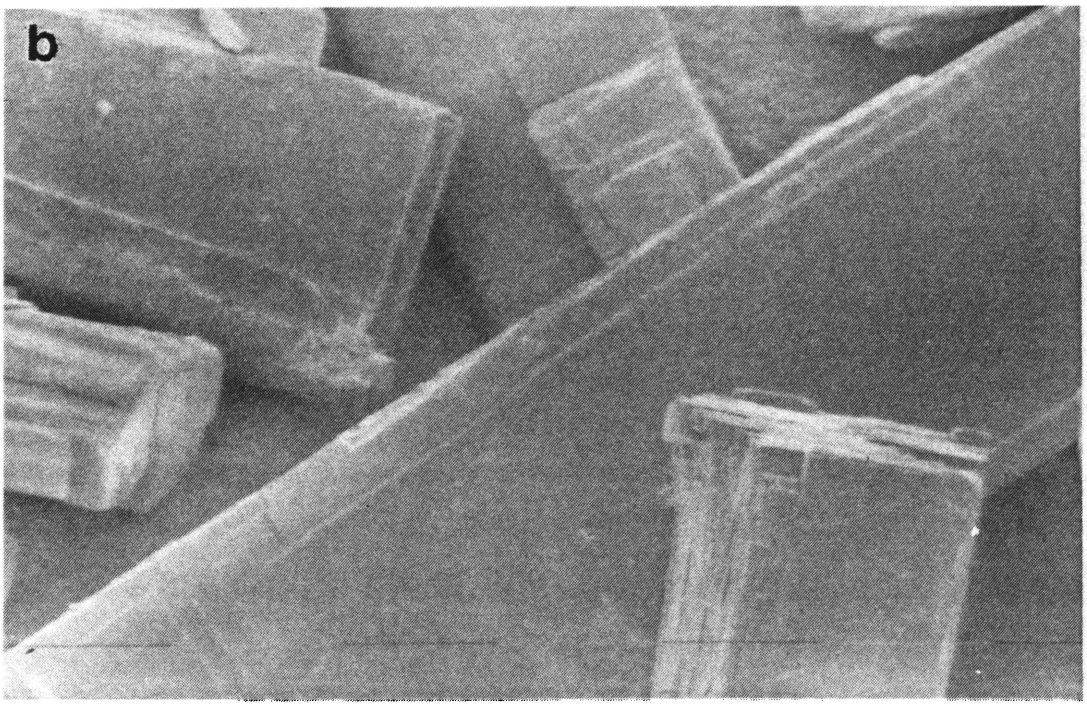

Figure 2.2 - Electron micrographs : (a) V_2O_5 powder X 5000
(b) V_2O_5 platelets X 160

On the other hand, the second type of V_2O_5 consists of well-developed platelike crystals with the largest faces corresponding to the (010) crystal plane. The average surface areas were found to be $<0.5 m^2.g^{-1}$ for crystals larger than 250μm, and $\pm$ $0.8 m^2.g^{-1}$ for crystals in the range of 125 - 250μm.

2.3.2. Reduction by CO

2.3.2.1 V_2O_5 powder

The corresponding dynamic TG and DTA curves for the reduction of the V_2O_5 powder by CO are given in figures 2.3(a) and (b) respectively.

At a heating rate of $5 K.min.^{-1}$, only a single exothermic reaction step is visible in the temperature range 540 - 750°C. The mass loss obtained is 17.0% which corresponds to the theoretical mass loss of 17.59% which is expected for the conversion of V_2O_5 to V_2O_3. XRPD analysis confirmed that the final product is V_2O_3.

At a higher heating rate of $10 K.min.^{-1}$, three exothermic steps become visible in the TG and DTA curves. The reaction steps obtained are summarized in table 2.1.

Table 2.1. - Reaction steps visible at $10 K.min^{-1}$.

Step no.	Temp. range °C	Obtained mass loss %	Corresponding stoich. composition	Expected mass loss %
1	550 - 670	± 5.6	V_6O_{13}	5.86
2	670 - 705	± 8.6	VO_2	8.80
3	705 - 830	± 17.0	V_2O_3	17.59

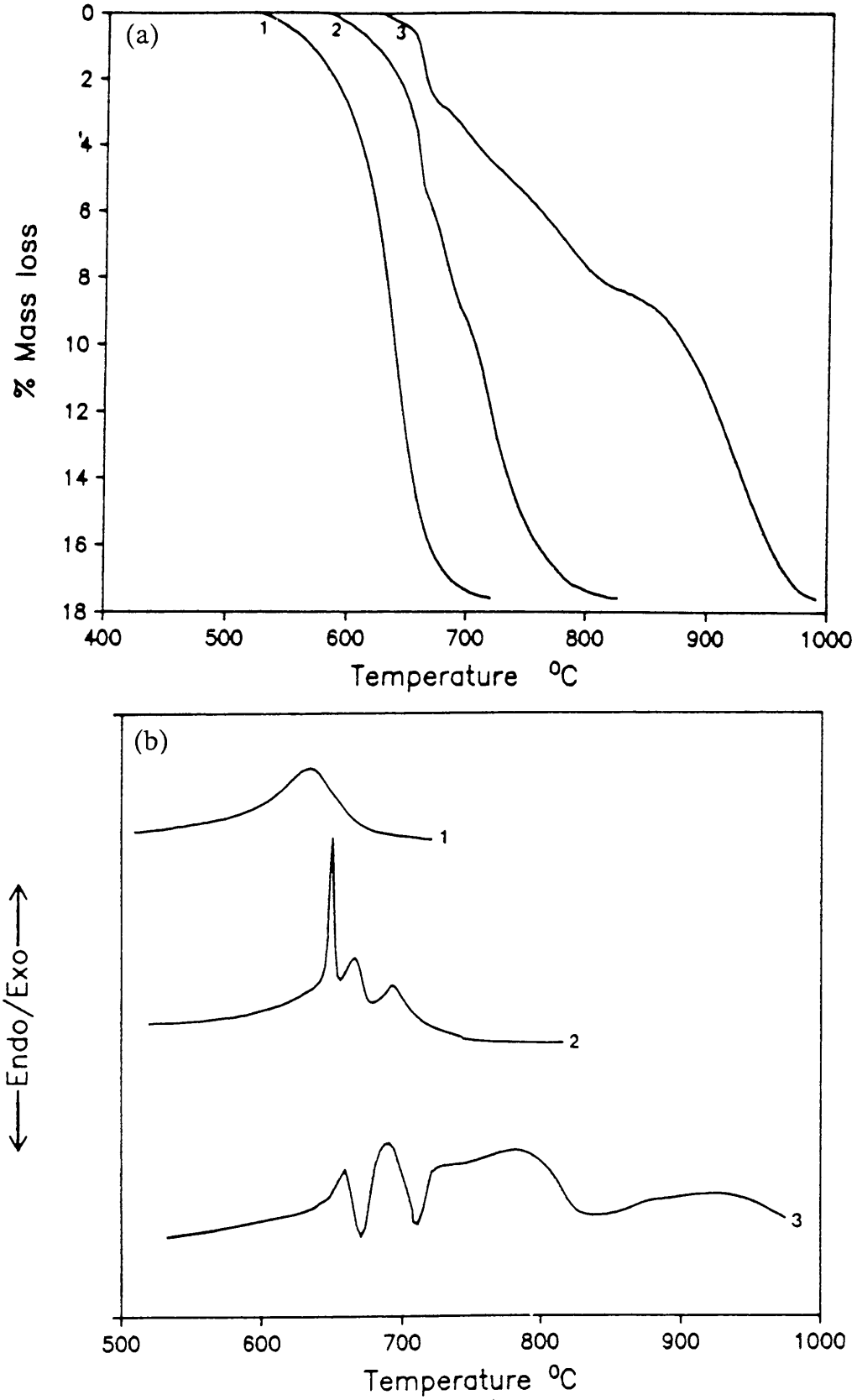

Figure 2.3 - (a) TG and (b) DTA* curves for the reduction of V_2O_5 powder by carbon monoxide.
Heating rates : (1) - 5 K.min.$^{-1}$
(2) - 10 K.min.$^{-1}$
(3) - 40 K.min.$^{-1}$
* - The enthalpies represented by the DTA-peaks are not to scale.

Note that the higher heating rate causes the reaction temperature range to shift to higher temperatures (a shift of ±80°C is observed). The reduction reaction was terminated after each of the DTA peaks observed, cooled to ambient temperatures in argon, and analysed by XRPD. The results obtained are summarized in table 2.2.

Table 2.2. - Oxide phases detected by XRPD.

Reaction step no.	V_2O_5	V_6O_{13}	VO_2 (rutile)	V_2O_3
initial sample	s	n.o.	n.o.	n.o.
1	n.o.	s	w	n.o.
2	n.o.	n.o.	s	w
3	n.o.	n.o.	n.o.	s

abbreviations :
n.o. = not observed
s = strong
w = weak

The observed XRPD data for the intermediate oxides that were identified are given in tables 2.3. to 2.5. The ASTM powder diffraction files that were used as reference are given in Appendix A. The intermediate oxides detected agree with the oxides found by Baiker et al. and Bosch et al.

At a higher heating rate of 40 K.min.$^{-1}$, a still higher reaction temperature range is observed and a temperature of ±970°C is needed for complete reduction. In the DTA curve, two endothermic peaks appear at ±674°C and ±708°C which overlap with the exothermic reduction peaks. They are ascribed to the melting of the V_2O_5 and V_6O_{13} phases respectively. A slight increase in reduction rate is observed in the TG curve in the vicinity of these melting processes. This is probably due to enhanced mobility of the ions in the oxide matrix which might contribute to changes in crystal structure near the melting temperature.

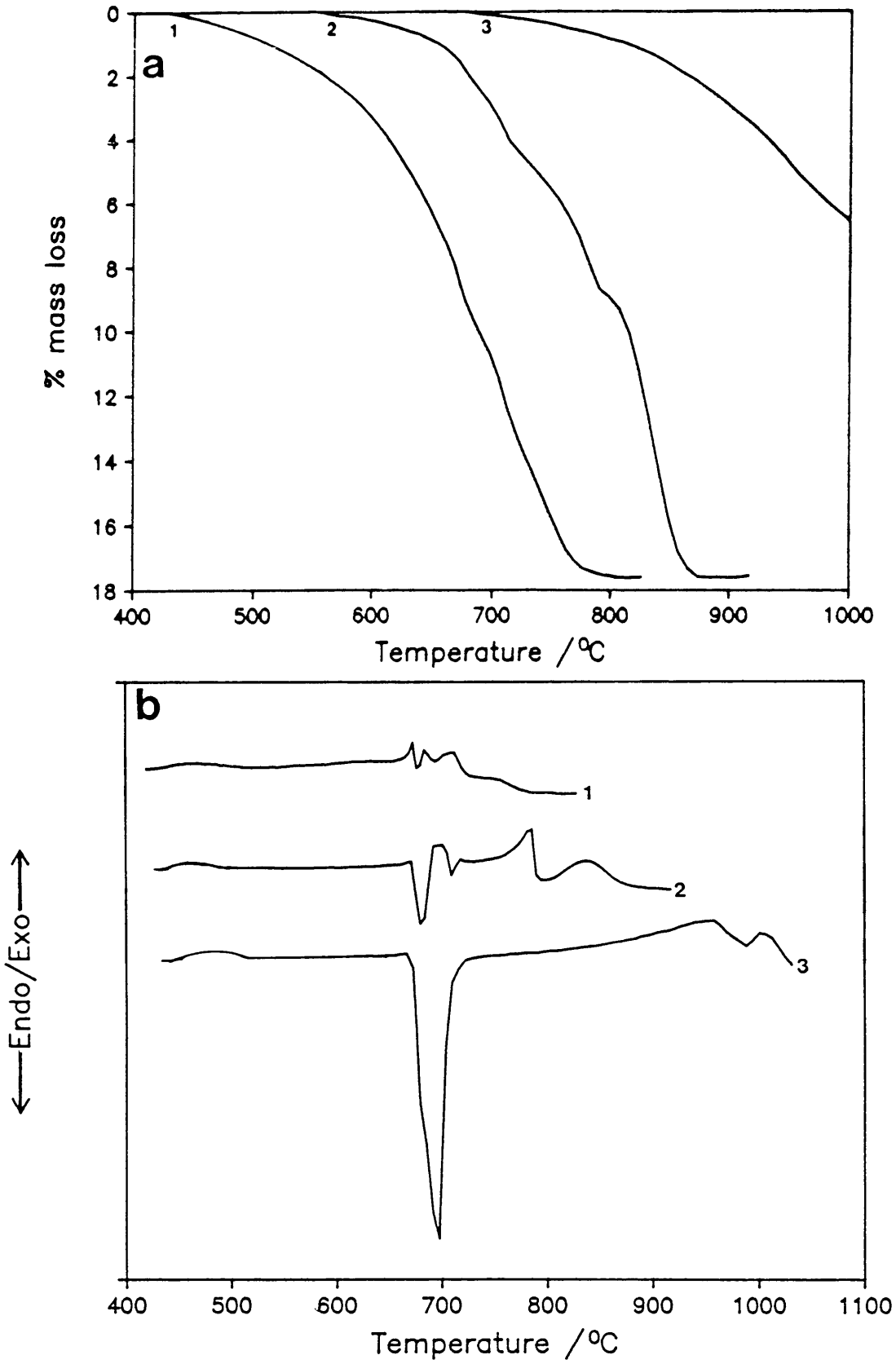

Figure 2.4 - (a) TGA and (b) DTA* curves for the reduction of V_2O_5 platelets by carbon monoxide.
Heating rates : (1) - 5 K.min.$^{-1}$
(2) - 10 K.min.$^{-1}$
(3) - 40 K.min.$^{-1}$

Table 2.3. - Obtained XRPD lines for V_6O_{13}

d / Å	I/I_1	d / Å	I/I_1
9.99	20	2.485	10
5.88	30	1.991	70
4.99	50	1.843	25
3.52	70	1.710	15
3.33	100	1.655	10
2.971	40	1.611	15
2.930	10	1.564	15
2.807	10	1.548	25
2.766	10	1.506	20
2.684	30	1.414	10
2.509	10	1.353	25
2.493	20		

Table 2.4. - Obtained XRPD lines for VO_2

d / Å	I/I_1	d / Å	I/I_1
3.31	20	1.731	8
3.22	100	1.655	25
2.655	10	1.618	8
2.427	20	1.605	15
2.274	6	1.438	10
2.143	15	1.436	10
2.027	6	1.337	6
1.876	5		

Table 2.5. - Obtained XRPD lines for V_2O_3

d / Å	I/I_1	d / Å	I/I_1
3.65	70	1.697	90
2.712	100	1.470	20
2.477	70	1.428	25
2.187	40	1.329	10
1.828	25		

2.3.2.2. V_2O_5 platelets

The corresponding TG and DTA curves for the reduction of V_2O_5 platelets by CO are given in figures 2.4(a) and (b).

If the reduction behaviour of the V_2O_5 platelets is compared to that of the V_2O_5 powder, it can be seen that the rate of reduction of the platelets is slower and is completed at higher temperatures. The higher temperatures which are needed for reduction result in slightly different TG-curves and complex DTA curves due to the overlapping of melting endotherms of V_2O_5 and V_6O_{13} with reduction exotherms. However, the same reduction intermediates were detected for the platelets as for the powder.

2.3.3. Reduction by hydrogen

2.3.2.1 V_2O_5 powder

The corresponding TG and DTA curves of the reduction of V_2O_5 powder by H_2 are given in figures 2.5(a) and (b).

At a heating rate of 10 K.min.$^{-1}$, only a single exothermic reaction is visible in the 450 - 650°C temperature range. The experimental mass loss corresponds to the stoichiometry of V_2O_3, as was confirmed by XRPD.

At a higher heating rate of 50K.min^{-1}, two steps are clearly visible in the TG-curve. The first step corresponds to the stoichiometry of VO_2 and the second to that of V_2O_3. In the DTA curve, however, four overlapping exotherms can be distinguished in the following temperature regions:

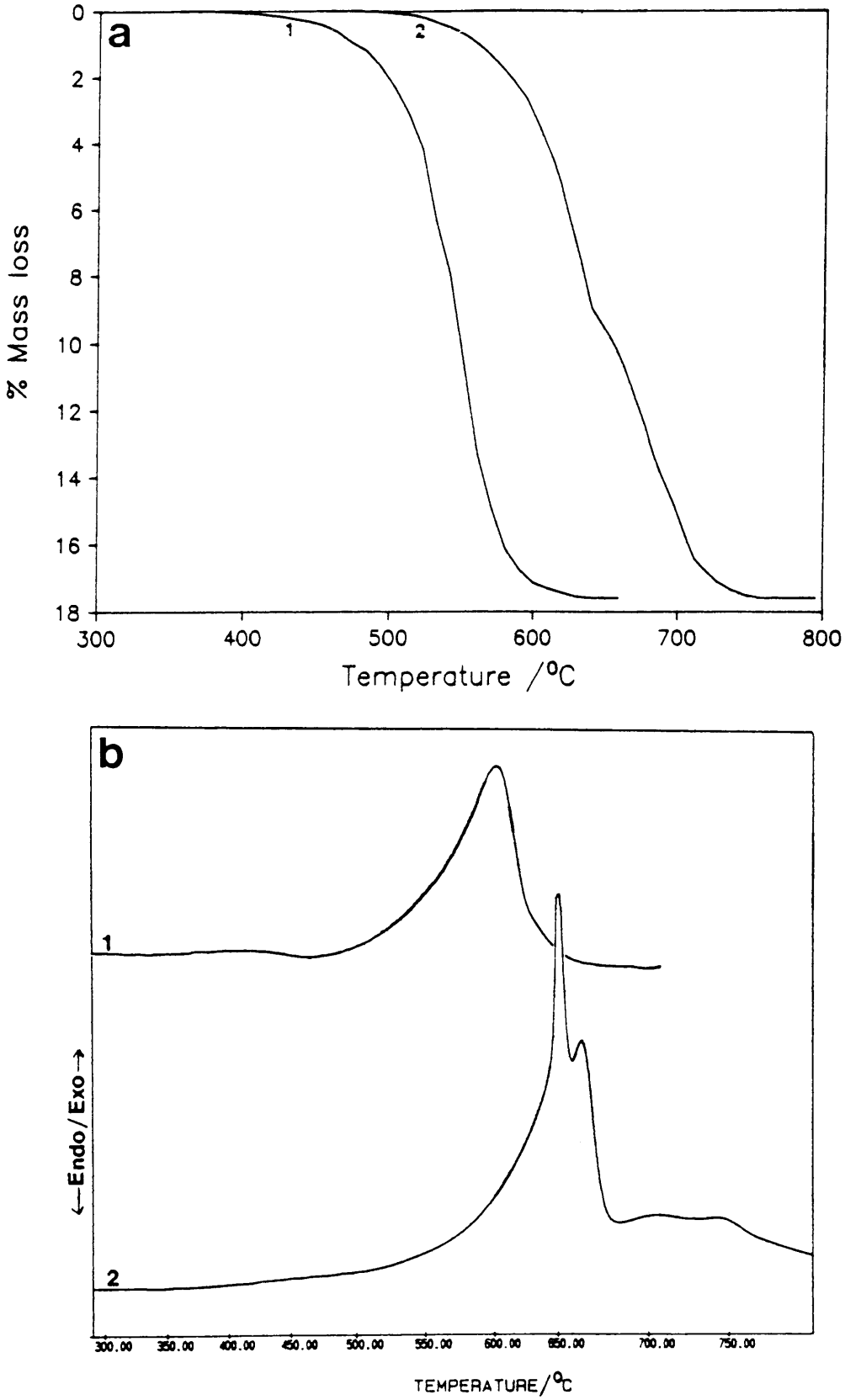

Figure 2.5 - (a) TG and (b) DTA* curves for the reduction of V_2O_5 powder by hydrogen.
Heating rates : (1) - 10 K.min.$^{-1}$
(2) - 50 K.min.$^{-1}$

Step 1 : 500 - 657°C
Step 3 : 682 - 725°C
Step 2 : 557 - 682°C
Step 4 : 725 - 780°C

The reaction was terminated after each of the peaks, the sample cooled to ambient temperature in argon and analysed by XRPD. The results obtained are summarized in table 2.6.

Table 2.6. - Oxide phases detected by XRPD

Reaction step	V_2O_5	V_6O_{13}	VO_2 (rutile)	V_nO_{2n-1} $(4\leq n\leq 8)$	V_2O_3
initial sample	s	n.o.	n.o.	n.o.	n.o.
1	w	s	w	n.o.	n.o.
2	n.o.	n.o.	s	n.o.	n.o.
3	n.o.	n.o.	w	w	n.o.
4	n.o.	n.o.	n.o.	n.o.	s

abbreviations :
s = strong
w = weak
n.o. = not observed

The oxides with composition V_nO_{2n-1} $(3\leq n\leq 8)$ are members of a homologous series of oxides [11] with a very limited stability range, as can be seen from the phase diagram of Kosuge (fig. 2.1.). The structures of all these oxides are based on rutile. Because their XRPD patterns are very similar, it is impossible to distinguish between them with low resolution XRPD. It is therefore not possible to determine whether only one or more of them are present. The XRPD-pattern obtained after step 3 consisted of broad bands which are probably the result of a number of overlapping peaks. In table 2.7., the d-value intervals of these bands are given, as well as the possible corresponding oxide peaks from literature.

Table 2.7 - Observed XRPD-bands after step 3 and possible corresponding oxide peaks

Observed bands d/Å I/I_1	possible corresponding oxide peaks d/Å I/I_1					
	VO_2	V_4O_7	V_5O_9	V_6O_{11}	V_7O_{13}	V_8O_{15}
3.84-3.56 25		3.70 40		3.83 60	3.73 60	3.65 60
3.33-3.29 100	3.31 30	3.33 100	3.32 100	3.31 100	3.30 100	3.29 100
3.11- 2.91 40-50		3.05 40 2.97 60	3.03 60	3.06 100 2.93 100	3.08 100 2.97 100	3.09 100 2.99 100
2.47-2.41 40-50	2.427 60	2.475 60 2.418 60	2.461 60 2.421 60	2.453 60 2.423 60	2.423 60	2.442 60 2.419 60
2.35-2.329 25			2.359 40	2.347 40 2.328 40	2.344 40 2.337 40	2.350 40
2.207-2.144 35		2.82 100	2.177 40 2.169 60 2.156 40	2.201 40 2.172 60 2.160 60	2.162 60 2.155 60	2.160 100 2.156 60 2.149 60
3.147-3.208 50	3.20 100			3.19 40		

(No corresponding V_3O_5 lines were found.)

A number of structures with the composition VO_2 have been described in literature [9,14,15]. The VO_2-phase detected in this study corresponds to that described by Andersson [9]. This oxide has a monoclinic structure consisting of an array of V_2O_4 molecules and a slightly distorted rutile lattice. On heating, it transforms at ±70°C into a tetragonal structure.

2.2.3.2 V_2O_5 platelets

The corresponding TG and DTA curves for the reduction of V_2O_5 platelets in H_2 are given in figures 2.6(a) and (b).

The differences observed for the reduction by H_2 of the V_2O_5 platelets compared to the V_2O_5 powder are similar to the differences observed for reduction by CO. The platelets are reduced slower than the powder and reduction is completed at higher temperatures. The same intermediate oxide phases were detected during reduction of the platelets as during reduction of the powder, although fewer reaction steps were visible in the TG and DTA curves.

2.4. DISCUSSION

From the results in section 2.3. it can be concluded that the reduction of V_2O_5 by H_2 probably proceeds through the formation of the following intermediate oxides:

$$V_2O_5 \longrightarrow 1/3\ V_6O_{13} \longrightarrow 2\ VO_2 \longrightarrow 2/n\ V_nO_{2n-1} \longrightarrow V_2O_3$$

These results are in agreement with the results of Baiker et al. [24] and Bosch et al. [23].

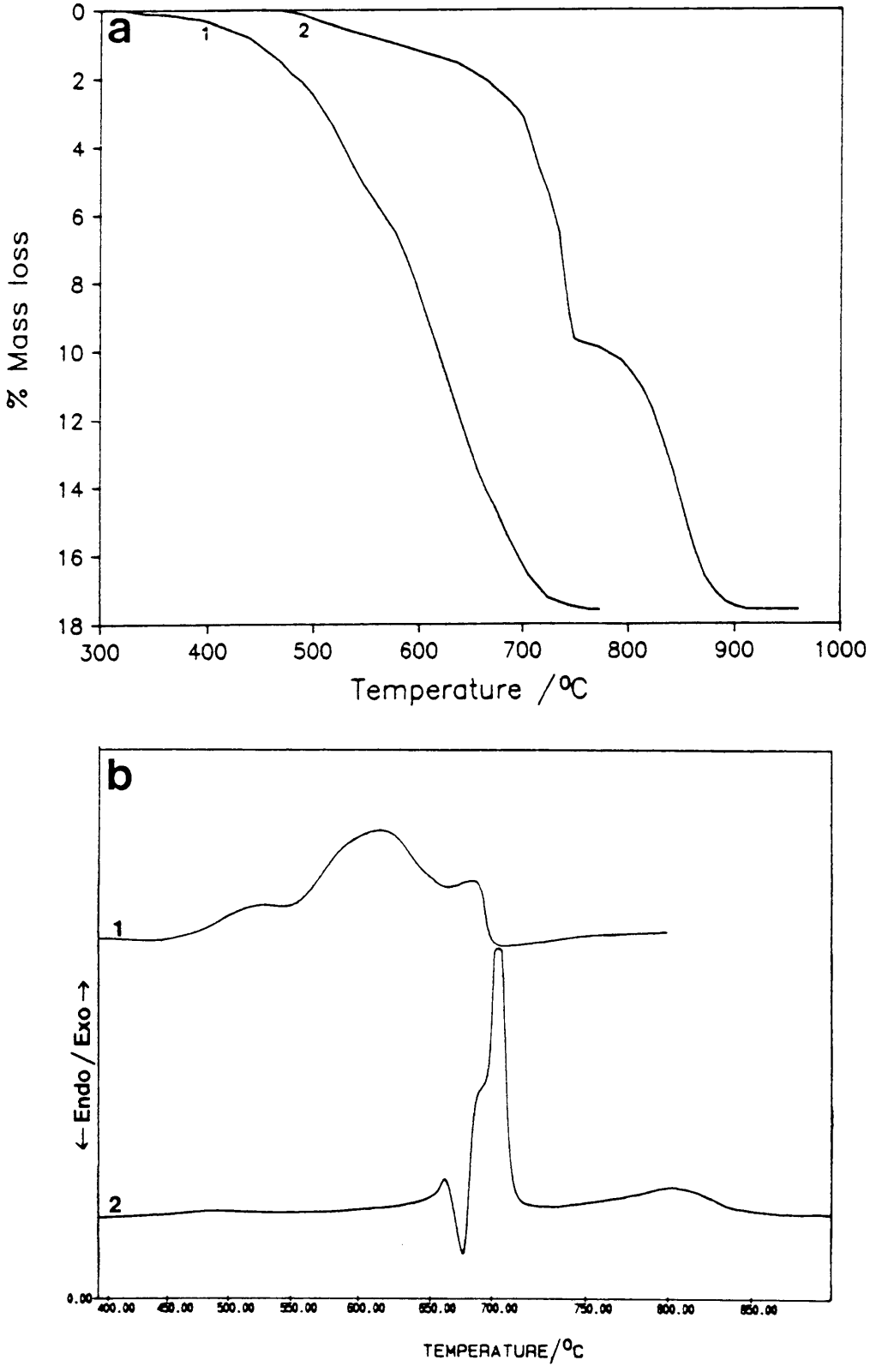

Figure 2.6 - (a) TGA and (b) DTA* curves for the reduction of V_2O_5 platelets by hydrogen.
Heating rates : (1) - 10 K.min.$^{-1}$
(2) - 50 K.min.$^{-1}$

With the exception of the phase V_nO_{2n-1}, the same phases were found to form during the reduction of V_2O_5 by CO. However, the possibility of the formation of these oxides cannot be rejected. Due to their limited stability range, it is possible that their presence could have been overlooked, using low resolution XRPD.

It is also clear from the results obtained that the reduction process is faster in hydrogen than in carbon monoxide. More attention will be given to this phenomenon in chapters 3, 4, and 5.

It was already mentioned in the introduction that the structures of vanadium oxides have been studied in great detail. In order to understand the mechanism of reduction of V_2O_5, some structural aspects of interest to this study will be discussed.

V_2O_5 has an orthorhombic structure [5] with lattice parameters a=1.1510Å, b=0.3563Å and c=0.4369Å. The structure of V_2O_5 is best described as five co-ordinate and consists of distorted square pyramids which are linked together by sharing corners in the x and z directions to form zig-zag chains (figure 2.7). These chains are linked together by weak Van der Waals forces, giving V_2O_5 a layered structure. Each V-atom has a single terminal O-atom in a double vanadyl bond (V=O). When the layers are stacked together to form the final crystal structure, each vanadium atom has another oxygen atom from an adjacent layer (trans to the V=O bond) which could be considered as occupying the sixth position in a very distorted octahedral co-ordination.

Under reducing conditions, lattice oxygen is removed, causing anion vacancies in the V_2O_5 lattice. The distorted structure formed through loss of oxygen is subjected to lattice strain. Shear and rearrangement of oxygen polyhedra

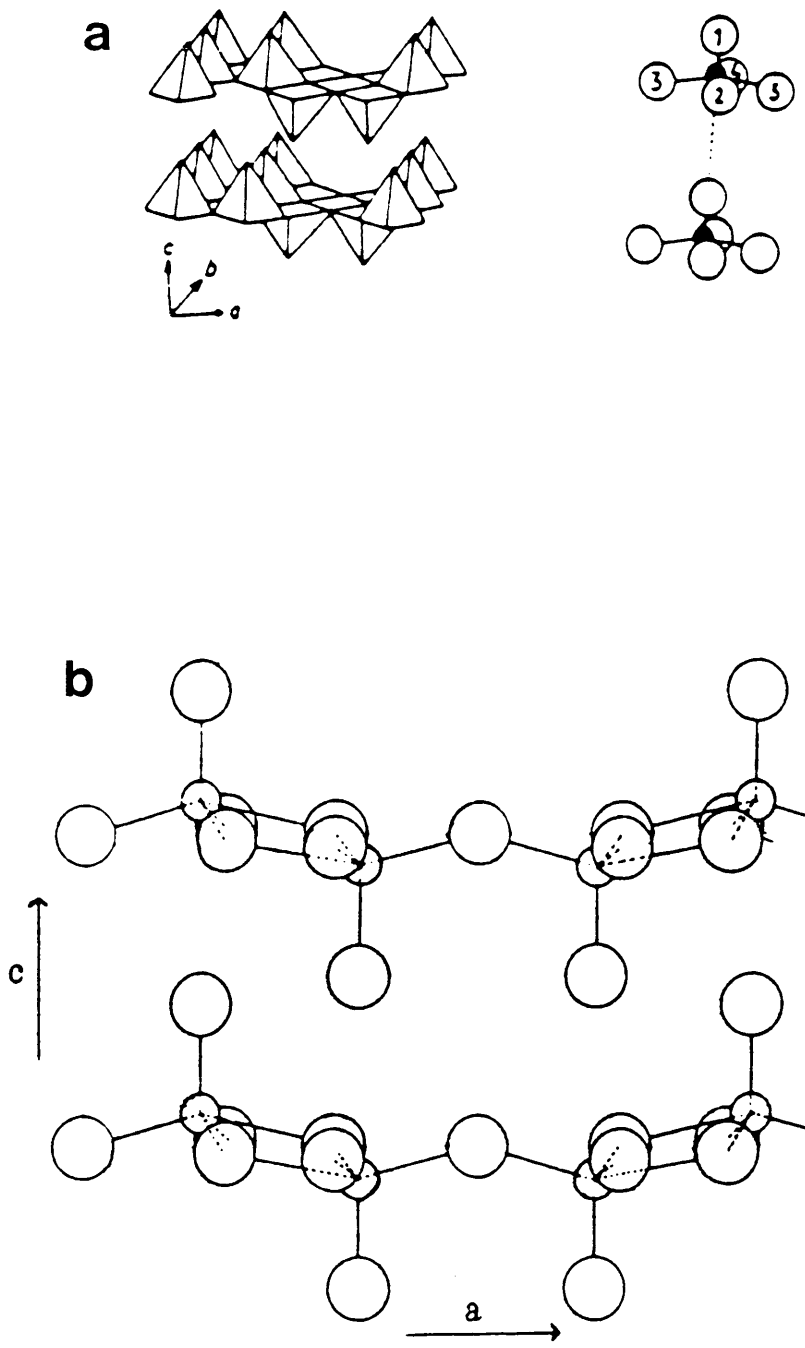

Figure 2.7 - The idealized structure of V_2O_5 projected in the (010) plane [17, 5]. Small circles denote V-atoms, large circles O-atoms.
(a) V_2O_5 square pyramids, linked to form chains
(b) Vanadium-oxygen co-ordination.

may then occur, leading to an energetically more favourable configuration [17].

According to Fiermans et al. [18], the mechanism of formation of lower oxides from V_2O_5 can be viewed as a series of steps involving the formation of vanadyl-oxygen vacancies and the introduction of (001) shear planes. The resulting phases (V_6O_{13} and VO_2) are known as shear structures of V_2O_5.

In view of this mechanism, the reduction process clearly involves the diffusion of oxygen and it can be understood that the reduction of V_2O_5 is probably diffusion controlled [17, 23]. The rate of reduction will be controlled by the flow of oxygen vacancies from the reacting surface.

It was shown in section 2.3 that higher rates of heating caused better resolution of the DTA-peaks. If the arguments in the preceding paragraphs are taken into account, attempts can be made to explain why lower heating rates do not resolve the reaction peaks.

According to Bosch et al. [23], at a certain temperature the degree of reduction of a sample reduced at a low heating rate is higher than the degree of reduction of a sample reduced at a high heating rate. Therefore, at lower heating rates a following phase can be formed at lower temperatures. Owing to the lower temperature, the conversion proceeds relatively slowly and the resulting reaction peaks are broad and overlap to a larger extent than when higher heating rates are used.

It was also shown in section 2.3. that the larger V_2O_5 platelets seem to have a slower reduction rate than the V_2O_5 powder which consisted of smaller crystallites. This is probably due to an accumulation of the product

gas (CO_2 or H_2O) in the lattice causing a relatively high partial pressure to build up. This effect would cause a decrease in reduction rate and would be more pronounced in larger crystals. It has also been mentioned that the reduction is probably diffusion controlled. Diffusion of oxygen vacancies into the lattices of the larger crystals would be slower and could also contribute towards their slower reduction rate. Although the V_2O_5 platelets seemed less reactive during dynamic reduction, it is hard to account for the influence of the different morphologies on reduction during isothermal conditions. This matter will receive more attention in chapter 4.

CHAPTER 3
THERMODYNAMIC ASPECTS OF THE REDUCTION OF V_2O_5

3.1. INTRODUCTION

In chapter 2, more knowledge was gained of the various reduction reactions that take place during the reduction process of V_2O_5 to V_2O_3. In view of this, a more effective study of the thermodynamic aspects of the reduction of V_2O_5 is possible at this stage. It was shown in chapter 2 that the rate of reduction of V_2O_5 by CO is markedly slower than the rate of reduction of V_2O_5 by H_2. A comparison of the systems V_2O_5-CO and V_2O_5-H_2 from a thermodynamic point of view was thought to be neccessary to gain a better understanding of the driving forces behind the reduction.

3.2. THERMODYNAMIC RESULTS

3.2.1. Gibbs free energy calculations

The Gibbs free energy changes associated with the following reactions were calculated :

$3/2\ V_2O_5 + CO \longrightarrow \frac{1}{2}\ V_6O_{13} + CO_2$ {R3.1}

$V_6O_{13} + CO \longrightarrow 6\ VO_2 + CO_2$ {R3.2}

$2\ VO_2 + CO \longrightarrow V_2O_3 + CO_2$ {R3.3}

$V_2O_3 + CO \longrightarrow 2\ VO_2 + CO_2$ {R3.4}

$3/2\ V_2O_5 + H_2 \longrightarrow \frac{1}{2}\ V_6O_{13} + H_2O$ {R3.5}

$V_6O_{13} + H_2 \longrightarrow 6\ VO_2 + H_2O$ {R3.6}

$2\ VO_2 + H_2 \longrightarrow V_2O_3 + H_2O$ {R3.7}

$V_2O_3 + H_2 \longrightarrow 2\ VO_2 + H_2O$ {R3.8}

The $\Delta G^{\ominus}$ values obtained for these reactions are contained in tables 3.1 and 3.2. $\Delta G^{\ominus}$ vs. temperature is plotted in figures 3.1 and 3.2. The thermodynamic data of the various substances that were used for the calculations are given in Appendix B.

From figures 3.1 and 3.2 it can be expected that reactions 3.1 to 3.3 and reactions 3.5 to 3.7 will be spontaneous, while reactions 3.4 and 3.8 will not be spontaneous. This is in agreement with the results obtained in chapter 2 where it was found that V_2O_5 is reduced to V_2O_3, but no further reduction of V_2O_3 to VO was observed. It can also be seen that $\Delta G^{\ominus}$ for reactions 3.3 and 3.7 is less negative than $\Delta G^{\ominus}$ for reactions 3.1, 3.2, 3.5 and 3.6. This explains the fact that VO_2 was observed to be the most stable intermediate during reduction since a reaction step in the TG-curves corresponding to the formation of VO_2 was most frequently observed (figures 2.3(a), 2.4(a), 2.5(a) and 2.6(a)).

According to tables 3.1 and 3.2, the reduction of V_2O_5 by CO is favoured above the reduction by H_2 since the $\Delta G^{\ominus}$-values for the reduction reactions in CO are more negative than the $\Delta G^{\ominus}$-values for the reduction reactions in H_2. This fact contradicts the results obtained in chapter 2 where reduction by H_2 was observed to be faster than reduction by CO.

3.2.2. Ellingham diagram

In the Ellingham-diagram in figure 3.3, the reduction by CO vs. reduction by H_2 can be viewed in a better perspective. Values of $\Delta G^{\ominus}$ vs. temperature for the following reactions are represented in figure 3.3 :

Table 3.1 - $\Delta G^{\ominus}$-values for the reduction of V_2O_5 by CO

Temperature		$\Delta G^{\ominus}$ kcal.mol^{-1}			
K	°C	R3.1	R3.2	R3.3	R3.4
298.15	25	-40.82	-30.81	-18.45	19.68
300	26.25	-40.81	-30.80	-18.46	19.69
400	126.25	-40.47	-31.60	-18.37	19.81
500	226.25	-39.98	-33.38	-17.99	19.96
600	326.25	-39.36	-35.34	-17.58	20.13
700	326.25	-38.65	-37.43	-17.16	20.33
800	426.25	-37.89	-39.59	-16.73	20.53
900	526.25	-37.13	-41.77	-16.29	20.74
1000	626.25			-15.85	20.95
1100	726.25			-15.41	21.16
1200	826.25			-14.97	21.37
1300	926.25			-14.53	21.57
1400	1026.25			-14.10	21.77
1500	1126.25			-13.68	21.96
1600	1226.25			-13.27	22.14

Table 3.2 - $\Delta G^{\ominus}$-values for the reduction of V_2O_5 in H_2

Temperature		$\Delta G^{\ominus}$ kcal.mol^{-1}			
K	°C	R3.5	R3.6	R3.7	R3.8
298.15	25	-34.13	-24.12	-11.77	26.37
300	26.25	-34.14	-24.14	-11.79	26.35
400	126.25	-34.79	-25.92	-12.69	25.49
500	226.25	-35.25	-28.65	-13.25	24.69
600	326.25	-35.53	-31.51	-13.75	23.96
700	326.25	-35.67	-34.47	-14.19	23.29
800	426.25	-35.76	-37.46	-14.60	22.65
900	526.25	-35.80	-40.45	-14.96	22.06
1000	626.25			-15.30	21.49
1100	726.25			-15.62	20.95
1200	826.25			-15.91	20.42
1300	926.25			-16.20	19.91
1400	1026.25			-16.47	19.41
1500	1126.25			-16.73	18.91
1600	1226.25			-16.99	18.42

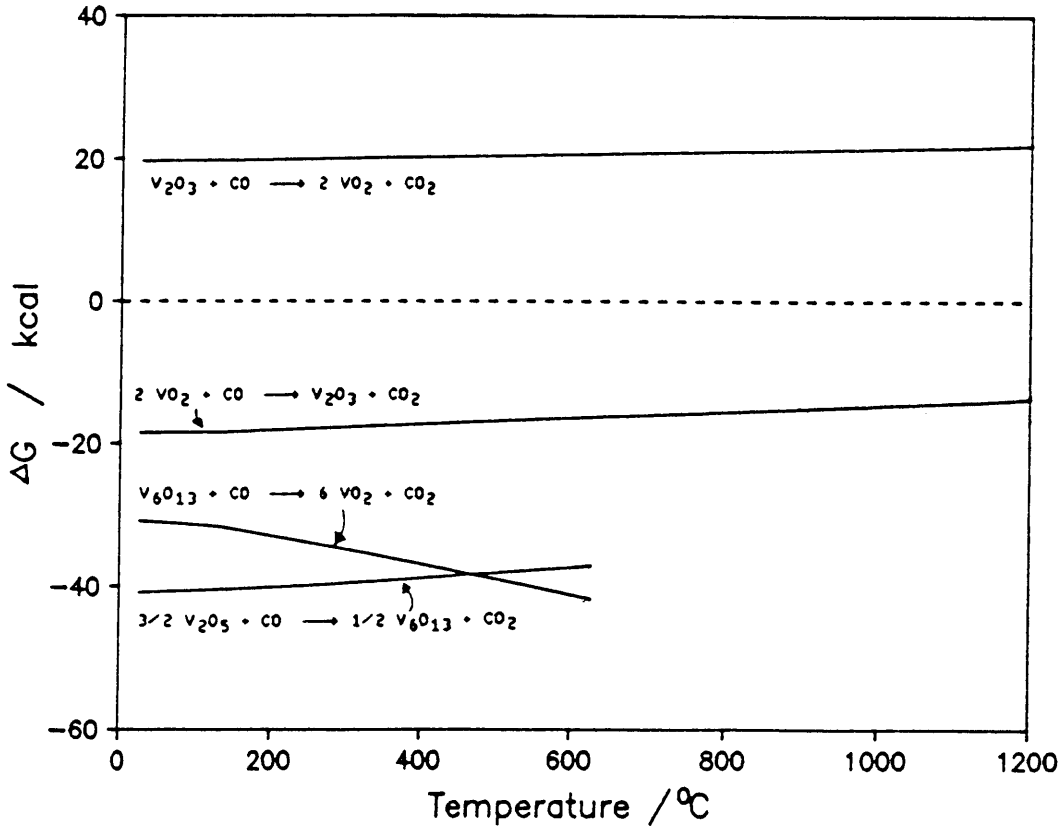

Figure 3.1 - $\Delta G^{\ominus}$ vs. temperature for the reduction of V_2O_5 by CO.

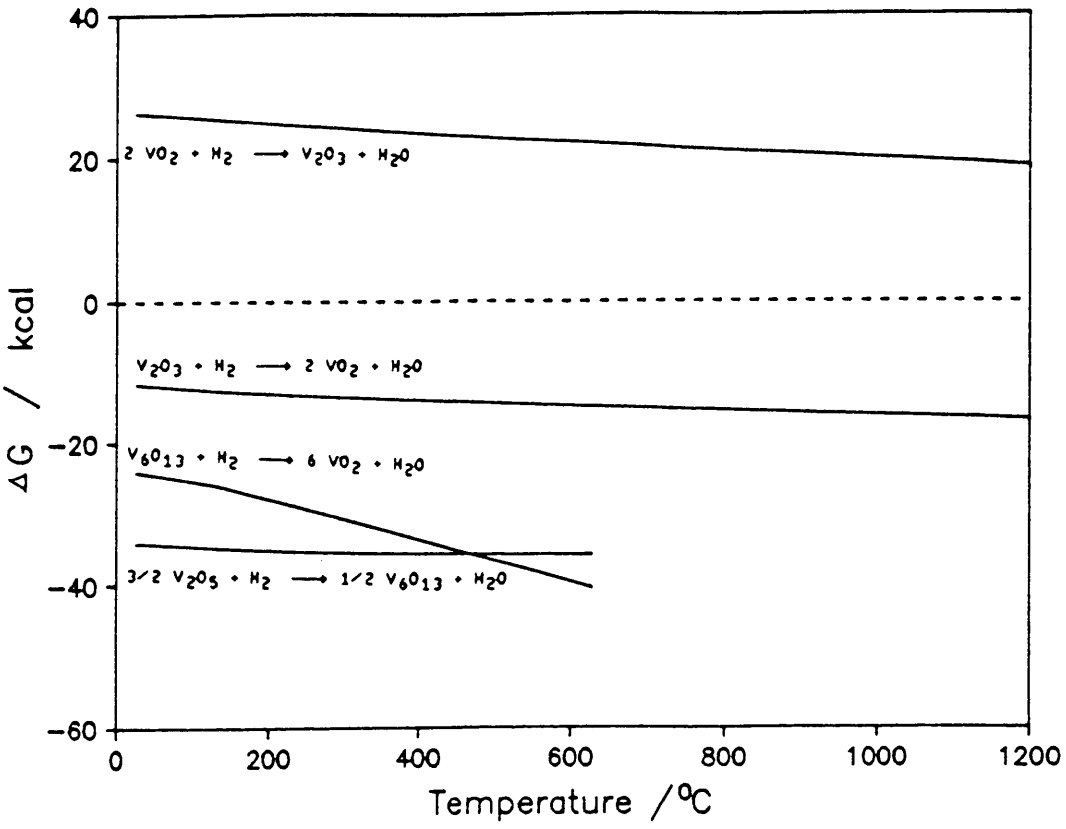

Figure 3.2 - $\Delta G^{\ominus}$ vs. temperature for the reduction of V_2O_5 by H_2.

$$CO + \tfrac{1}{2} O_2 \rightarrow CO_2 \quad \{R3.9\}$$

$$H_2 + \tfrac{1}{2} O_2 \rightarrow H_2O \quad \{R3.10\}$$

$$2\,VO + \tfrac{1}{2} O_2 \rightarrow V_2O_3 \quad \{R3.11\}$$

$$V_2O_3 + \tfrac{1}{2} O_2 \rightarrow 2\,VO_2 \quad \{R3.12\}$$

$$6\,VO_2 + \tfrac{1}{2} O_2 \rightarrow V_6O_{13} \quad \{R3.13\}$$

$$\tfrac{1}{2} V_6O_{13} + \tfrac{1}{2} O_2 \rightarrow 3/2\,V_2O_5 \quad \{R3.14\}$$

According to figure 3.3, reduction by CO is favoured below ~800°C while reduction by H_2 is favoured above ~800°C. It was shown in chapter 2 that reduction takes place roughly in the temperature range ±400°C - ±1000°C, depending on the heating rate and sample morphology. In this temperature range the thermodynamics of reactions 3.9 and 3.10 seem quite comparable, according to figure 3.3. Although reduction by CO is slightly more favourable below 800°C, reduction by CO and H_2 should almost be equally favourable in the temperature range where reduction of V_2O_5 takes place.

3.3 DISCUSSION

The faster reduction rate of V_2O_5 by H_2 as compared to that by CO, cannot be explained from a thermodynamic point of view. On the contrary, thermodynamics predicts that the reverse should take place. The Ellingham diagram (figure 3.3) shows that the thermodynamics of CO reduction does not differ appreciably from H_2 reduction. It is possible that this phenomenon might be due to kinetic factors. In chapters 4 and 5, a study of the kinetic and mechanistic aspects of the reduction reactions will be made.

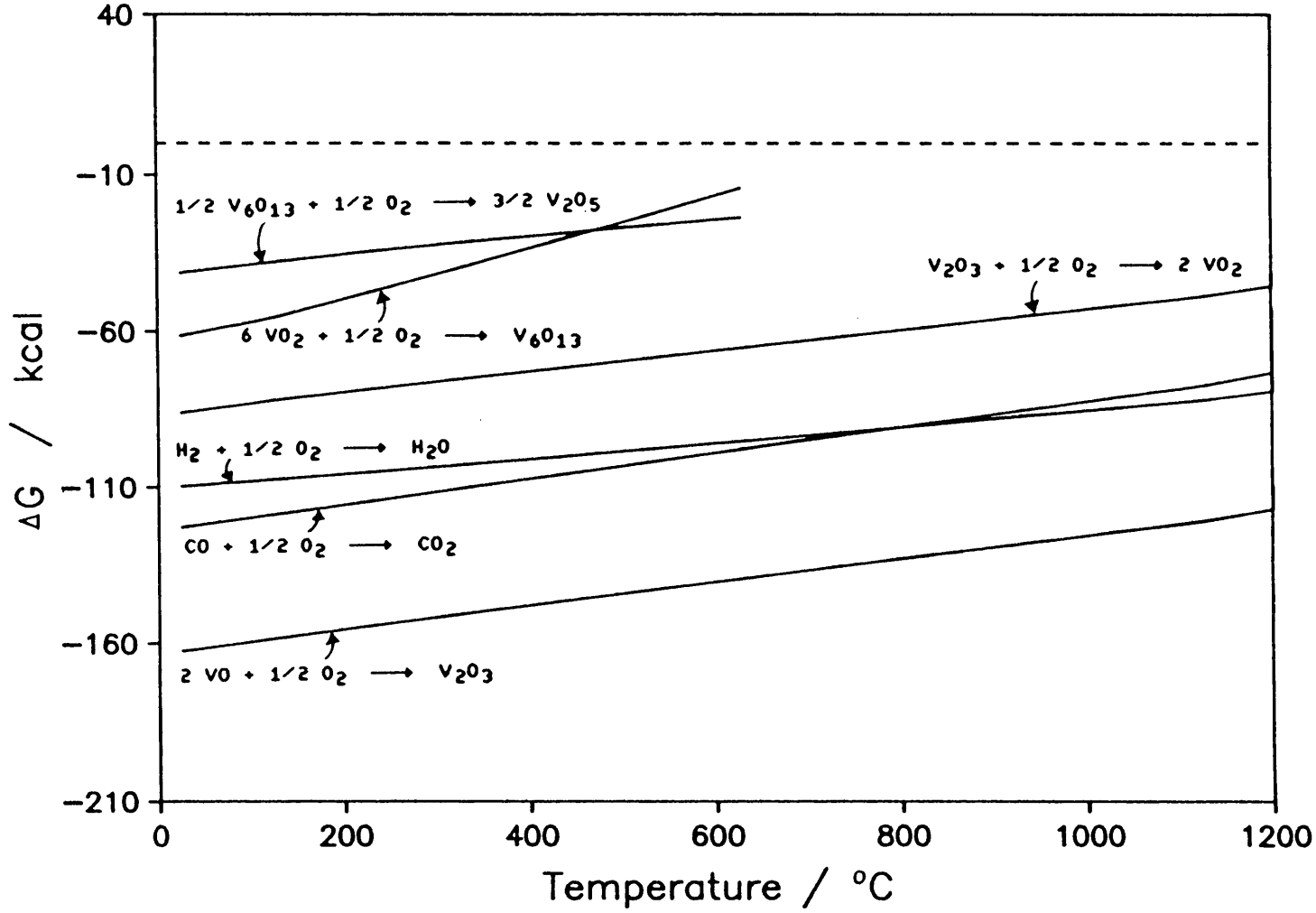

Figure 3.3 - Ellingham diagram : ΔG vs. temperature for the oxidation reactions of vanadium oxides, CO, and H_2.

CHAPTER 4
THE MECHANISM OF REDUCTION : SOLID - GAS INTERACTION

4.1. INTRODUCTION

During isothermal reduction experiments done on V_2O_5 at various temperatures, unexpected tendencies were observed in the behaviour of different morphological types of V_2O_5. These observations will be discussed in this chapter and possible explanations, in terms of the mechanism of reduction of V_2O_5, will be presented.

Although extensive research has been done on the mechanism of oxidation of CO and H_2 on V_2O_5 catalysts [25, 28-34], little effort has been made to study the mechanism of reduction of V_2O_5. The object of this chapter is therefore to contribute to a better understanding of the processes which are involved in the mechanism of reduction of V_2O_5.

4.2. EXPERIMENTAL PROCEDURE

4.2.1. Materials

Two types of V_2O_5 with different morphologies were used in the studies conducted in this chapter. Their preparation and characterization were discussed in sections 2.2.1 and 2.3.1 respectively.

4.2.2. Instrumental techniques

4.2.2.1. Thermal analysis studies

The isothermal reduction of V_2O_5 by CO and H_2 was studied in the 380°C to 590°C temperature range using isothermal TG. The instrumentation used was described in section 2.2.2. Sample masses were in the range 20mg to 30mg, and dynamic atmospheres of ±50ml.min.$^{-1}$ were used in all studies.

4.2.2.2. X-ray powder diffraction

XRPD analysis was used for identification of intermediate and final compounds. The instrumental details were given in section 2.2.3.

4.2.2.3. Carbon analysis

The carbon content of samples was determined by the LECO-technique at Mintek.

4.3. RESULTS

4.3.1. Reduction by CO

The isothermal reduction curves for the V_2O_5 powder and platelets are given in figures 4.1 and 4.2 respectively. The reduction of V_2O_5 by CO at various temperatures is represented by single, sigmoidal TG-curves consisting of induction periods, acceleration and decay periods. In all cases, the total mass losses obtained corresponded to the formation of V_2O_3 which was confirmed by XRPD to be the final product.

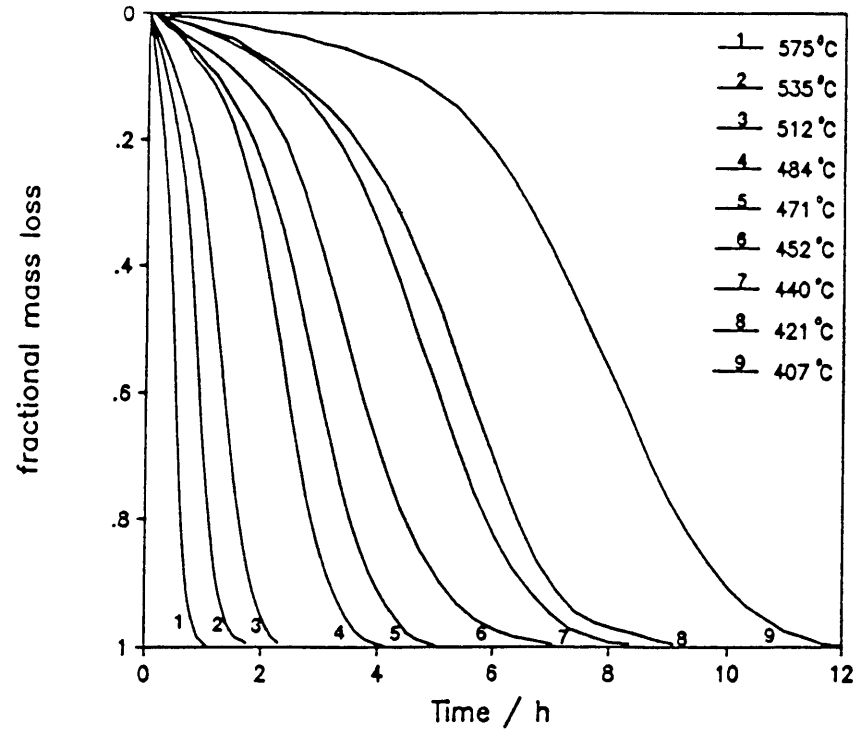

Figure 4.1. - Isothermal TG-curves for the reduction of V_2O_5 powder by CO

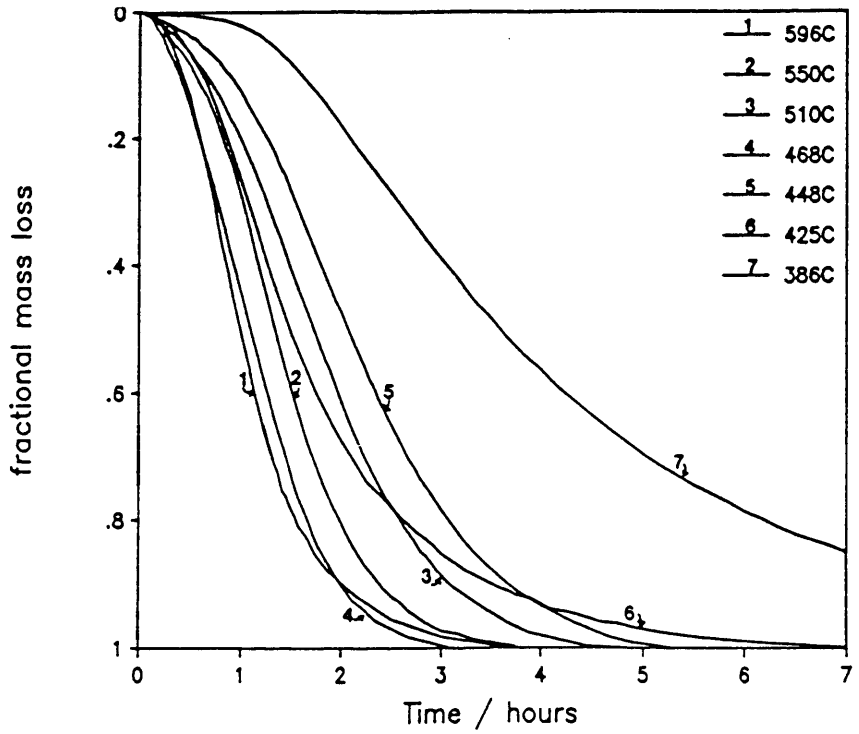

Figure 4.2 - Isothermal TG-curves for the reduction of V_2O_5 platelets by CO

The isothermal reduction of V_2O_5 powder at 550 °C was terminated at various stages of the reduction to study the formation of intermediate oxide phases. A qualitative study was done by plotting the relative intensities of the main peak of each of the oxides against α to follow the course of reduction (figure 4.3).

The oxide phases identified were V_6O_{13}, VO_2 and V_2O_3, in accordance with the results of the dynamic studies (chapter 2). During isothermal reduction, V_2O_5 is reduced gradually through these intermediate oxides to V_2O_3 without discreet reaction steps, in such a way that there exists a gradient of oxygen between the surface and the centre of the material. Therefore only single reaction steps are observed in figures 4.1 and 4.2.

An increase in isothermal reduction temperature leads to an increase in reduction rate of the V_2O_5 powder (figure 4.1). However, as the reduction temperature is raised, the rate of reduction of the platelets seems to reach a maximum at 460°C (figure 4.2).

This effect is clearer in figures 4.4(a) and (b). In these figures the reduction time versus the isothermal reduction temperature is plotted for reduction to a fractional mass loss of 0.5 (figure 4.4(a)) and 0.9 (figure 4.4(b)). These α values were chosen instead of using the α-values at the end of the reduction curves in order to minimize the influence of experimental error which is more pronounced at $\alpha = 1$.

At temperatures below ~480°C, the V_2O_5 powder is reduced more slowly than the V_2O_5 platelets, while at temperatures above ~480°C the reverse effect is observed. In the temperature range ±460°C to ±500°C a decrease in the reduction rate of the platelets is observed, after a maximum reduction rate at 460°C. An explanation for this effect will be suggested in section 4.4.

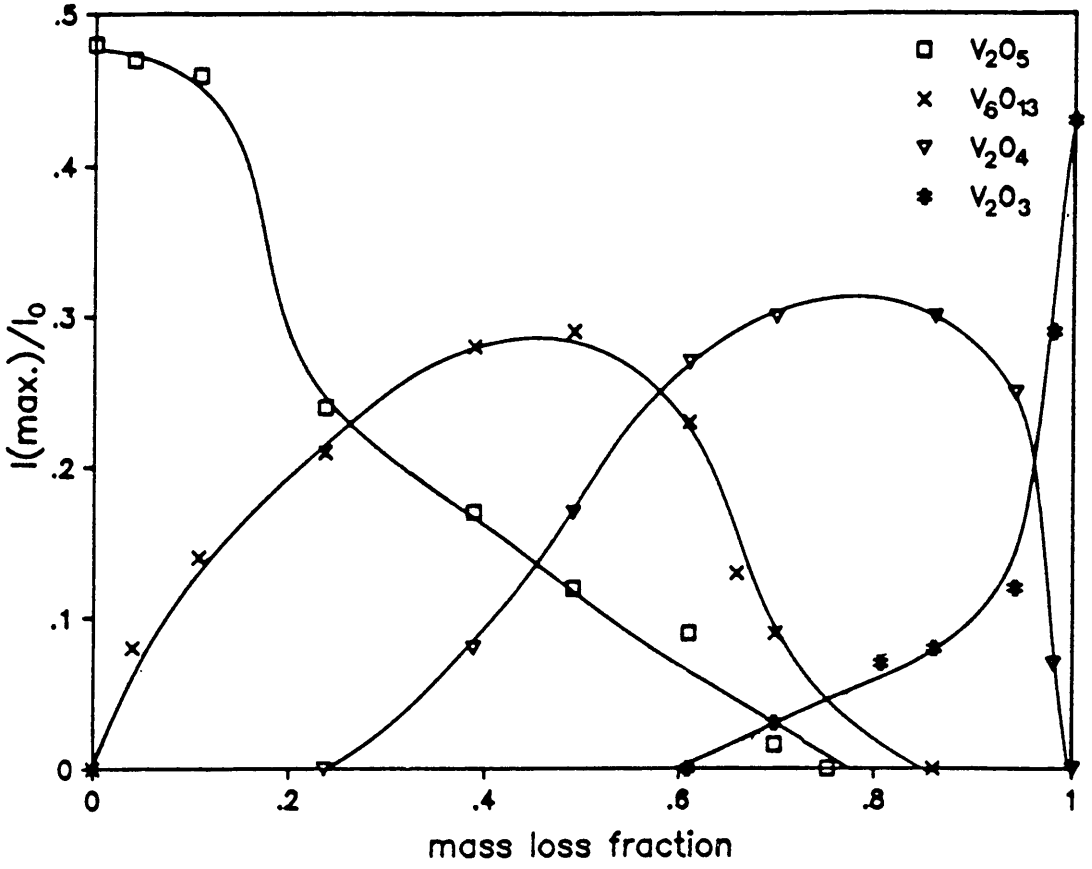

Figure 4.3 - I_{max}/I_0 versus α for intermediate oxides during isothermal reduction

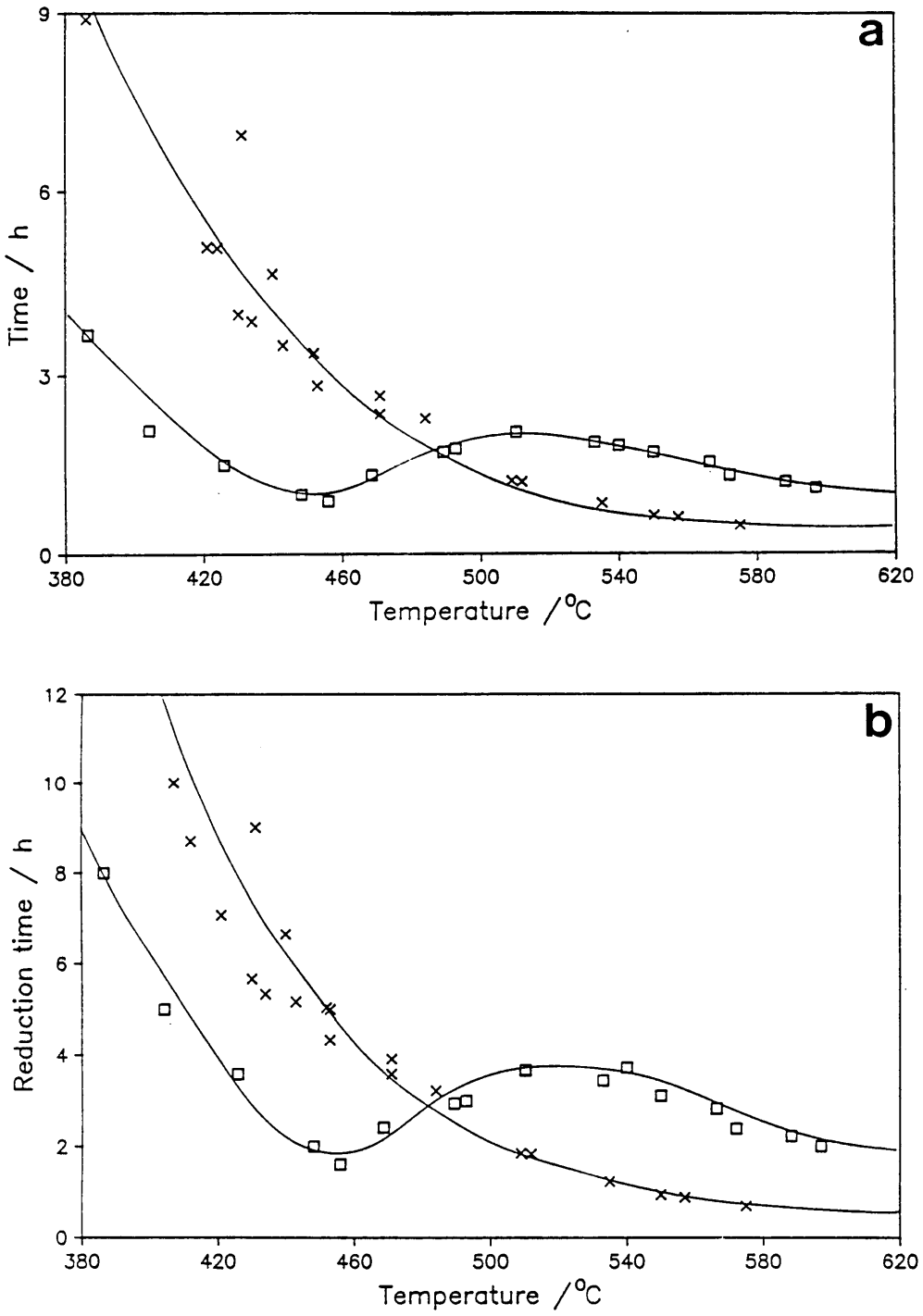

Figure 4.4 - Reduction time versus isothermal reduction temperature of V_2O_5 in CO to (a) $\alpha = 0.5$ (b) $\alpha = 0.9$

4.3.2. The formation of carbon

During reduction experiments of V_2O_5 by CO it was observed that the thermocouples and sample holders as well as the inner surfaces of the furnace were blackened due to carbon deposition. The carbon is expected to form due to the decomposition of CO according to :

$$2CO \longrightarrow C(s) + CO_2 \qquad \{R4.1\}$$

Since V_2O_5 has been reported in literature to catalyze the decomposition of CO with a maximum rate at 480°C [35], it was thought at first that the observed coking was caused by the catalytic decomposition of CO on the V_2O_5 surface. It was further thought that this process was responsible for the effect observed in figures 4.4(a) and (b). However, this theory was rejected after further considerations, as will become clear shortly.

Samples of V_2O_5 powder and platelets were completely reduced by CO at various temperatures after which the carbon content of the final V_2O_3 products was determined. The results obtained are contained in table 4.1.

From table 4.1 it seems that the carbon content of the final samples is not markedly dependent upon reduction temperature or sample morphology. The carbon contents of the reduced platelets at 500°C and 550°C seem to be somewhat lower than the other values in table 4.1. A possible reason for this discrepancy is that these samples were mistakenly kept at the indicated temperatures for shorter time periods than the rest of the samples. It seems, therefore, that the carbon deposition is a function of time rather than of temperature or grain morphology.

Table 4.1 - Carbon content of final samples after CO reduction at various temperatures

Temperature of reduction °C	Carbon content / mass %	
	Powder	Platelets
400	1.01	1.07
450	0.88	0.93
480	0.82	1.03
500	0.89	0.46
550	1.00	0.55

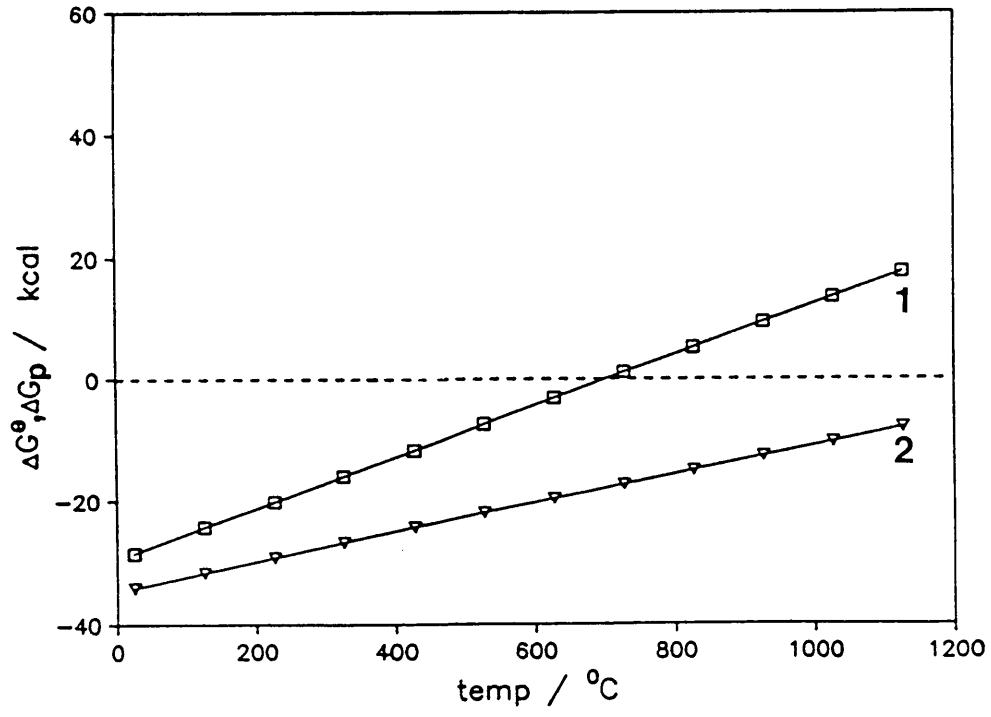

Figure 4.5 - ΔG versus temperature for the decomposition of CO according to reaction 4.1
curve 1 : p(CO) = 0.5 atm.
curve 2 : p(CO) ~ 1 atm.

If the decomposition of CO was catalyzed by V_2O_5 with a maximum rate at 480°C, the carbon content of the V_2O_5 samples should accordingly have reached a maximum amount at this temperature. The extent of coking of the platelets should also have been higher than that of the powder since the active plane for the catalytic decomposition of CO would most probably be the (010) plane.

If the thermodynamics of reaction 4.1 are considered (figure 4.5) it can be seen that ΔG for the reaction at a CO partial pressure of ~1 atmosphere is negative in the temperature range 25 - 1200°C. Therefore it is possible that coking of the samples is due to spontaneous rather than catalytic decomposition of CO.

4.3.3. Reduction by H_2

The isothermal TG-curves for the reduction of V_2O_5 powder and platelets by H_2 are given in figures 4.6 and 4.7.

Similar to the TG-curves obtained in CO, the TG-curves in figures 4.6 and 4.7 consist of sigmoidal, single-step reactions with total mass losses corresponding to the formation of V_2O_3.

An increase in isothermal temperature causes a higher reduction rate of the powder, while there seems to be a deviation from this behaviour by the platelets, although to a lesser extent than when CO was used as reducing agent.

In figures 4.8(a) and (b) the reduction time for reduction to $\alpha=0.5$ and $\alpha=0.9$ is plotted versus isothermal temperature. The same behaviour is observed in these figures as in figures 4.4(a) and (b), although less

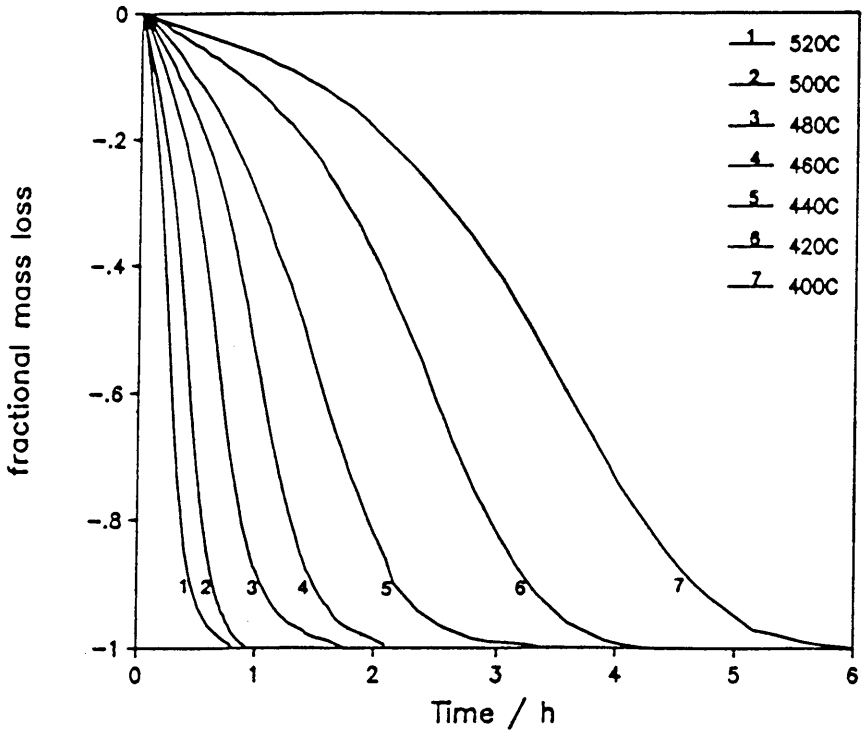

Figure 4.6 - Isothermal TG-curves for the reduction of V_2O_5 powder by H_2

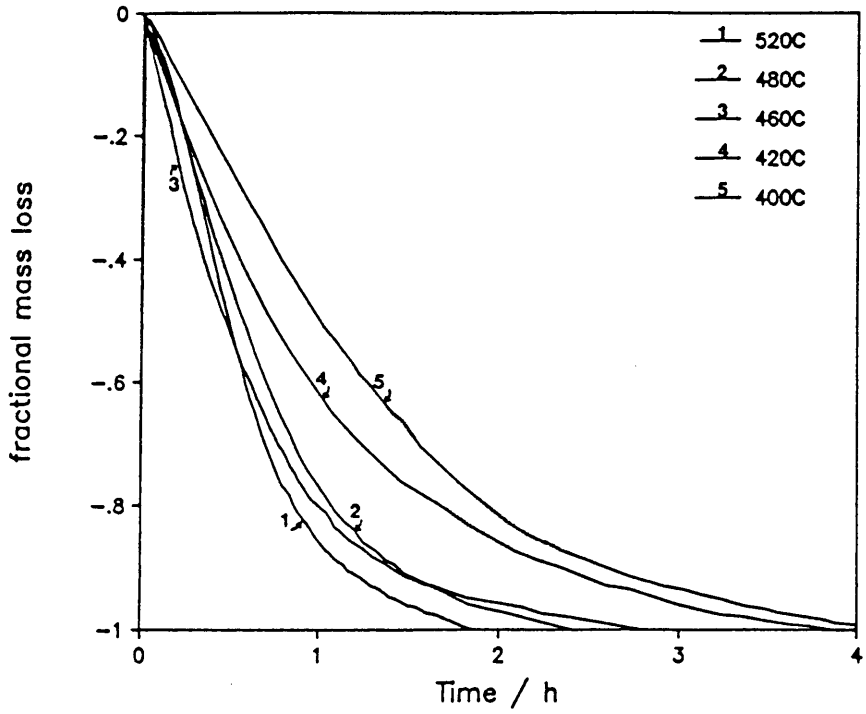

Figure 4.7 - Isothermal TG-curves for the reduction of V_2O_5 platelets by H_2

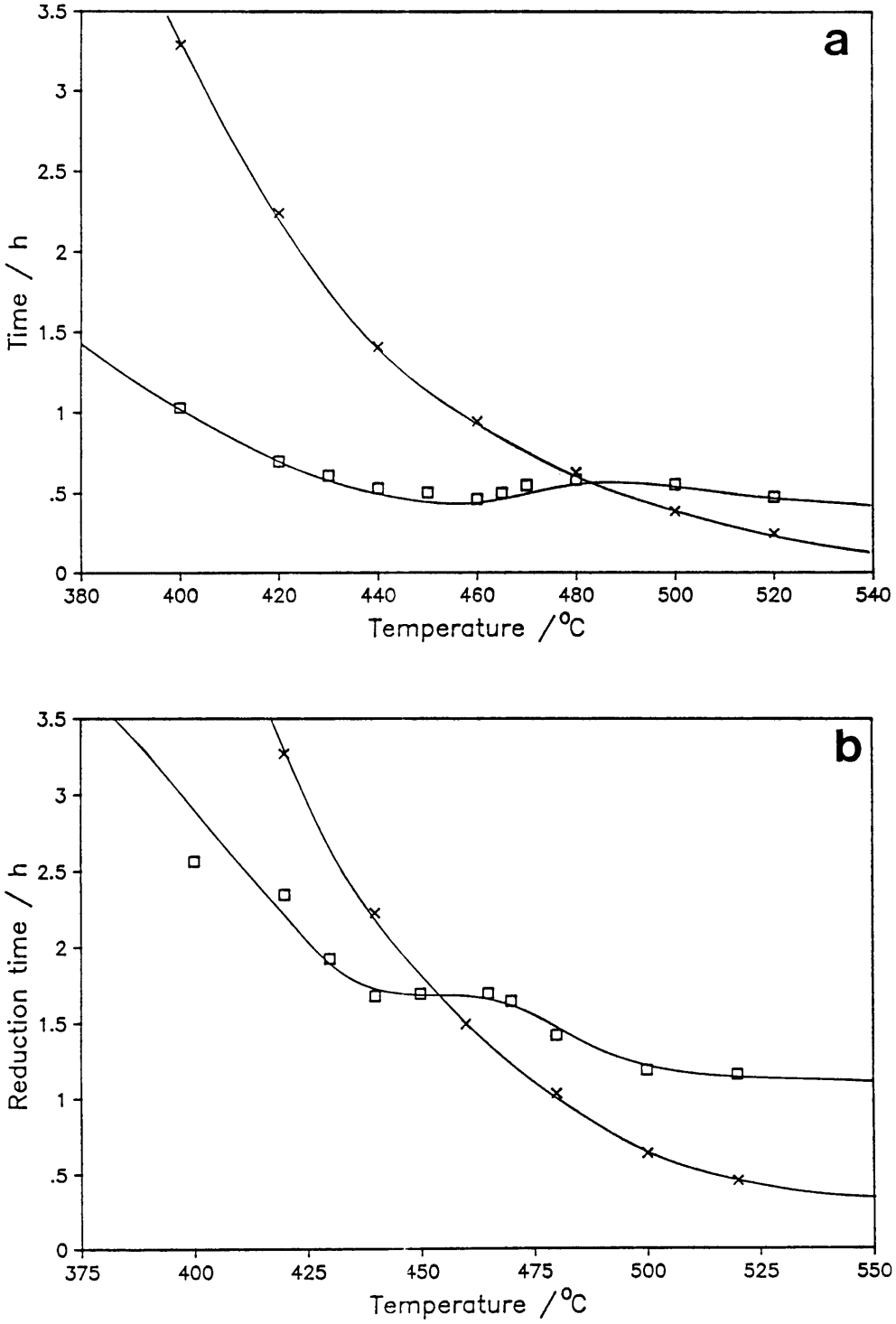

Figure 4.8 - Reduction time versus isothermal reduction temperature of V_2O_5 in H_2 to (a) $\alpha = 0.5$ (b) $\alpha = 0.9$

pronounced. It can be seen that at temperatures below ~480°C the reduction rate of platelets is faster than the reduction rate of the powder, while above these temperatures the reverse is observed. The reduction rate of the platelets also passes through a maximum at ~460°C after which a decrease is observed.

4.4. DISCUSSION

From the results obtained it seems that the reduction of V_2O_5 is a structure sensitive process. Although the surface area of the platelets ($<0.5 m^2.g^{-1}$) is much smaller than the surface area of the powder ($2.87 m^2.g^{-1}$), the platelets are reduced faster at lower temperatures ($<480°C$) than the powder. This is contrary to expectation. Above a temperature of ~460°C, a decrease in the reduction rate of the platelets is observed. At higher temperatures ($>480°C$) the reduction rate of the platelets is slower than the reduction rate of the powder. An attempt will be made to explain these phenomena by proposing that two competing reduction mechanisms are contributing towards the overall reduction process, viz. reduction through adsorption and direct reduction.

4.4.1 The contribution of reduction through adsorption

It was mentioned in section 2.1 that vanadium-based catalysts are used as oxidation catalysts in various industrial processes. In their study of the oxidation of CO on an unsupported V_2O_5 catalyst, Baiker et al. [31, 33] found that catalysts consisting of well-developed thin plates of V_2O_5 with a large contribution of the (010) face to the surface area, were about 30 times more active for CO oxidation than agglomerates of needle type V_2O_5 without predominant exposure of this face. They ascribed this effect to the

activity of the V=O species in the (010) face. Their measurements indicated that the active sites for CO adsorption and oxidation are these V=O species and attributed the higher activity af the V_2O_5 plates to their larger number of V=O active sites per unit surface area.

In addition to this, it has also been stated by Fiermans et al. [18] that reduction of the V_2O_5 lattice occurs by removal of vanadyl oxygen. At this stage it seems that prior to reduction of V_2O_5, the reducing gas (CO or H_2) is adsorbed onto the V=O species after which rupture of this vanadyl bond occurs, leading to reduction.

A possible representation of the mechanism of chemisorption of CO on the V=O species and the consequent desorption of CO_2 following reduction, is given in the following diagram:

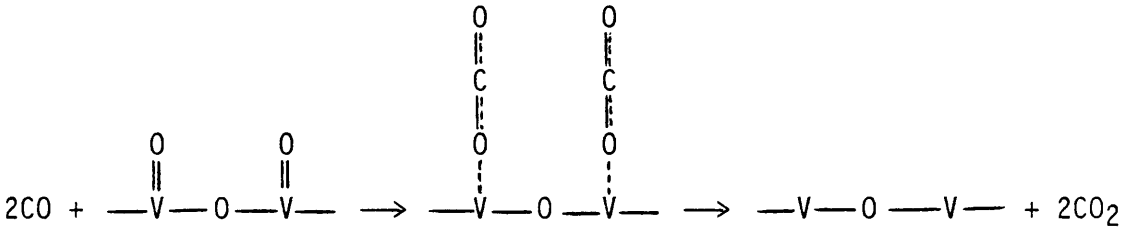

On the other hand, according to the literature [34,54], the mechanism of adsorption (chemisorption) of H_2 on the V=O species, involves the dissociation of the hydrogen bond with the formation of V-O-H species, according to the following mechanism:

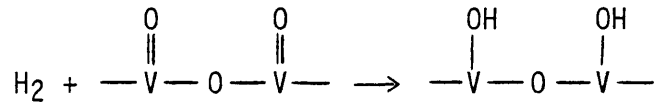

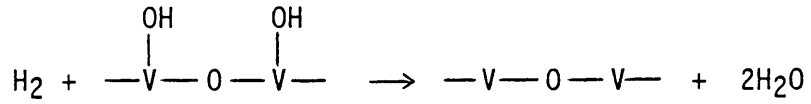

For argument's sake, consider at first only the reduction of the platelets and powder up to a temperature of about 460°C in figures 4.4 and 4.8. It is possible that the rate of reduction of the platelets could be faster than that of the powder because the larger number of V=O species per unit surface area of the platelets as compared to that of the powder, ensures a higher rate of chemisorption on the (010) plane of the platelets.

Considering the nature of the adsorption of the reducing gas onto the V_2O_5 surface, the process should rather be viewed as a chemical adsorption (chemisorption) process. This is because full chemical bonding should occur between the adsorbate (V_2O_5) and the adsorbent (CO or H_2) for reduction to occur.

It is possible that the gas is only physically adsorbed at first, and then enters into a chemical reaction with the surface of the solid. A further increase in temperature would lead to the normal decrease in the rate of chemisorption. It would thus appear as if chemisorption would reach a maximum rate at 460°C.

If the DTA-curves of the dynamic reduction of V_2O_5 by CO and H_2 are reconsidered (figures 2.4(b), 2.5(b) and 2.6(b)), exothermic DTA signals are observed in the 450°C to 500°C temperature range. If these exotherms are interpreted as heat being evolved during chemisorption of the reducing

gases onto the V_2O_5 surface, it is possible to explain the maximum reduction rate of the platelets at 460°C. The reduction rate of the powder should also be affected in the same manner, but only to a smaller extent. The contribution of chemisorption on the (010) planes to the overall reduction process in these crystals is much smaller so that a small decrease in reduction rate could occur without being noticed.

4.4.2. The contribution of direct reduction

The slower reduction rate of the platelets above 480°C as compared to the powder, can possibly be ascribed to a different reduction mechanism governing the rate of reaction above this temperature. This mechanism probably involves direct reduction of the solid reactant by the gas, and would not involve adsorption of the gas onto the V=O species, but merely physical contact through solid-gas collisions.

It is known [26] that CO molecules adsorbed on an oxide surface react with the oxygen of the lattice more readily than CO molecules in the gas phase. Therefore it can be expected that reduction following an adsorption process would be faster than reduction by a direct mechanism.

The contribution of the direct mechanism towards the overall reduction rate below 460°C will be very small for the platelets as compared to the contribution of the adsorption mechanism. When it comes to the powder, it can be understood that the direct mechanism would have a larger contribution towards the overall reduction rate than reduction through adsorption because of the poorly developed (010) planes of these crystals and a consequent poor capacity for gas adsorption.

These arguments correlate well with the results obtained by Marshneva et

al. [29]. They studied the kinetics and mechanism of CO oxidation on V_2O_5 and found that at temperatures below 450°C, a mechanism associated with reactions of the reagents in an adsorbed layer, makes the main contribution to the process rate. At higher temperatures, the share of this mechanism in the overall process rate is reduced due to a decrease in catalyst coverage by the reagents, and at 590°C essentially the whole reaction rate is ensured by a direct reduction-oxidation mechanism.

4.4.3. The contribution of diffusion

Other contributing factors towards the behaviour observed in figures 4.4 and 4.5, are the diffusional processes which occur during reduction. If these processes are considered rate determining above 460°C, it can be understood that the reduction rate of the powder would be the highest.

These diffusional processes would involve the diffusion of the reactive gas through the product layer towards the reaction interface and the diffusion of gaseous products from the reaction interface through the product layer towards the surface of the crystal. The inhibitive effect of these processes would be more pronounced in the platelets due to their smaller surface areas and larger dimensions.

The effect of diffusion can also be seen by comparing figures 4.4(a) and (b) or figures 4.7(a) and (b). The difference between the reduction time of the powder and the platelets at temperatures below the temperature of intersection is larger at $\alpha=0.5$ than at $\alpha=0.9$. Inversely, the difference between the reduction time of the powder and the platelets at temperatures above the intersection is larger at $\alpha=0.9$ than at $\alpha=0.5$. This can be ascribed to the increasing inhibiting effect of product gas diffusion through a product layer which becomes thicker as the reduction proceeds. This

proceeds. This effect would be much more pronounced in the platelets, causing the observed effect.

However, this is not the sole reason for the observed effects in figures 4.4 and 4.5, since there would be a more gradual change in the curve of the platelets and no actual decrease in reduction rate would be observed if diffusion alone was responsible for this effect.

4.4.4. The influence of reducing gas

It is clear from the results obtained during the isothermal reduction experiments that the reduction rate of V_2O_5 using H_2 as reducing gas, is significantly faster than when CO is used. This behaviour is not explained from a thermodynamic point of view. The next chapter will be devoted to a kinetic study of the reduction of V_2O_5 in order to gain a better understanding of this system.

CHAPTER 5
THE KINETICS AND MECHANISM OF REDUCTION

5.1. INTRODUCTION

Although the extent of reaction can be predicted by thermodynamics, the actual rate of reaction can only be described by kinetics. Thermodynamics is a powerful tool for investigating conditions at equilibrium, but the time required for reaction lies beyond the scope of thermodynamics. Kinetics deals with the rate of reaction, with all the factors that influence the reaction rate and offers an explanation of the reaction in terms of a reaction mechanism.

Unfortunately, kinetics and the reaction mechanism are based on theory which strives to explain (often crudely) experimental observations. However, useful information can be obtained from a kinetic study performed with discretion. With this goal in mind, a kinetic study of the reduction of V_2O_5 was undertaken.

This chapter is concerned with the kinetics of the reduction of V_2O_5 and the determination of a kinetic model which is best suited to describe the experimental course of reduction. The influence of the following factors on the kinetics and rate of reduction will also be discussed:

(i) solid-gas interaction, which is a continuation of the issue dealt with in the previous chapter,

(ii) the grain morphology of the V_2O_5 reactant,

(iii) the reducing gas (CO versus H_2),

(iv) the reduction temperature.

5.2. EXPERIMENTAL PROCEDURE

5.2.1. Kinetic calculations

The experimental, isothermal TG-curves (figures 4.1, 4.2, 4.6, 4.7) which were obtained for the reduction of V_2O_5 powder and platelets in CO and H_2, were used for the kinetic calculations. The experimental data, α (fraction reacted) versus t (time), were fitted to nineteen different equations (listed in appendix C), representing different kinetic models. A computer program developed by Wagener et al. [36] was used for these calculations. The linearity of the plots of calculated values of $f(\alpha)$ versus t for each kinetic expression was taken as criterion for identification of the rate equation. Both the correlation coefficient (R) and the standard deviation (σ) were considered in the determination of each of these rate equations. In appendix C a detailed explanation is given of the method used to process the data and to decide on the best kinetic model.

The relationship between the rate of reaction and temperature was assumed to be described by the Arrhenius equation:

$$k = Ae^{-Ea/RT} \qquad \{R5.1\}$$

$$\Rightarrow \ln k = \ln A-(Ea/R)(1/T) \qquad \{R5.2\}$$

Ea : activation energy
k : rate constant
T : isothermal temperature
A : frequency factor

An Arrhenius plot was made by plotting ln k versus 1/T. The activation energy was then calculated from the slope, according to equation 5.2. The values of the rate constant in the Arrhenius plot were calculated with the computer program for each α versus t data set recorded at each isothermal temperature.

5.2.2. Microscopy studies

Both optical microscopy and SEM were used in addition to the kinetic calculations to study the reduction mechanism. The instrumental details for the surface studies were discussed in section 2.2.5. For cross-section studies, the crystals were mounted in perspex holders with epoxy resin after which the crystals were cross-sectioned by polishing to a smooth finish. A Jeol JSM 840M scanning electron microscope was used in these studies.

5.3. RESULTS

5.3.1. Reduction by CO

5.3.1.1. V_2O_5 powder

Determination of the rate equation

The experimental α vs. t data for the isothermal reduction of V_2O_5 powder by CO (figure 4.1) were treated according to the method described in appendix C. The kinetic equation $f(\alpha)=[-\ln(1-\alpha)]^{1/4}$, which is an Avrami-Erofe'ev type equation, was found to describe the data the best.

The correlation coefficients and standard deviations obtained for the fit of the kinetic model to the experimental data sets recorded at various temperatures in the 380 - 575°C temperature interval, are listed in table 5.1. The linearities of the $f(\alpha)$ vs. t plots for some of the temperatures, are shown in figure 5.1.

The Avrami-Erofe'ev mechanism describes a process of nucleation and growth at sites of higher activity in the crystal such as dislocations and defects

in the crystal lattice. The nucleation period is represented by the induction period in the TG-curve. The general form of the Avrami-Erofe'ev equation is as follows:

$$k(t-t_0) = [-\ln(1-\alpha)]^{1/n} \qquad \{R5.3\}$$

α : the fractional mass loss at time t
k : the rate constant
t_0 : the delay time

The exponent $n = \beta + \alpha$, where β is the number of steps involved in nucleus formation and λ is the number of dimensions in which the nuclei grow.

For the isothermal reduction of V_2O_5 powder by CO, the value of n was found to be equal to 4. The physical significance of this value of n can not be explained at this stage because further experimental evidence is needed to do so. More attention will be given to the interpretation of the Avrami-Erofe'ev equation regarding the reduction of V_2O_5 at a later stage in this chapter.

Determination of the activation energy

The Arrhenius plot (ln k vs. 1/T) for the reduction of the powder is given in figure 5.2.

If the points on the Arrhenius plot above temperatures of 450°C, ($1/T < 1.38\times10^{-3}$), are considered, it can be seen that a good linear correlation of these data points exists. At lower temperatures, ($1/T \geq 1.38\times10^{-3}$), the points are more scattered. It is also observed from table 5.1 that at these lower temperatures, the Avrami-Erofe'ev (n=4) equation gives a poorer fit to the experimental data.

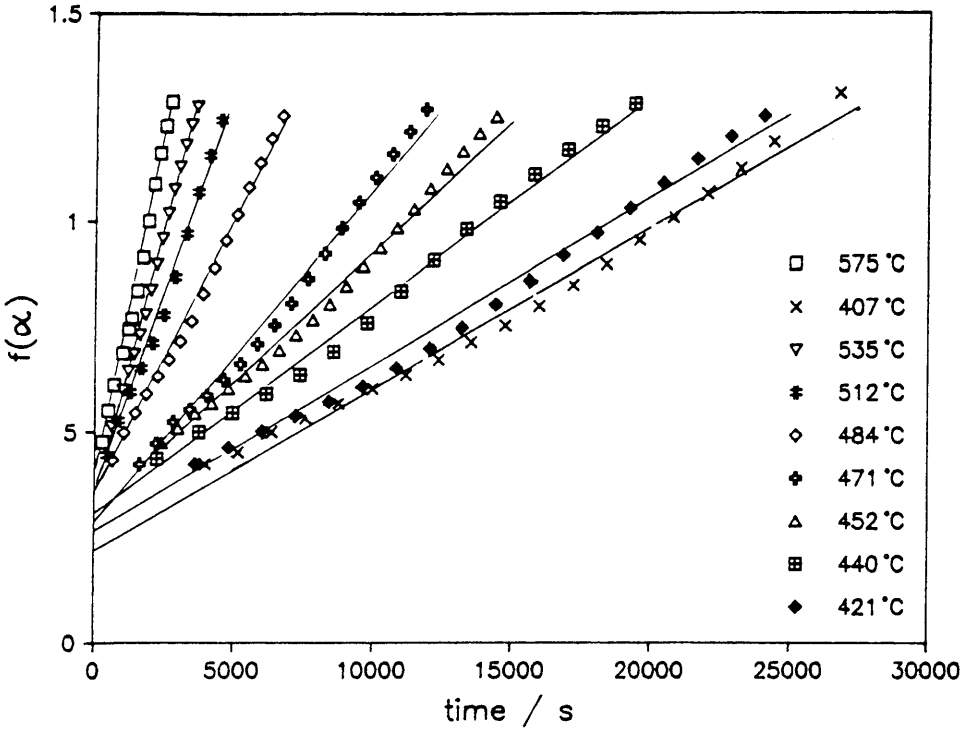

Figure 5.1. - Reduction of V_2O_5 powder by CO : $f(\alpha) = [-\ln(1-\alpha)]^{1/4}$ versus t.

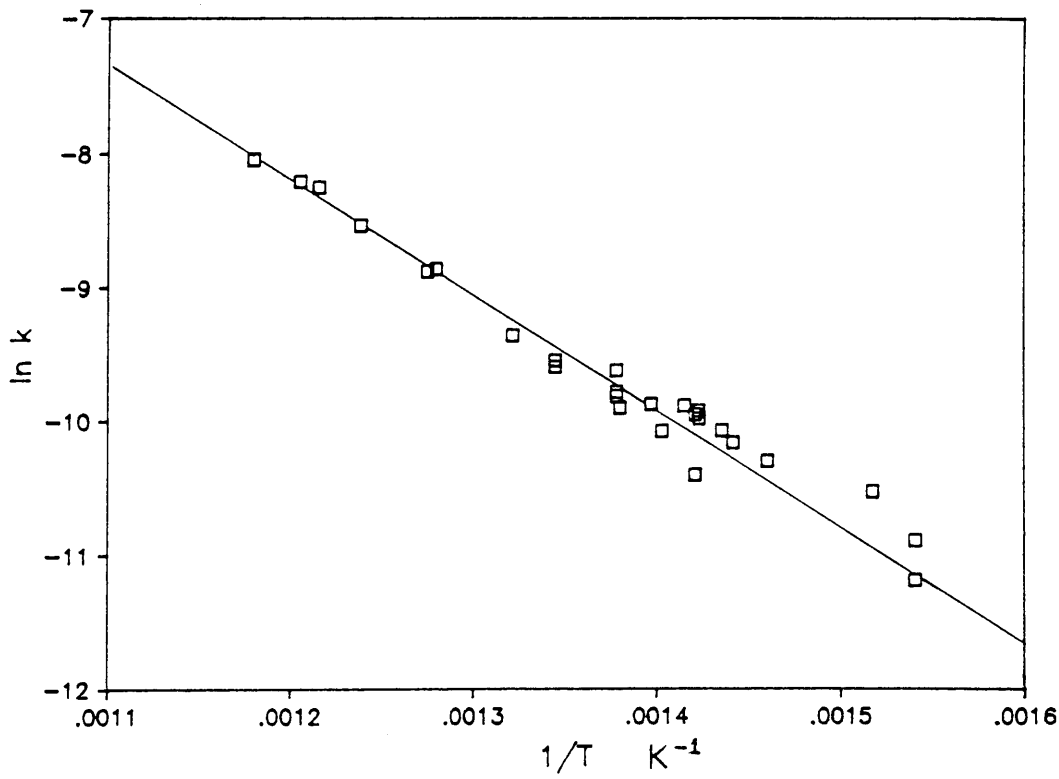

Figure 5.2. - Reduction of V_2O_5 powder by CO : Arrhenius plot.

The activation energy and frequency factor were calculated using:

(i) data points with $1/T < 1.38\times10^{-3}$

(ii) data points with $1/T \geq 1.38\times10^{-3}$

(iii) all data points.

The results are summarized in table 5.2.

Table 5.1 - The reduction of V_2O_5 powder by CO : R, σ and k for f(α) vs. t

Temp. / °C	R	σ	k / s^{-1}
376	.9471	.1122	1.388×10^{-5}
376	.9800	.0781	1.867×10^{-5}
386	.9838	.0780	2.494×10^{-5}
407	.9863	.1725	3.000×10^{-5}
412	.9908	.0387	3.373×10^{-5}
421	.9940	.0308	3.866×10^{-5}
424	.9941	.0460	4.236×10^{-5}
430	.9955	.0361	4.631×10^{-5}
430	.9985	.0214	4.918×10^{-5}
431	.9950	.0381	4.779×10^{-5}
431	.9882	.0604	3.040×10^{-5}
434	.9967	.0345	5.099×10^{-5}
440	.9976	.0276	4.221×10^{-5}
443	.9986	.0196	5.163×10^{-5}
452	.9985	.0216	5.018×10^{-5}
453	.9897	.0580	5.653×10^{-5}
453	.9873	.0650	6.660×10^{-5}
471	.9991	.0155	7.179×10^{-5}
471	.9974	.0268	6.842×10^{-5}
484	.9970	.0305	8.670×10^{-5}
509	.9972	.0285	1.425×10^{-4}
512	.9987	.0186	1.396×10^{-4}
535	.9966	.0318	1.964×10^{-4}
550	.9987	.0195	2.612×10^{-4}
557	.9987	.0260	2.727×10^{-4}
575	.9963	.0299	3.217×10^{-4}

Table 5.2. - Activation energies calculated for V_2O_5 powder in CO

Points used	R	Ea kJ.mol^{-1}	A s^{-1}
$1/T < .00138$	-.997	79.97	28.47
$1/T \geq .00138$	-.938	52.78	0.036
all	-.975	64.54	2.70

5.3.1.2. V_2O_5 platelets

Determination of the rate equation

The experimental α vs. t data for the isothermal reduction of V_2O_5 platelets by CO (figure 4.2) were treated according to the method described in appendix C.

The Avrami-Erofe'ev equation with $n=2$, $f(\alpha)=[-\ln(1-\alpha)]^{1/2}$, was found to give the best description of the experimental data.

The correlation coefficients and standard deviations obtained for the fit of this kinetic model to the experimental data sets recorded at various isothermal temperatures in the range 386 - 596°C, are listed in table 5.3.

The linearities of the $f(\alpha)$ vs. t plots are shown in figure 5.3(a) (510 - 588°C) and (b) (386 - 449°C). In the temperature range (510 - 588°C) the $f(\alpha)$ vs. t plots give very good linear correlations, as can be seen in both figure 5.3(a) and table 5.3. In the lower temperature range (386 - 449°C), poor linear correlations and fits to the Avrami-Erofe'ev equation with $n=2$, are observed.

Determination of the activation energy

On considering the Arrhenius plot (figure 5.4), it can be seen that the data fail to obey the Arrhenius law. This can be taken as evidence that the kinetics of the reaction is complex. This anti-Arrhenius behaviour is indicative of a multistep mechanism that changes as temperature increases [37]. This result supports the hypothesis that was made in the previous chapter, viz. the existence of two reduction mechanisms taking part in the overall reduction process. It could also explain the scatter that was observed at lower

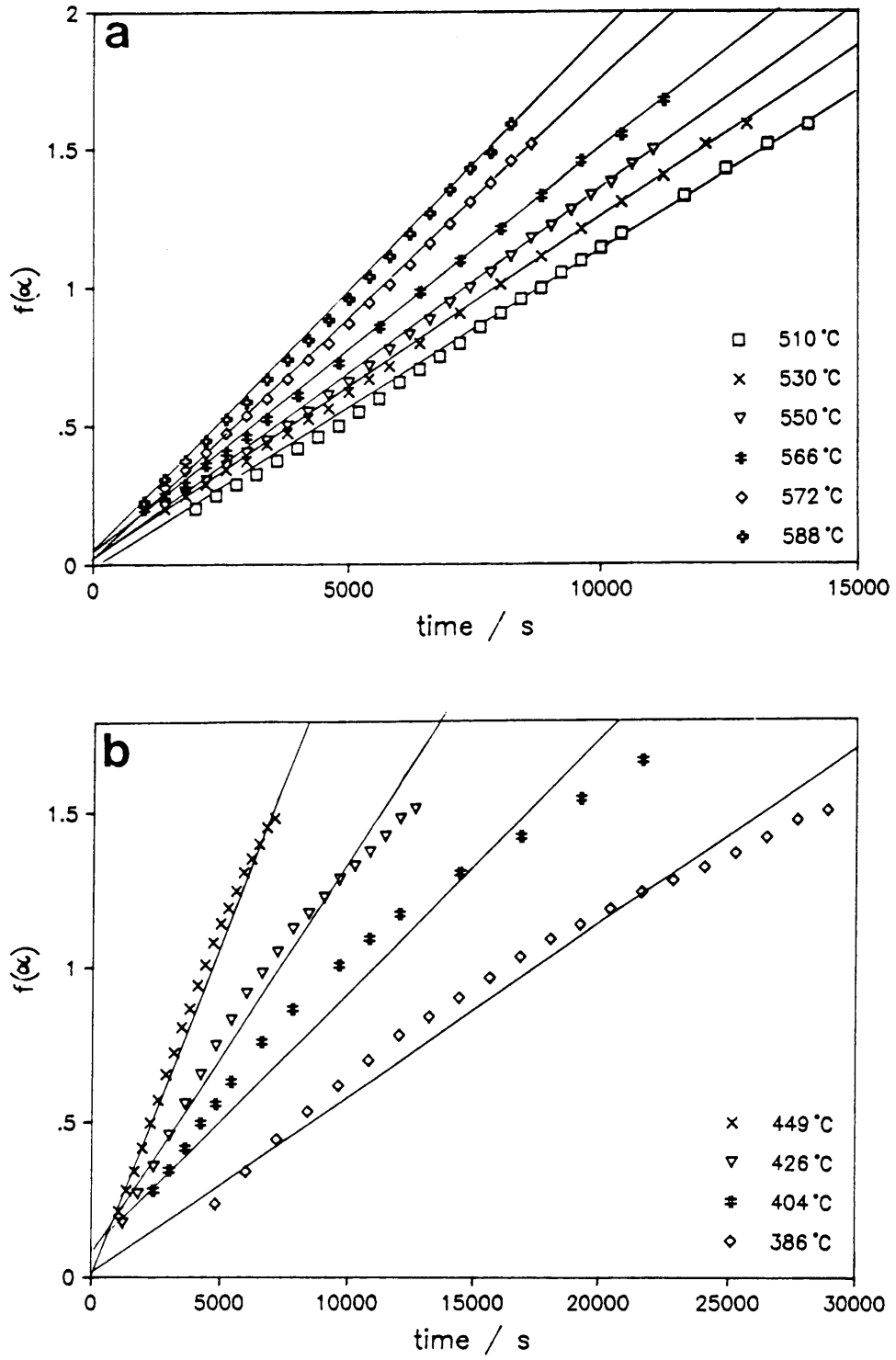

Figure 5.3. - Reduction of V_2O_5 platelets by CO : $f(\alpha) = [-\ln(1-\alpha)]^{1/2}$ versus t.

(a) 510 - 588°C (b) 386 - 449°C

Table 5.3 - The reduction of V_2O_5 platelets by H_2 : R, σ, and k for f(α) vs. t

Temp. / °C	R	σ	k / s^{-1}
386	.9906	.0513	5.115×10^{-5}
404	.9856	.0808	7.309×10^{-5}
425	.9980	.0680	1.127×10^{-4}
448	.9847	.0506	1.532×10^{-4}
468	.9993	.1077	1.816×10^{-4}
489	.9996	.0113	1.513×10^{-4}
492	.9996	.0126	1.454×10^{-4}
510	.9997	.0105	1.193×10^{-4}
533	.9997	.0110	1.242×10^{-4}
540	.9986	.0220	1.128×10^{-4}
550	.9996	.0107	1.358×10^{-4}
566	.9998	.0095	1.476×10^{-4}
572	.9996	.0106	1.173×10^{-4}
588	.9999	.0069	1.873×10^{-4}
597	.9998	.0083	2.053×10^{-4}

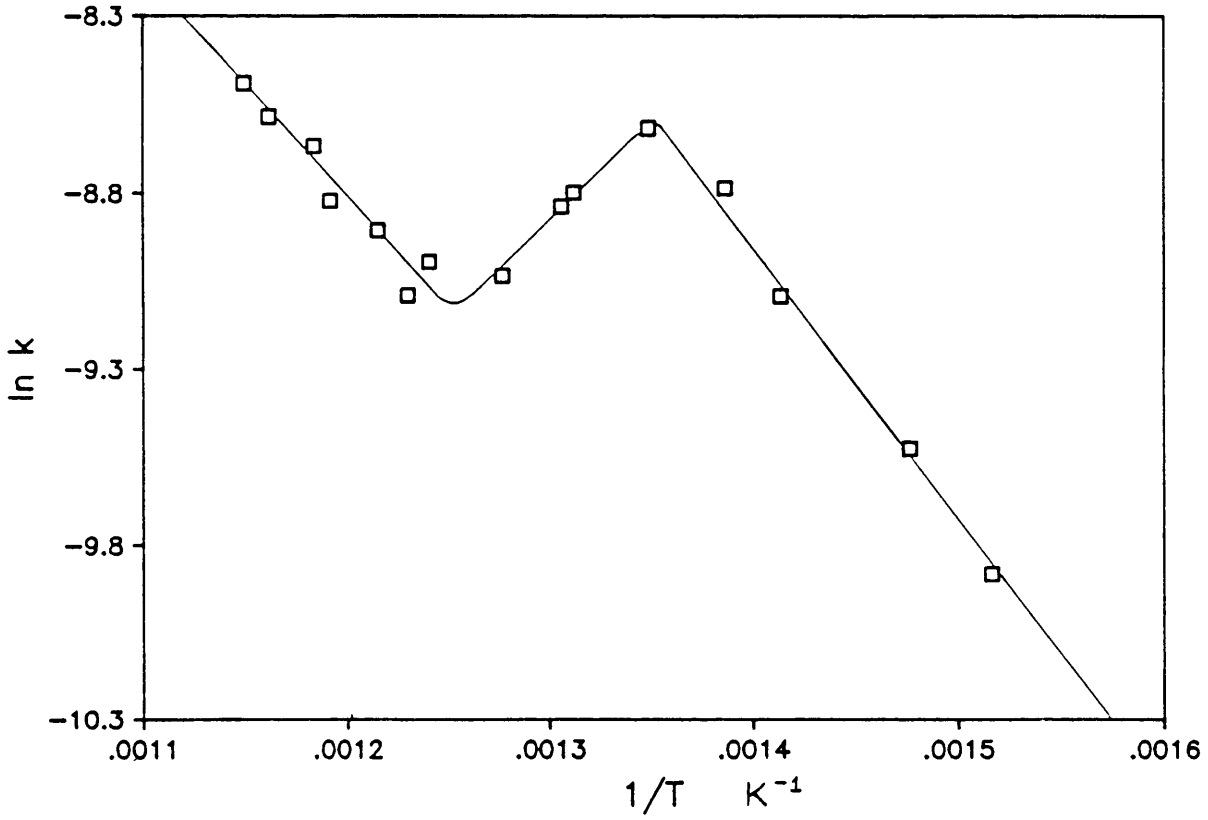

Figure 5.4. - Reduction of V_2O_5 platelets by CO : Arrhenius plot.

temperatures in the Arrhenius plot (figure 5.2) of the reduction of V_2O_5 powder by CO. The deviation from linearity observed for the powder is smaller than for the platelets because the contribution of reduction via adsorption onto V=O bonds to the overall reduction, is smaller for the powder than for the platelets, as was already discussed in detail in chapter 4.

Due to the anti-Arrhenius behaviour of the platelets, uncertainty exists as to the validity and significance of the activation energy determined from these plots. It is also difficult to decide which data points to use for the determination of the activation energy and frequency factors. The activation energies were calculated for the data points with $1/T \geq 1.35x10^{-3}$, as well as for data points with $1/T \leq 1.28x10^{-3}$. The results are summarized in table 5.4.

Table 5.4 - Activation energies calculated for the reduction of V_2O_5 platelets in CO

Data points used	R	Ea / kJ.mol^{-1}	A / s^{-1}
$1/T \leq 1.28x10^{-3}$	-0.9670	51.9	0.264
$1/T \geq 1.35x10^{-3}$	-0.9921	64.2	6.475

5.3.2. Reduction by H_2

5.3.2.1. V_2O_5 powder

Determination of the rate equation

The experimental α vs. t data for the reduction of V_2O_5 powder by H_2 (figure 4.6) were treated according to the method described in appendix C. The kinetic equation $f(\alpha) = [-\ln(1-\alpha)]^{1/4}$, gave the best description of the experimental data. This kinetic model was also found to give the best

description of the mechanism of reduction of the powder by CO (section 5.3.1.1). Table 5.5 gives the correlation coefficients, standard deviations, and rate constants which were calculated for the fit of the kinetic model to the isothermal data sets recorded in the 400°C - 520°C temperature range.

Table 5.5 - The reduction of V_2O_5 powder by H_2 : R, σ, and k for f(α) vs. t.

Temp. / °C	R	σ	k / s^{-1}
400	.9966	.0209	5.419×10^{-5}
420	.9967	.0185	7.371×10^{-5}
440	.9993	.0085	1.058×10^{-4}
460	.9994	.0082	1.601×10^{-4}
480	.9991	.0101	2.341×10^{-4}
500	.9992	.0093	3.701×10^{-4}
520	.9960	.0220	5.329×10^{-4}

The linearity of the f(α) vs. t plots for the experimental data sets are shown in figure 5.5.

Determination of the activation energy

The Arrhenius plot (figure 5.6) indicates good linear correlation of the data, with a correlation coefficient of .9998. No scatter similar to that observed for CO reduction is detected, possibly due to the smaller number of data points in the plot, or otherwise the effects which caused the deviations during CO reduction do not have a marked influence on the course of hydrogen reduction.

The activation energy calculated from the slope is 77.35 $kJ.mol^{-1}$ with a frequency factor of 51.65 s^{-1}. This value obtained for the activation energy corresponds with the activation energy of 79.79 $kJ.mol^{-1}$, calculated for the reduction of the powder by CO, using the data points with $1/T < 1.38\times10^{-3}$ (table 5.2) in the linear part of the Arrhenius plot.

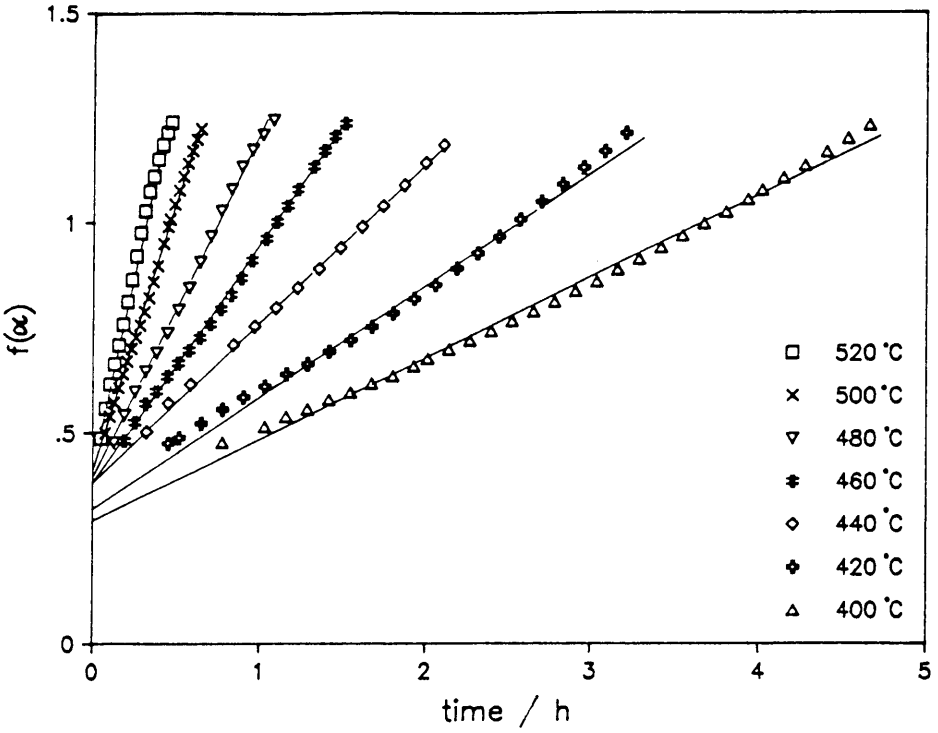

Figure 5.5. - Reduction of V_2O_5 powder by H_2 : $f(\alpha) = [-\ln(1-\alpha)]^{1/4}$

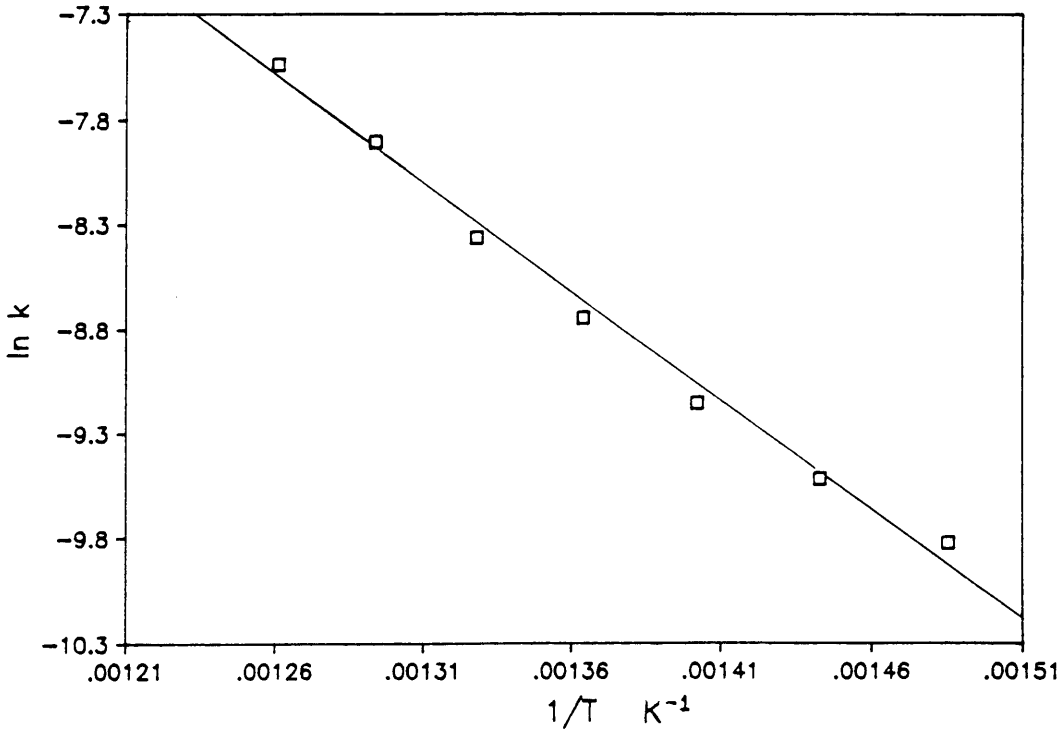

Figure 5.6. - Reduction of V_2O_5 powder by H_2 : Arrhenius plot.

If the activation energy is identified as the energy barrier that must be surmounted during transformation of the reactant into products, then the corresponding activation energies obtained for the reduction of the powder by CO and H_2 indicate that the same energy barrier must be overcome during both reduction processes.

The frequency factors, however, differ. For CO reduction, A = 28.47 s^{-1} while for reduction by H_2, A = 51.65 s^{-1}.

According to literature [38], the frequency factor, A, is identified with the frequency of occurrence of the reaction configuration, first identified as a molecular encounter (a collision) and later as a specific vibration in the reaction co-ordinate. If this interpretation for A is applied to the systems under consideration, then the values of A obtained give an indication that in the temperature interval studied, the rate of reduction using H_2 is about twice the rate of reduction using CO. The exact reason for this difference has not yet been ascertained.

5.3.2.2. V_2O_5 platelets

Determination of the rate equation

The kinetics of isothermal reduction of V_2O_5 platelets using H_2 were found to be significantly faster than when CO was used. It was observed, that in the temperature range studied (380 - 570°C), a certain period of time elapsed prior to any observable mass loss due to reduction by CO, after the isothermal temperature was reached. This indicates a period of slow nucleation. On the other hand, when H_2 was used, reduction commenced immediately when the furnace reached the isothermal temperature. In some instances, at higher temperatures, reduction had already occurred to a noticeable extent before the

isothermal temperature was reached. Consequently, the induction periods were shorter and liable to be more influenced by experimental error than was the case with the CO reduction.

The Avrami-Erofe'ev equation, $f(\alpha) = [-\ln(1-\alpha)]$ with $n = 1$, gave the best fit to the experimental data. Table 5.6 gives the correlation coefficients, standard deviations and rate constants obtained for the fit.

Table 5.6 - The reduction of V_2O_5 platelets by H_2 : R, σ and k for $f(\alpha)$ vs. t

Temp. / °C	R	σ	$k/10^{-4}$ / s^{-1}
400	.9958	.0640	2.563
420	.9998	.0124	2.762
430	.9999	.0095	3.317
440	.9996	.0180	3.703
450	.9999	.0073	3.898
460	.9988	.0318	4.873
465	.9996	.0200	3.939
470	.9995	.0228	4.118
480	.9967	.0560	4.774
500	.9929	.0820	5.682
520	.9952	.0713	6.025

The linearities of the $f(\alpha)$ vs. t plots are shown in figure 5.7.

Determination of the activation energy

The Arrhenius plot (figure 5.8) does not show good linear correlation of the data. Although acute anti-Arrhenius behaviour such as in figure 5.4 is not observed, the data points are scattered. This could either be due to the same effect that was responsible for the behaviour in figure 5.4, seemingly to a lesser extent, or simply to errors introduced by the incorrect recording of the TG-curves. In the temperature range studied, nucleation was almost instantaneous and some reduction had already occurred by the time the furnace reached the appropriate temperature, causing a shorter induction period to be recorded.

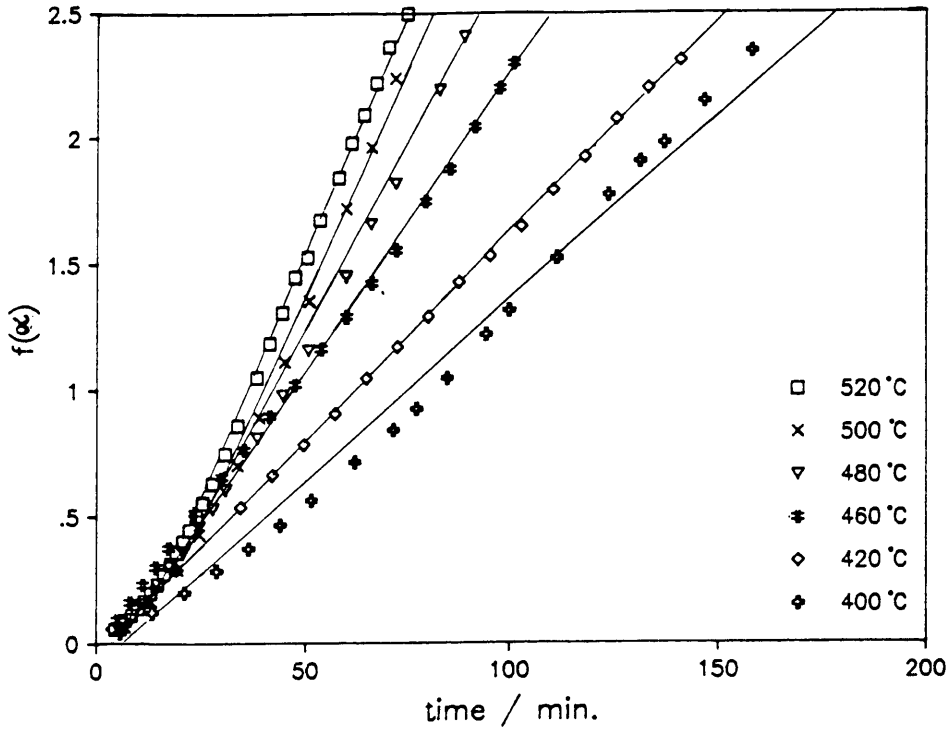

Figure 5.7. - Reduction of V_2O_5 platelets by H_2: $f(\alpha) = [-\ln(1-\alpha)]$

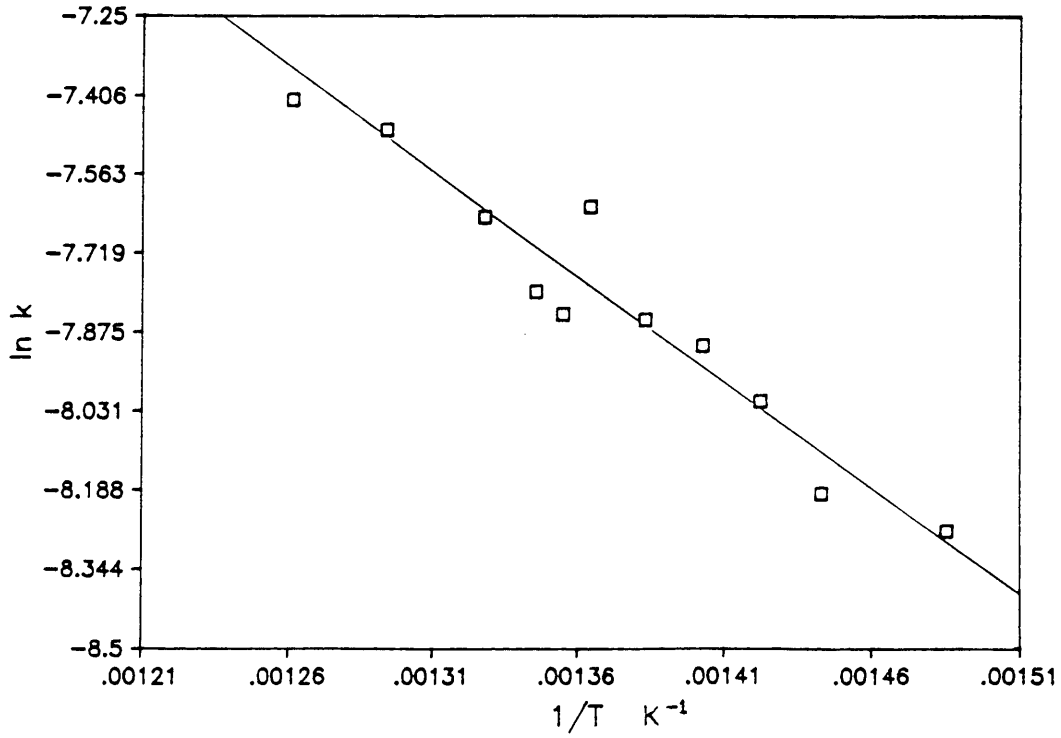

Figure 5.8. - Reduction of V_2O_5 platelets by H_2 : Arrhenius plot.

Table 5.7 gives the activation energies and frequency factors calculated from the Arrhenius plot.

Table 5.7 - Activation energies calculated for the reduction of V_2O_5 platelets by H_2

Data points used	Ea / kJ.mol^{-1}	A / s^{-1}	R
$1/T \geq 1.36\times10^{-3}$	43.26	0.547	-0.97
$1/T < 1.36\times10^{-3}$	39.22	0.241	-0.97
all	33.23	0.096	-0.96

These values are much smaller than all the other activation energies calculated in this study. The reliability of these values is doubted due to possible experimental errors.

5.3.3. Microscopy studies

All the reduction processes of V_2O_5, independent of morphology or reducing atmosphere, were found to be described by Avrami-Erofe'ev equations which describe a process of nucleation and growth. The sites of nucleation are described as possessing locally enhanced reactivity.

Although much research has been done on the oxidation of CO and H_2 on V_2O_5 catalysts, the active sites for reaction have been a subject of controversy [32-34]. It has generally been found that the (010) plane of the V_2O_5 lattice exhibits a high activity for CO and H_2 oxidation, but different opinions exist as to the exact active sites.

Mori and co-workers [32] stated that for CO oxidation, the activity of surface defects such as steps, kinks and vacancies, is much higher than that of the surface V=O species in the smooth (010) face of V_2O_5. As regards H_2 oxidation [34], they stated that the number of V=O species on the catalyst determines the activity of the catalyst. Baiker and co-workers [33] found that

at higher temperatures (600°C), the vanadyl groups which are predominantly exposed on the (010) faces of V_2O_5, contribute most to the activity of CO oxidation. They stated that at lower temperatures (400°C), the most active sites are the lattice defects which exhibit a lower activation energy than the V=O species.

According to the Avrami-Erofe'ev theory, the value of the exponent n is related to the number of steps involved in nucleus formation and the number of dimensions in which the nuclei grow. In order to make any such conclusions regarding nucleation during the reduction of V_2O_5, further experimental evidence is required apart from the kinetic calculations. For this reason and to examine the controversial site where nucleation starts, optical microscopy and SEM were utilized.

V_2O_5 crystals were heated in CO and H_2 atmospheres up to temperatures of about 300 - 350°C where no noticeable mass losses had occurred in the TG-curves. However, when the crystals were removed from the furnace, a slight darkening of their usual orange colour was observed.

Optical microsopy of the darkened crystals revealed a colour change to occur along steps, kinks and dislocations in the (010) crystal plane. Photographs of these crystals are shown in figure 5.9(b), from which it seems that reduction starts preferably at these defects. The same tendency was observed for crystals heated in CO and in H_2.

SEM studies of the (010) crystal plane of the slightly darkened V_2O_5 platelets, indicated the presence of the structures shown in figure 5.10(a). These structures represent an advanced stage of nuclei growth with the formation of cracks due to shear and lattice collapse. This proves that reduction already starts at temperatures below 350°C although it is not

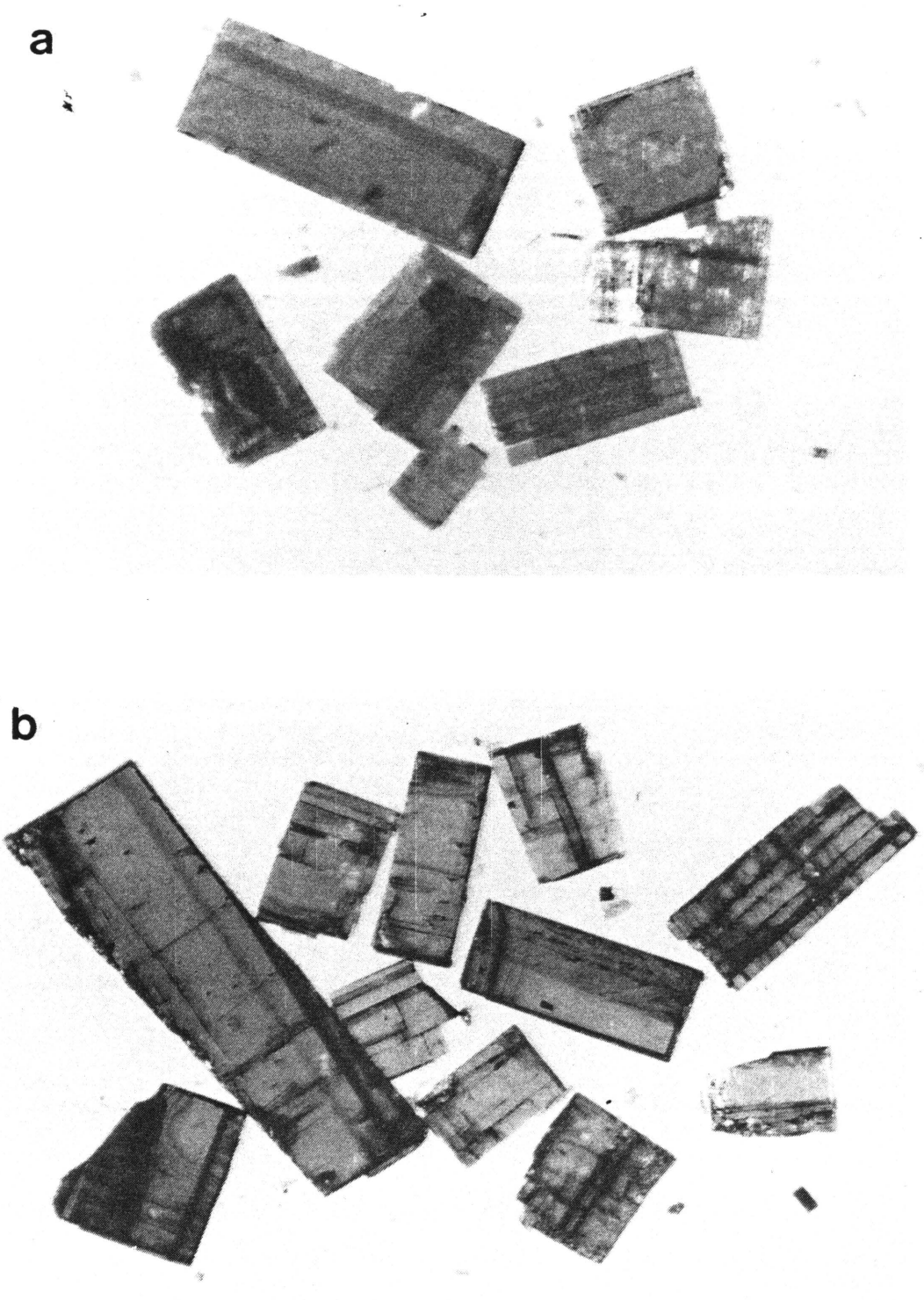

Figure 5.9. - Microscope photographs of V_2O_5 crystals × 50

(a) before heating,

(b) after heating in CO or H_2 to 300 - 400°C.

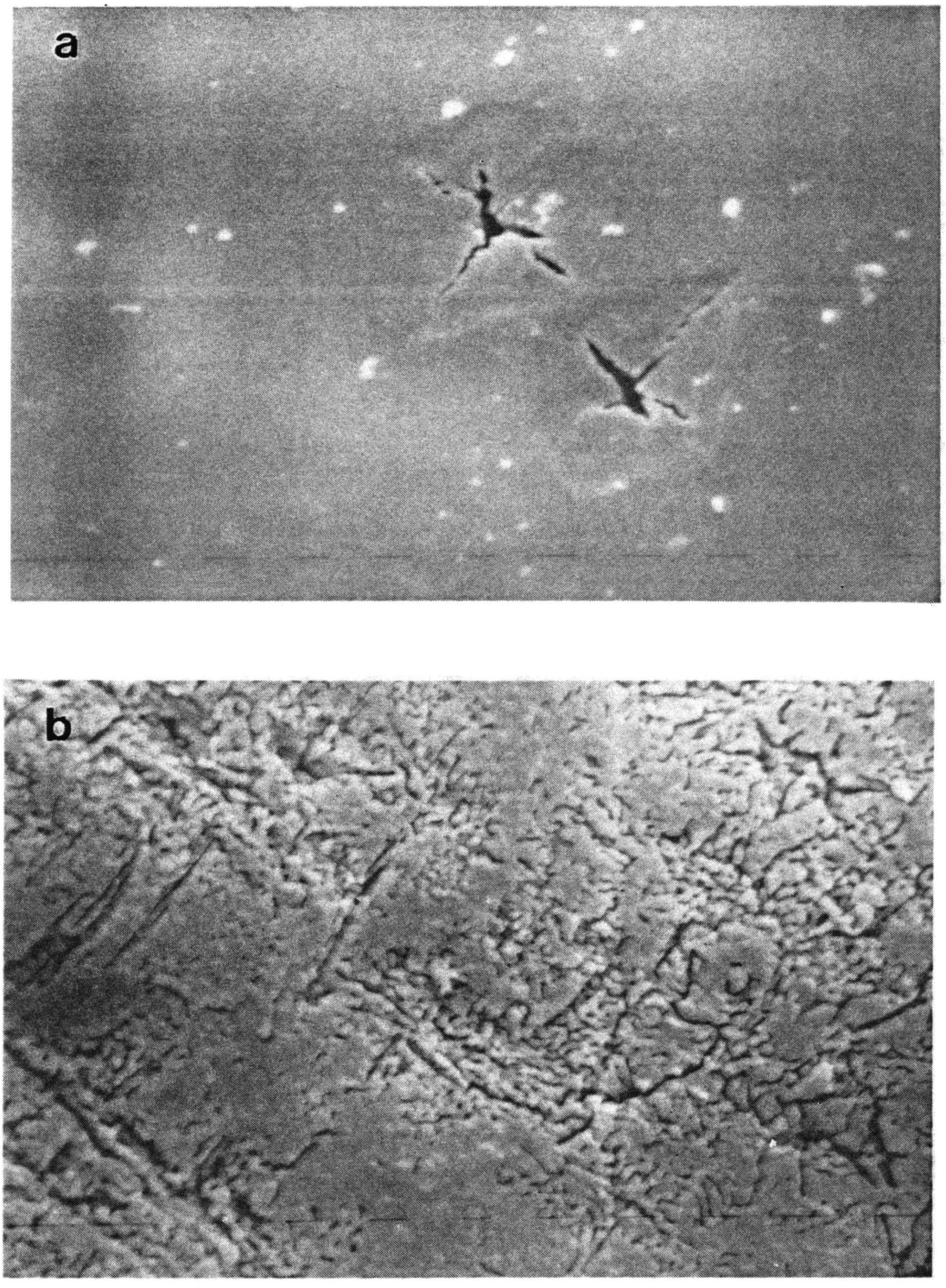

Figure 5.10. - Electron micrographs of V_2O_5 crystals × 5000

(a) after heating to 300 - 400°C in CO or H_2,

(b) after complete reduction.

visible in the TG-curves. The induction periods of the isothermal TG-curves used for the kinetic calculations do not represent the true nucleation and growth period of the reaction. The exact site of nucleation could not be determined from these studies because by the time that a nucleus has developed sufficiently to be examined by low resolution SEM, it has entered the growth phase. Reduction could have started at a point defect in the (010) plane such as an oxygen vacancy, but the possibility also exists that a V=O specie in the (010) face could have been the active site. The same tendency was again observed for the crystals heated in CO and in H_2. Figure 5.10(b) shows the roughened appearance of the (010) plane after reduction has been completed.

Unfortunately, no definite conclusions can be made regarding the dimensions of growth of the nuclei, judging from figure 5.10(a), although it seems that two- or three-dimensional growth would be the most likely to result in such a structure. In his studies on the reduction kinetics of mixed oxides (NiO - V_2O_5) with hydrogen, Pospišil [22] found that the reduction kinetics can be expressed by the Erofe'ev equation, $\alpha = 1\text{-}\exp[-kt^n]$. In accordance with a morphological examination of the partially reduced samples, he found that n=2 gives evidence for two-dimensional growth of the nuclei.

A further study of the reduction mechanism was done by terminating the reduction of V_2O_5 platelets when a fractional mass loss of 0.5 was reached. The crystals were then polished to reveal a cross-section of the partly reduced crystals. Figures 5.11(a) and (b) show electron micrographs of such a cross-sectioned crystal in which a zone of reduced oxide can be seen to form from the surfaces of the crystal as well as from cracks through which gaseous products can escape and reducing gas can enter. It is also clear that reduction is not confined to a specific crystal face, but apparently proceeds equally from all the surfaces visible in the electron micrograph. Most probably the cleavage

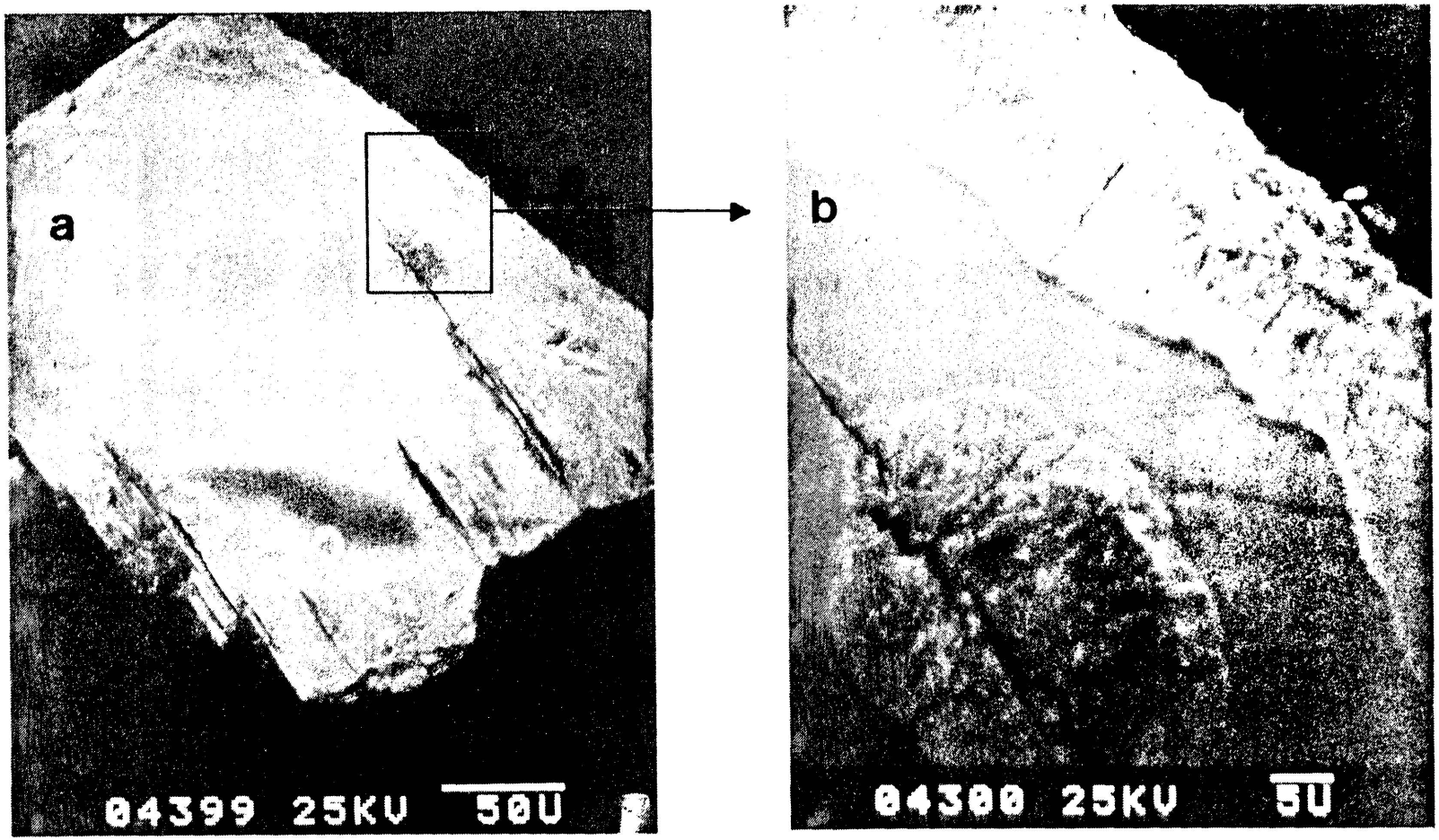

Figure 5.11. - Electron micrographs, showing a cross-section of a partly reduced V_2O_5 crystal (α = 0.5).

of the crystal has occurred along the (010) plane (which is an easy cleavage plane), so that the reaction interface proceeding from this plane, is not visible from the electron micrograph. It is suspected that reduction would proceed faster from the (010) plane, for the following reason: Assuming that reduction starts at the terminal vanadyl oxygens which are located in the (010) plane, it can be understood that reduction would proceed faster from this plane.

5.4 DISCUSSION

5.4.1. Problems encountered and their implications on the kinetic studies

It is clear that the kinetics of reduction is complex. It was found to change with temperature and is therefore probably determined by more than one mechanism, as was discussed in chapter 4. It was proposed that two mechanisms contribute towards the overall reduction process, with the extent of contribution of each mechanism depending on the grain morphology and temperature.

Although all the reduction processes of V_2O_5 can quantitatively be described by Avrami-Erofe'ev equations (equation 5.3), the value of the parameter n in the equation was found to depend on the morphology of the sample. For reduction of the V_2O_5 powder, long induction periods were observed (figures 4.1 and 4.6) and the value of n in equation 5.3 was found to be four for both reduction in CO and H_2. On the other hand, shorter induction periods were observed for the reduction of the platelets (figures 4.2 and 4.7) with the parameter $n=2$ for reduction by CO and $n=1$ for reduction by H_2. Various studies [38] have confirmed that the parameter n is sensitive to particle dimensions and shape. In addition to this, it is also shown that errors in t_0, the delay time (equation 5.3), exert an important control over the

magnitude of n. These errors arise from inaccurate measurements of the true induction period due to very slow processes preceding the main reaction.

Gai [17] used a gas-reaction cell in a high voltage electron microscope to study the reduction of V_2O_5 in H_2, CO and C_2H_4, and observed that reduction already started at very low temperatures of ~80 - 100°C. This result gives reason to suspect that slow reduction processes have already started at much lower temperatures than the temperature range (±380 - 580°C) covered in the present study, introducing errors into the measured induction periods and subsequently influencing the value of n. This temperature range was studied since reduction was extremely slow and did not proceed at a measureable rate at temperatures below ±380°C.

5.4.2. Reduction kinetics : CO versus H_2

The rate of reduction by H_2 was throughout this study markedly faster than that of reduction by CO, at the same temperature, although the same kinetic model apparently applies in both cases. The exact cause for the faster reduction rate when using H_2 is still uncertain.

A possible explanation might lie in the different mechanisms of solid-gas interaction of the V_2O_5-CO and V_2O_5-H_2 systems, that were proposed in section 4.4.1. Reduction by H_2 involves the dissociation of the hydrogen bond and the formation of V-O-H groups while reduction by CO occurs through the formation of V-O-C-O groups. It is possible that the hydroxyl groups that form on the V_2O_5 surface during H_2 reduction have a larger destabilizing effect on the V_2O_5 lattice than the V-O-C-O groups, and could serve as active adsorption sites for further chemisorption of H_2. The larger destabilization of the V-O bonds could lead to a faster reduction rate.

Another possible contributing factor to the faster reduction observed with hydrogen concerns the H_2 and CO molecules. Considering the smaller size and higher mobility of the H_2-molecule as compared to that of the CO-molecule, it can be appreciated that H_2 would be prone to faster and better diffusion than CO. The same argument would apply to the products of reduction, i.e. H_2O and CO_2. It is not known to what extent this factor could influence the reduction rate.

It is also known that hydrogen gas is catalytically dissociated into atoms by platinum and other metals [39]. It has further been found by Batley and co-workers [40] that V_2O_5 can be catalytically reduced by H_2 using a separated platinum catalyst at temperatures above 350 °C. They postulated that the H_2 gas is dissociated on the platinum surface after which the atomic hydrogen diffuses through the gas phase to the oxide surface where reduction occurs.

If this is true, then the possibility exists that the H_2 reduction experiments done in the present study could have been catalyzed by the platinum sample holders which were used. However, in studies performed by other workers [4], alumina crucibles were used and it was reported that the hydrogen reduction rate was still higher than CO reduction. It is possible that the reduction in the present study was catalyzed by the platinum sample holders to a certain extent, increasing the H_2 reduction rate (which is higher than the CO reduction rate even if uncatalyzed reduction occurs), leading to a deceptively high reduction rate. This possibility needs further investigation.

The results obtained from the kinetic study on the reduction of V_2O_5 seem disappointing in the sense that the different rates of CO and H_2 reduction could not be successfully quantified. Neither can any definite conclusions be made regarding the activation energies, frequency factors and the value and

significance of the parameter n in equation 5.3.

5.4.3. The mechanism of the reduction

The Avrami-Erofe'ev kinetic model was found to give a general description of the mechanism of reduction, starting as a nucleation process at sites of higher activity in the crystal (represented by the induction period), followed by growth of the nuclei. Microscopy studies supported this model and showed that reduction starts at defects such as kinks, steps and dislocations in the (010) plane.

Extensive studies have been conducted by Fiermans et al. [6] on the defect structure of V_2O_5 and lower oxides. They concluded that the V=O bonds in the vicinity of distorted regions such as defects, are less tightly bound than those in the unstrained lattice due to steric hindrance which distorts the nature of the bond. This effect would cause the V=O bonds in the vicinity of steps, kinks and dislocations to be more easily reduced. It is stated that reduction of V_2O_5 occurs by removal of the vanadyl oxygen species in the (010) plane, preferably those that are located in the vicinity of defects.

The kinetic model further implies that after coverage of the surface, the reaction interface proceeds inwards to the centre of the particle, resembling a contracting volume mechanism. A contracting reaction interface was observed by SEM in a cross-sectioned, partly reduced crystal.

The kinetic calculations were thus not totally meaningless with regard to the mechanism of reduction, although further studies are required to refine the kinetic parameters and to determine their physical and/or empirical significance.

CHAPTER 6
IMPORTANT INDUSTRIAL PARAMETERS

6.1. Introduction

In the process of going from laboratory reduction experiments to larger scale industrial reduction of V_2O_5, certain experimental conditions which exert a significant influence on the reduction rate change and have to be adapted and optimized to obtain the best possible results. Although a detailed study was not conducted of such parameters, some of them have emerged from the fundamental studies and will be discussed briefly in this chapter.

6.2. Sample morphology

It is clear from the results of the previous chapters that the reduction of V_2O_5 is a structure-sensitive process which depends largely on the morphology of the sample. In the experiments carried out, the two different types of V_2O_5 used showed different reduction behaviour.

The question arises as to how the morphology of the V_2O_5 flakes (the product of the industrial roast-leach process) would influence the course of reduction. The flakes are also obtained from molten V_2O_5, similar to the V_2O_5 platelets prepared in this study, with the difference that the flakes are prepared by quenching the V_2O_5 melt on a cooling wheel, while the platelets were formed through very slow cooling of the melt. The flakes have larger dimensions (in the order of centimetres) and do not consist of distinguishable platelike crystals. They are also darker in colour. By crushing the flakes, however, similar platelike crystals were obtained. These crystals were sieved to fall in the same ranges as the platelets, i. e. 75 - 125μm, 125 - 250μm and >250μm. They were then reduced, using CO, to compare their reduction

patterns with that of the platelets. The results are shown in figures 6.1(a) and (b) at two different reduction temperatures.

The reduction curves of the flakes, similar to those of the platelets, are s-shaped, indicating that the same reduction mechanism applies in both cases. There exists, however, slight differences in the TG-curves. The induction periods of the flakes are shorter than those of the platelets while the decay periods are longer. The shorter induction periods probably indicate a faster nucleation and growth process while the longer decay periods are caused by a larger inhibiting effect of diffusion in the flakes.

6.3.Sample purity

It has been mentioned that the V_2O_5 flakes have a darker colour than the V_2O_5 platelets. This is probably due to impurities which were present in the initial AMV sample and which have consequently been included in the flakes. Microprobe analyses indicated that traces of phosphorus, sulphur, alumina, silicon and iron are present in the flakes. According to Rohrmann [2], a typical analysis of fused vanadium pentoxide flakes is as follows :

V_2O_5 : 95.5%

V_2O_4 : 3.5%

Na_2O : 0.25%

Fe : 0.15%

S : 0.006%

P : 0.002%

Colpaert and co-workers [41] studied the surface reaction that occurs through thermal induced oxygen loss in V_2O_5 single crystals. They found that the surface reaction of impure V_2O_5 crystals was faster than that of clean crystals

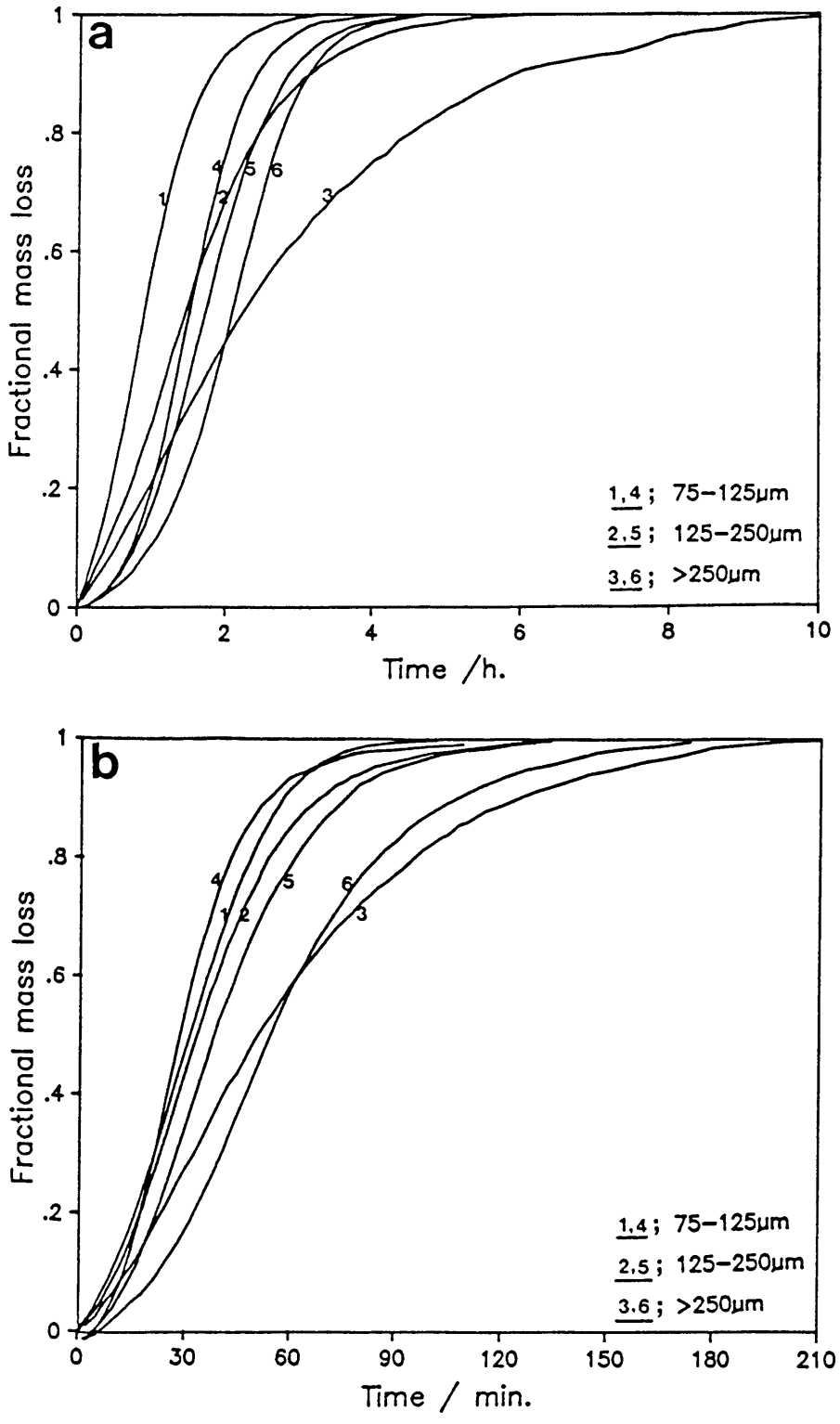

Figure 6.1. - The reduction of V_2O_5 flakes (curves 1, 2, and 3) and platelets (curves 4, 5, and 6) by CO at (a) 400°C and (b) 450°C.

and concluded that during transition of V_2O_5 to V_6O_{13}, the surface reaction was greatly enhanced by the interaction of contaminating molecules at the surface with lattice oxygen.

In view of these results, it is possible that the impurities which are present in the V_2O_5 flakes are responsible for the faster surface reaction than that of the platelets, as indicated by the shorter induction periods in the TG-curves of the flakes as compared to that of the platelets (figures 6.1(a) and (b)).

The flakes probably crystalize with a larger degree of defectivity than the platelets, due to the faster quenching process employed in the production process. The presence of these defects in the crystal structure of the flakes could also contribute to a higher reducibility.

The longer decay periods of the flakes can probably be ascribed to the inhibition of diffusion by the impurities during the reduction. The effect of impurities on the reduction rate of V_2O_5 requires further investigation.

6.4. Grain size

From figures 6.1(a) and (b) it is clear that a decrease in the size of the V_2O_5 grains leads to a higher reduction rate. This can be explained by considering the diffusional processes that occur during reduction, i.e. the diffusion of the reducing gas to the reaction interface and the diffusion of product gases from the reaction interface to the surface. These processes would be hampered by larger crystal sizes, causing a decrease in reduction rate. This effect would be much more pronounced in industrial size flakes. The reduction rate, and probably also the degree of conversion of the starting material, would definitely benefit by a decrease in the grain size of the starting material by means of mechanical grinding or crushing.

6.5. CO versus H_2 as reducing gas

From the reduction experiments conducted, it is evident that a faster reduction rate is obtained when H_2, rather than CO, is used as reducing gas, although complete conversion of V_2O_5 to V_2O_3 is possible by using either of these two gases. When CO is used, it is important to take into account the possible deposition of carbon, as was found to occur during reduction experiments conducted in this study (section 4.3.2). The presence of carbon in the V_2O_3 product and in the final vanadium metal will have a significant effect on the properties of the steel produced, as was discussed in section 1.2.

6.6. Gas purity

In this study, high purity gases were used for the reduction experiments. In industry, however, technical grade gases with certain impurity levels are used, and the effects of these contained impurities on the reduction behaviour have to be considered in order to obtain optimum reaction conditions.

Unfortunately, a detailed study of the effects of these reducing gas impurities was not conducted although some preliminary reduction experiments with CO/CO_2 gas mixtures were done. The isothermal TG-curves of the reduction of V_2O_5 powder at 500°C with various CO/CO_2 gas mixtures can be found in figure 6.2 from which it can be seen that an increase in the CO_2 content of the CO reducing gas leads to a decrease in reduction rate. With all the mixtures, total conversion of V_2O_5 to V_2O_3 was achieved at this temperature.

When the thermodynamics of V_2O_5 reduction with CO/CO_2 mixtures is considered (figures 6.3(a) to (c)), it can be seen that only at very high partial pressures of CO_2, total conversion of V_2O_5 to V_2O_3 becomes unfavourable.

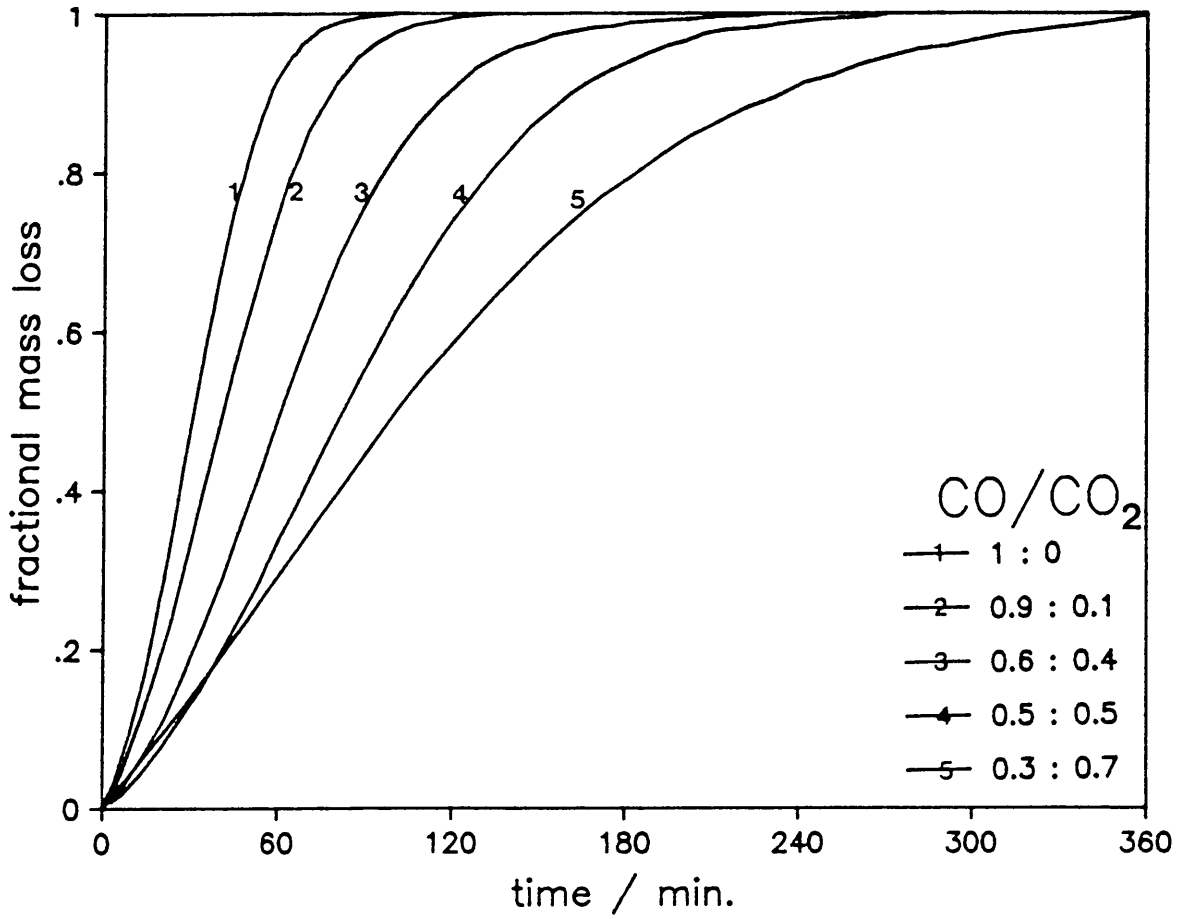

Figure 6.2 - The reduction of V_2O_5 platelets (75-125μm) by CO/CO_2 mixtures at 500°C.

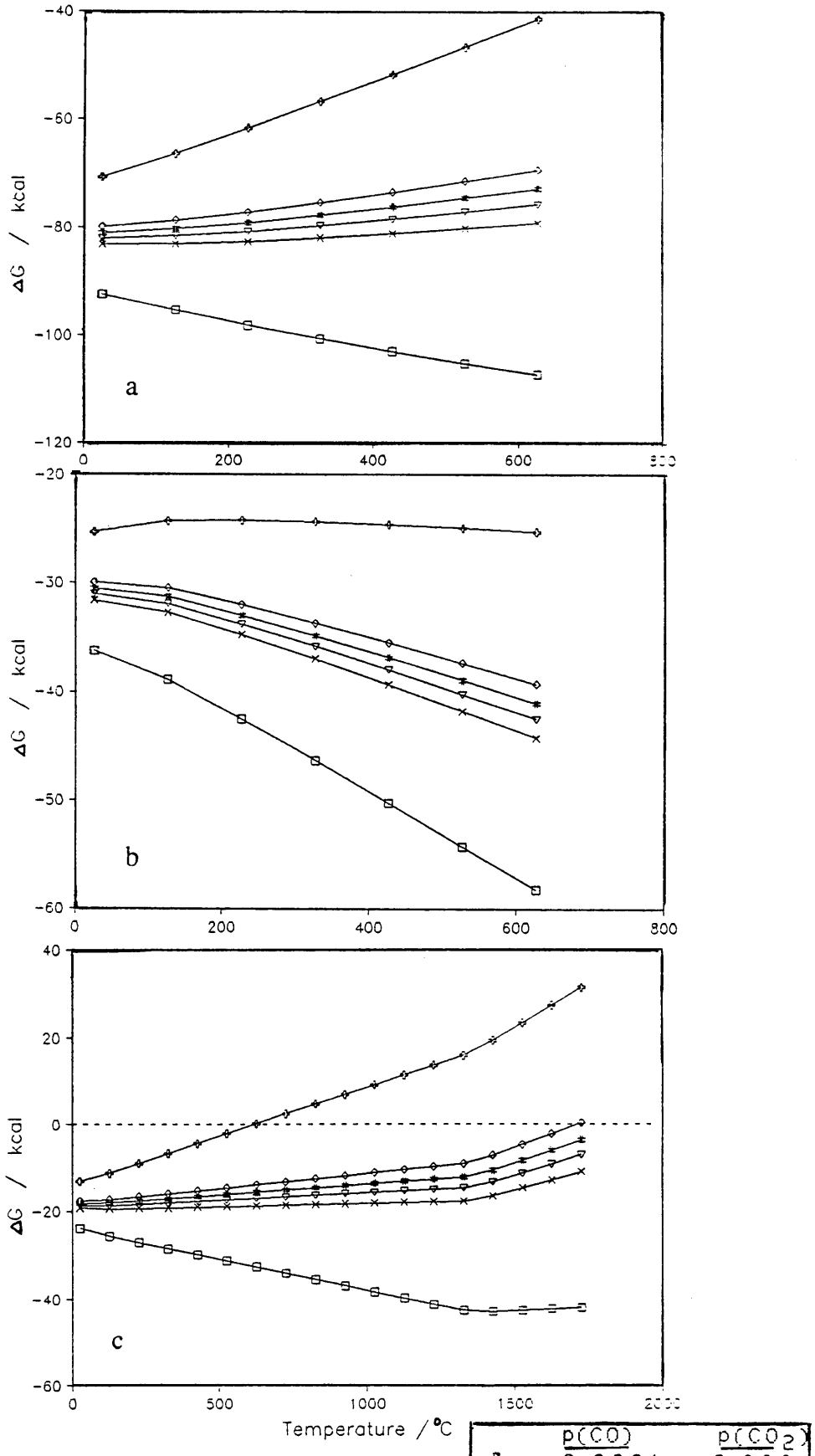

Figure 6.3 - ΔG vs. temperature for the reduction of
(a) V_2O_5 to V_6O_{13},
(b) V_6O_{13} to VO_2,
(c) VO_2 to V_2O_3, by CO/CO_2 mixtures.

At these high partial pressures of CO_2, reduction is only favourable up to the intermediate V_2O_4.

It is possible that factors such as large grain sizes could serve to inhibit the reduction to such an extent that total conversion to V_2O_3 becomes unfavourable, even at partial pressures of CO_2 lower than that predicted by thermodynamics.

Thermodynamic calculations were also done for the reduction of V_2O_5 by various H_2/H_2O partial pressure ratios. The results are shown in figures 6.4(a) to (c) which predict that an increase in the partial pressure of water in the reducing gas would lead to an decrease in the reduction rate. In agreement with these predictions, Bosch et al. [23] found that the presence of water had a considerable effect on their temperature programmed reduction (TPR) profiles, causing the reduction to be completed at higher temperatures. Maciejewski et al. [24] also studied the influence of a lowering of the hydrogen concentration on the reduction behaviour by diluting the hydrogen stream with nitrogen. They found that the reduction rate of the diluted system was considerably lower than that of the undiluted system. The onset of reduction was also found to be shifted to higher temperatures.

From these findings it can be expected that the employment of technical grade reduction gases on an industrial scale would lead to lower reduction rates than those achieved with high purity gases. The extent to which these impurities would influence the degree of conversion requires further investigation.

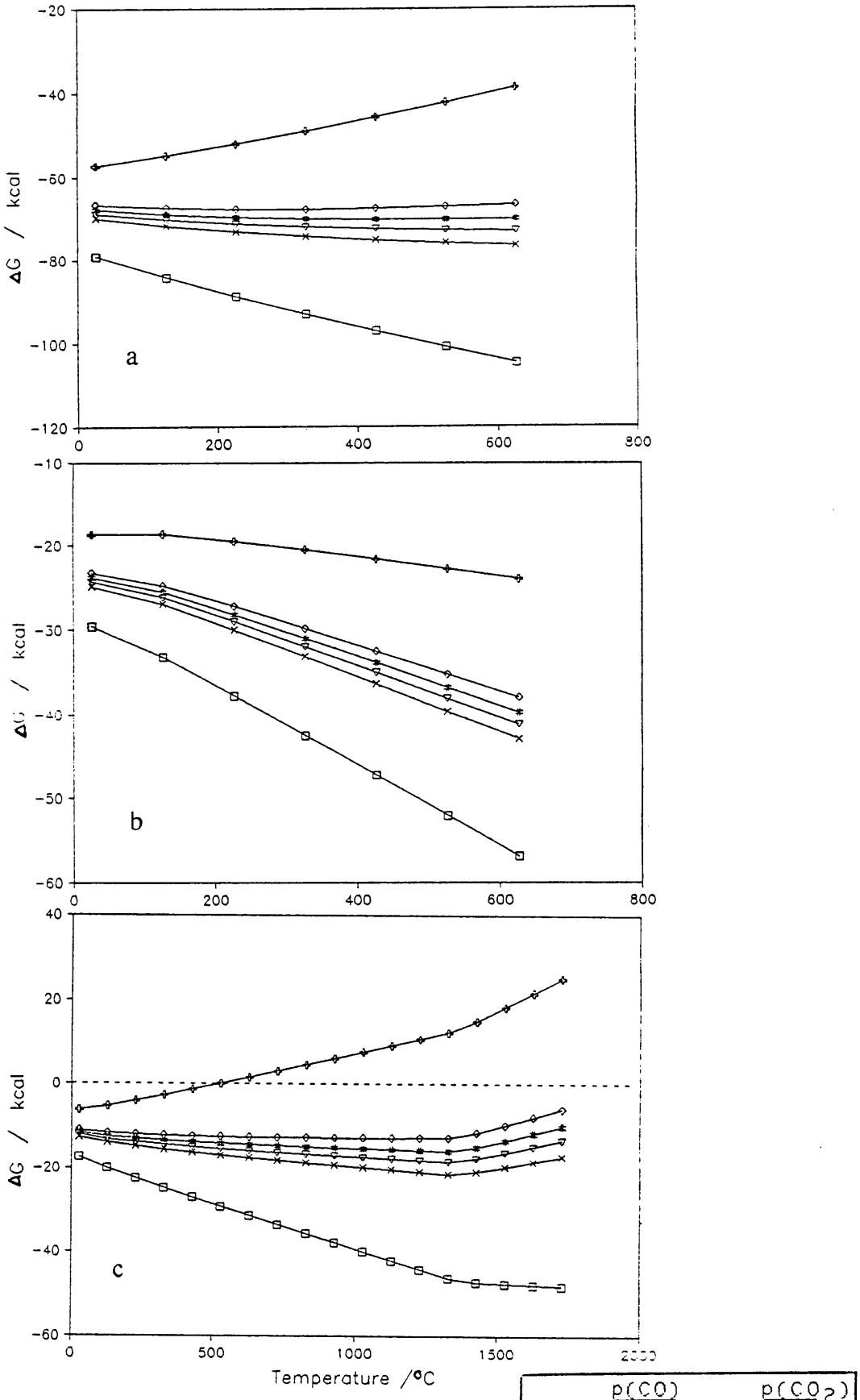

Figure 6.4 - ΔG vs. temperature for the reduction of
(a) V_2O_5 to V_6O_{13},
(b) V_6O_{13} to VO_2,
(c) VO_2 to V_2O_3, by H_2/H_2O mixtures.

6.7. Reduction temperature

When finding the optimum reduction temperature, the melting points of the oxides under consideration (given in table 6.1) should be taken into account.

Table 6.1. - Melting points of vanadium oxides.

oxide	melting point / °C
V_2O_5	±680
V_6O_{13}	708
VO_2	1967
V_2O_3	1970

Using reduction temperatures close to and higher than the melting point of V_2O_5 would cause considerable loss of the oxide through volatilization. Starting at temperatures where V_2O_5 is still in the solid form and increasing the reduction temperature, would lead to an increase in the reduction rate, but at temperatures close to the melting point a decrease in reduction rate would be observed. This is due to a decrease in surface area of the solid and thus in the solid-gas contact area through sintering and/or melting of the oxide. Raising the temperature further would cause the reduction rate to increase again, but considerable volatilization of the oxide would then occur, making these higher temperatures unsuitable for industrial application.

Reduction of V_2O_5 in the liquid state would also complicate recovery of the product which would be sticking to the sides of the sample holder, causing further losses.

Another factor that has been mentioned [4] is the formation of a solid crust of a lower oxide (VO_2 or V_2O_3) on the molten V_2O_5, since these oxides have higher melting points (table 6.1) than V_2O_5. This effect would serve to inhibit diffusion and would consequently lead to a decrease in the reduction rate.

From these aspects it seems that the optimum reduction temperature would be ±600°C where V_2O_5 is still in the solid form and no significant volatilization occurs.

CHAPTER 7
THE REDUCTION OF AMMONIUM METAVANADATE

7.1. INTRODUCTION

The main reason for the interest in the reduction of ammonium metavanadate (AMV) was briefly outlined in chapter 1. During preliminary studies done at Mintek [4] it was found that V_2O_3 is formed at much lower temperatures when AMV instead of V_2O_5 is used as starting material for reduction. It was also found that CO-reduction leads to a higher degree of conversion of AMV to V_2O_3 than H_2-reduction. This finding is unexpected since the reverse tendency was observed when V_2O_5 was used as starting material.

It is known that the actual transition of AMV to V_2O_3 is composed of two different processes. The first part does not involve a reduction process, but is a thermal decomposition reaction whereby AMV gives off ammonia and water to yield V_2O_5. The second part involves reduction of the freshly formed V_2O_5 to V_2O_3 by the prevailing CO or H_2 atmosphere.

If it is true that V_2O_5 is formed as an intermediate of decomposition and is reduced in situ, why would reduction proceed at lower temperatures than when V_2O_5 is used as starting material? To answer this question, a fundamental study of the processes involved in decomposition of AMV was carried out.

Several studies have been done in the past on the thermal decomposition of AMV [42-50], and the decomposition is well-known to proceed as follows :

$$3\ \underset{\text{AMV}}{(NH_4)_2O.V_2O_5} \longrightarrow \underset{\text{AHV}}{(NH_4)_2O.3V_2O_5} + 2\ H_2O + NH_3 \qquad \{R7.1\}$$

$$\underset{\text{AHV}}{(NH_4)_2O.3V_2O_5} \longrightarrow 3\ V_2O_5 + H_2O + 2\ NH_3 \qquad \{R7.2\}$$

AMV : ammonium metavanadate
AHV : ammonium hexavanadate

There still exists uncertainties as to the number of stable intermediates which form during the course of decomposition of AMV to AHV (reaction 7.1). Nevertheless, the present study is mainly concerned with the second step (reaction 7.2), i.e. the transition of AHV to V_2O_5, as well as further reduction of V_2O_5.

Previous studies have also brought to light that there exists a high degree of structural control on the course of decomposition of AMV [42].

The structure of AMV consists of zig-zag chains of distorted tetrahedra of oxygen about vanadium. These tetrahedra are linked by their corners to form chains. The NH_4^+ ions of AMV are then located between these V–O chains so that each NH_4^+ ion is irregularly surrounded by ten O-atoms.

The decomposition of AMV involves scission of the V–O chains in the AMV structure (accompanied by a simultaneous evolution of gaseous ammonia and water) with a subsequent rearrangement and cross-linking of V–O units to form AHV. Further decomposition of AHV to V_2O_5 is a similar but less ordered process.

It has also been shown [43] that the surrounding atmosphere has a marked influence on the stoichiometry and structural order of the intermediates of decomposition, as well as on the final V_2O_5 product [45, 46, 48].

It has generally been found that decomposition in an oxidizing atmosphere led to a stoichiometric V_2O_5 product, while in the absence of oxygen (in inert atmospheres) a V_2O_{5-x} product with an average vanadium valence of less than five, was obtained.

Taniguchi et al. [45] ascribed this phenomenon to catalytic decomposition of gaseous ammonia (evolved during decomposition) on the surface of V_2O_5, causing slight reduction. Trau [51] and Sas et al. [46] also mentioned the possibility of reduction of V_2O_5 by gaseous ammonia. Dziembaj and co-workers [48] proposed that the following redox processes occur :

$$2\,NH_4^+(s) + O^{2-}(s) \rightleftharpoons 2\,NH_3(g) + H_2O(g) \qquad \{R7.3\}$$

$$2\,NH_4^+(s) + O^{2-}(s) \rightleftharpoons N_2(g) + 4\,H_2O(g) + 6\bar{e} \qquad \{R7.4\}$$

$$2\,NH_4^+(s) + O^{2-}(s) \rightleftharpoons N_2O(g) + 4\,H_2O(g) + 8\bar{e} \qquad \{R7.5\}$$

$$2\,NH_4^+(s) + O^{2-}(s) \rightleftharpoons 2\,NO(g) + 4\,H_2O(g) + 10\bar{e} \qquad \{R7.6\}$$

The electrons (indicated by $\bar{e}$) in the above equations are localized at the vanadium atoms, causing their reduction.

From these results and opinions of previous workers, it seems that two factors play an important role during the decomposition process : the surrounding atmosphere and structural order/disorder. Consequently, the influence of these factors on the reducibility of the intermediate V_2O_5 was studied.

7.2. EXPERIMENTAL PROCEDURE

7.2.1. Instrumental techniques

The experimental techniques used in this study are TG, DTA and DSC as well as X-ray powder diffraction analysis. A detailed description of

the instrumentation used, was given in section 2.2. Heating rates of 5 $K.min^{-1}$ were used throughout since the best seperation of reaction peaks were obtained at this rate.

7.2.2. Materials and sample preparation

Commercial AMV supplied by Riedel de Haën (analytical grade) was used as starting material. To obtain AHV intermediates of varying degree of structural order, the commercial AMV was subjected to different treatments.

AHV 1 - very ordered structure

A very ordered AHV intermediate was prepared from solution according to the method of Kelmers [52].

A solution of approximately 1 molar NH_4VO_3 was prepared and pre-heated to 85°C. A quantity of acid (sulphuric, hydrochloric or perchloric acid) equivalent to that required by the following reaction was added :

$$6\ NH_4VO_3 + 4\ H^+ \longrightarrow (NH_4)_2V_6O_{16} + 4\ NH_4^+ + 2\ H_2O \qquad \{R7.7\}$$

Bright orange crystals formed slowly and the resulting slurry was stirred for ±24h at 85°C. The precipitate was filtered, washed with water and dried at 110°C. The X-ray powder diffraction spectrum obtained for the crystals, corresponded to the spectrum obtained by Kelmers and is given in appendix A.

AHV 2 - less ordered structure

During decomposition of AMV a certain degree of disorder is introduced into

the crystal lattice due to rearrangement of oxygen polyhedra and evolution of gaseous products. An intermediate AHV with a less ordered structure was thus obtained as intermediate during decomposition of commercial AMV.

AHV 3 - most disordered structure

A disordered AHV was obtained according to the method described by Brown et al. [43]. This method involves the reaction of V_2O_5 (which is a product of decomposition of commercial AMV in air at 400°C) with damp ammonia to form a "recombined" AMV according to the following reversible reaction :

$$V_2O_5 + 2NH_3(g) + H_2O(g) = 2NH_4VO_3 \qquad \{R7.8\}$$

7.3. RESULTS

7.3.1. The influence of atmosphere n the decomposition of AMV

The thermal decomposition of AMV was studied in oxygen, argon, carbon monoxide and hydrogen atmospheres, using commercial AMV. The TG and DTA-traces for the various reactions are given in figures 7.1 to 7.4 respectively.

As was anticipated from the results of previous workers, the first part of the decomposition process, i.e. the decomposition of AMV to AHV (reaction 7.1), was found to occur independently of the prevailing atmosphere. In all cases, the intermediate AHV was found to form with a simultaneous mass loss of 15.5% wich corresponds to the theoretical mass loss of 14.85% expected for this reaction. The plateaus in the TG-curves which represent the formation of AHV, are indicated in figures 7.1 to 7.4. The AHV intermediate was

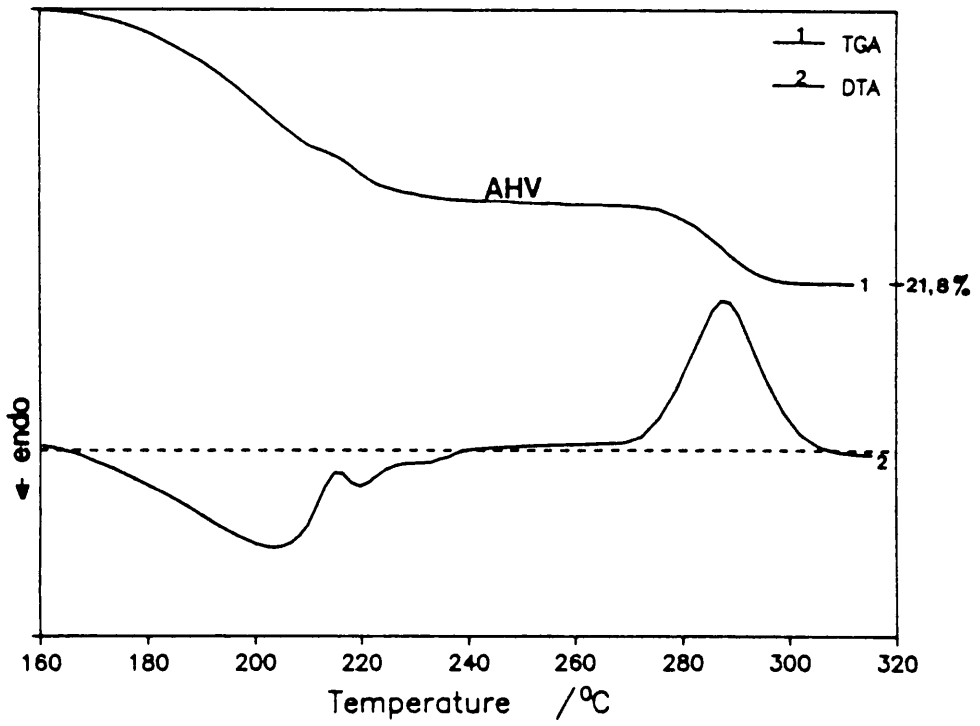

Figure 7.1. - TG and DTA curves for the thermal decomposition of commercial AMV in O_2.

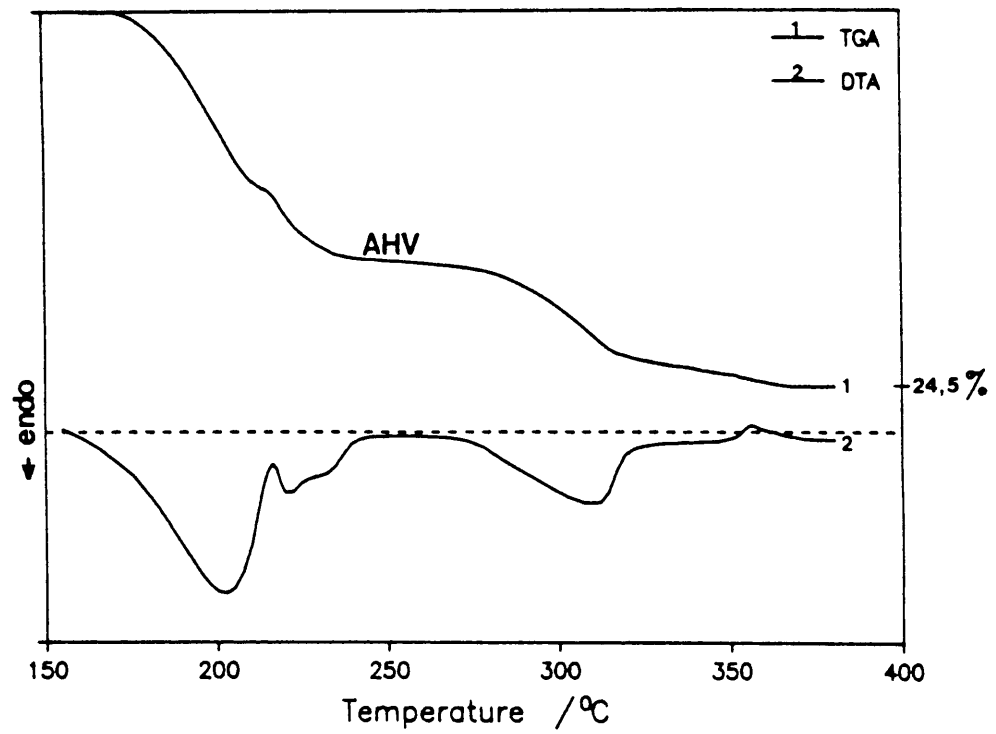

Figure 7.2. - TG and DTA-curves for the decomposition of commercial AMV in an inert atmosphere.

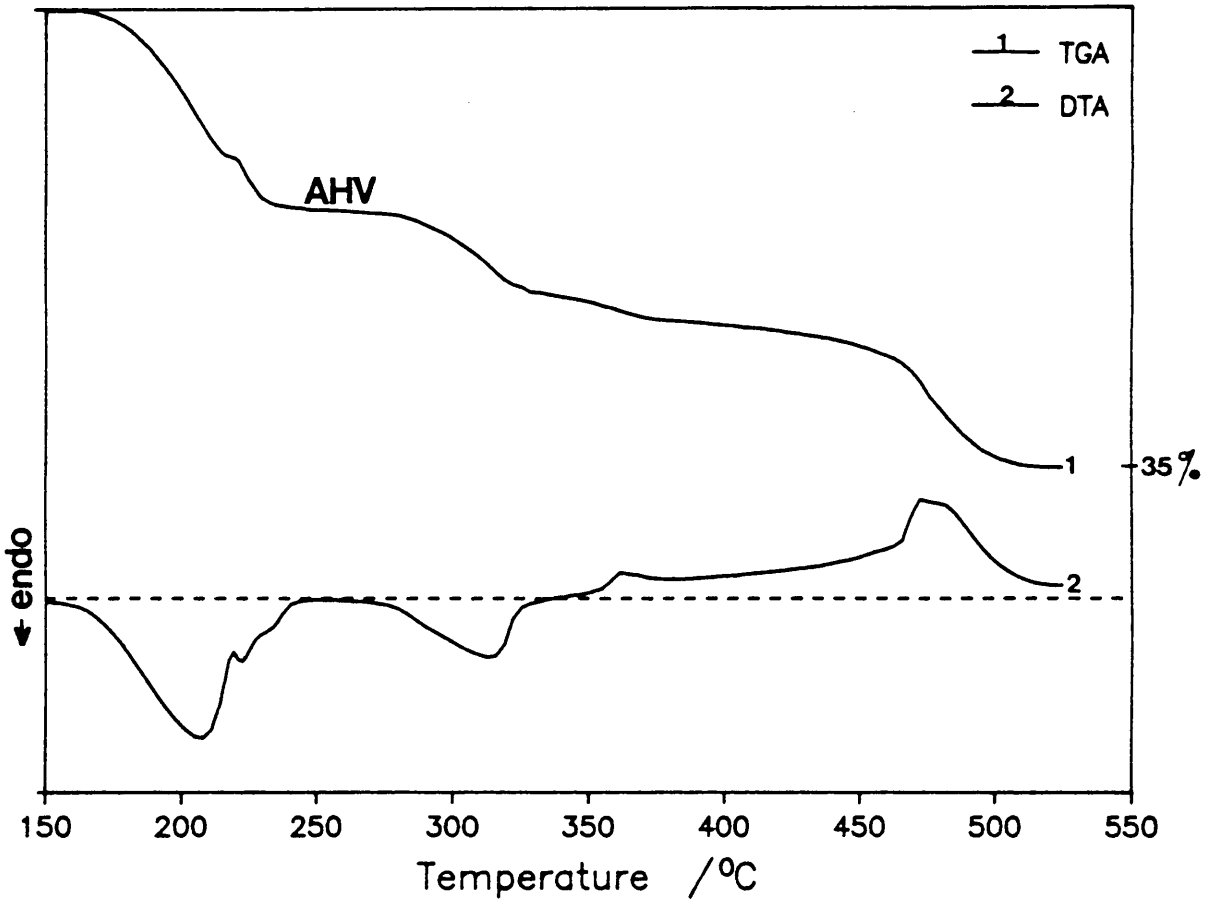

Figure 7.3. - TG and DTA-curves for the reduction of commercial AMV in CO.

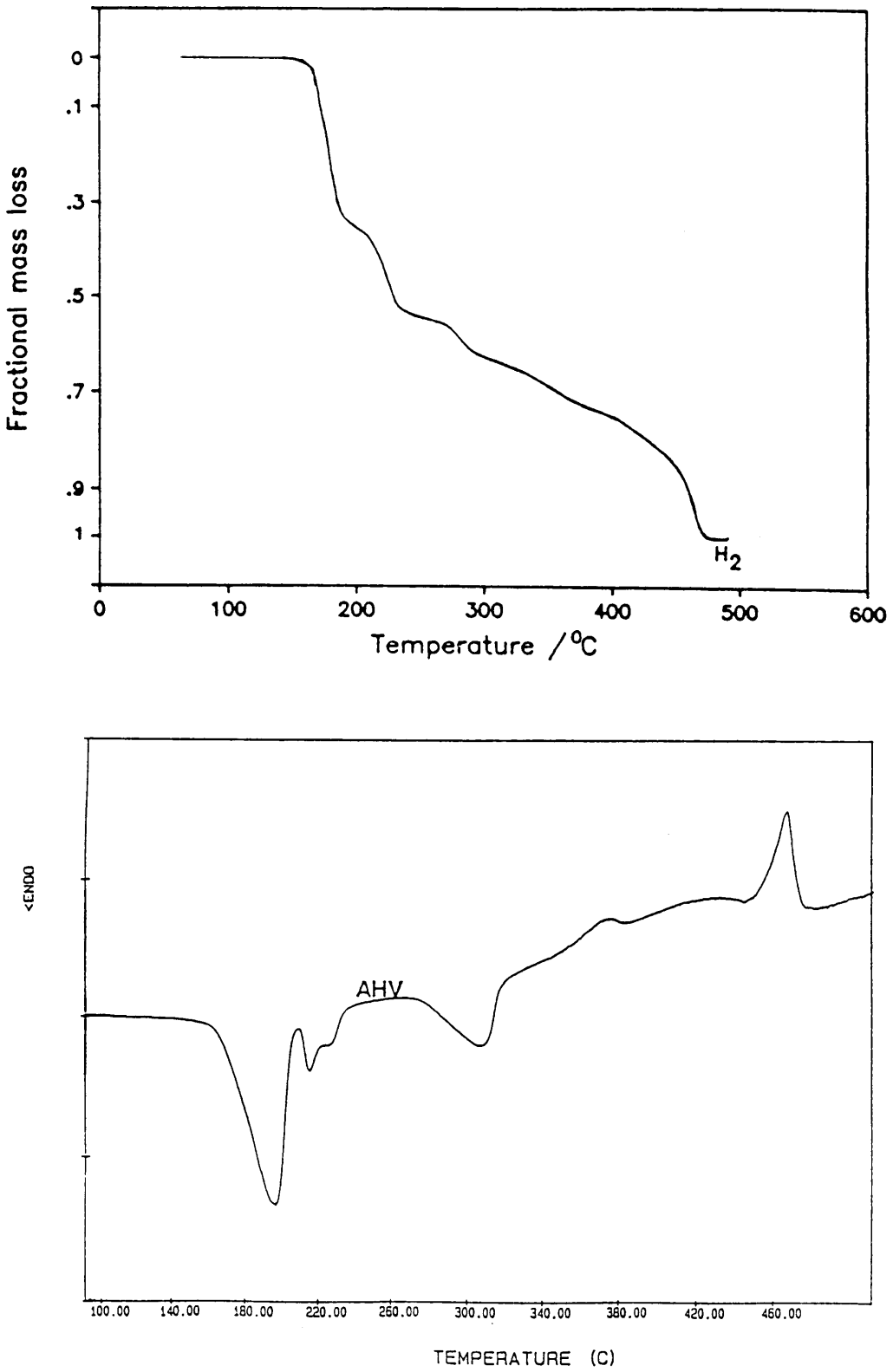

Figure 7.4. - TG and DTA curves for the reduction of commercial AMV by H_2.

identified by XRPD analysis in all cases, and the XRPD-pattern obtained corresponded to that obtained by Kelmers et al. [52].

The second part of the decomposition process (reaction 7.2) was found to be sensitive to the surrounding atmosphere.

7.3.1.1. Oxidizing atmosphere

The total mass loss obtained for the decomposition in oxygen (figure 7.1), was 21.8%, corresponding to the theoretical mass loss of 22% for the formation of V_2O_5. The final product had the characteristic orange colour of V_2O_5, and XRPD-analysis confirmed that the final product was V_2O_5.

From the DTA-profile, it can be seen that the decomposition of AHV to V_2O_5 is represented by an exothermic process in the 270 - 315°C temperature range.

7.3.1.2. Inert atmosphere

In nitrogen and argon atmospheres (figure 7.2), a total mass loss of 24.5% was obtained which is more than the expected 22% for the decomposition of AHV to V_2O_5.

XRPD-analysis indicated the presence of lines of lower oxides i.e. V_3O_7 and V_6O_{13}, together with the V_2O_5 lines. The final product was also darker in colour than expected for V_2O_5. From the DTA-curve, it can be seen that the decomposition of AHV is represented by two peaks. An endothermic peak is observed in the 280 - 330°C temperature range and a smaller exotherm in the 350 - 380°C range. The endotherm is associated with a mass loss of 22.0%, while the exotherm corresponds to a further mass loss of ±2.5%.

To study this process in more detail, the decomposition reaction in argon was terminated at the stages A to D, indicated in figure 7.5, and the sample analysed by XRPD. In patterns A and B, lines of AHV and V_2O_5 are visible (the most prominent lines of V_2O_5 are indicated by numbers 1 to 4). In patterns C and D, the arrows indicate the main lines of the lower oxides, V_3O_7 and V_6O_{13}. On comparing patterns B and C, it can be seen that V_2O_5 lines in pattern B are shifted to lower d-spacings. This is probably due to a uniform stress that exists in the V_2O_5 crystal lattice at stage B because of the presence of non-stoichiometric and non-crystalline material, as well as some occluded ammonia. The alleviation of this stress in the V_2O_5 lattice is coupled by the formation of V_3O_7 and V_6O_{13}, shown in patterns C and D. This process is exothermic, as observed in the DTA-curve, and probably represents the reduction of V_2O_5 and/or the oxidation of ammonia.

7.3.1.3. Reducing atmospheres

The total mass loss observed in CO (figure 7.3) was 35.5% which corresponds to the theoretical value of 35.94% for the conversion of AMV to V_2O_3. XRPD-analysis confirmed that the final product was V_2O_3.

The processes which are observed in the DTA-curve between 150 and 380°C are similar to those observed in inert atmospheres in the same temperature range. At higher temperatures (380 - 530°C), further reduction of V_2O_5 to V_2O_3 by CO occurs, accompanied by an exothermic DTA signal. It is important to notice that reduction to V_2O_3 is completed at ±530°C which is much lower than the temperature that was needed to reduce commercial V_2O_5 to V_2O_3 in figure 2.3. V_2O_5 produced through the the decomposition of AMV in the presence of O_2, had a similar morphology to the commercial V_2O_5, shown in the electron micrograph in figure 2.2(a). Reduction of both these V_2O_5 samples is complete at ±740°C.

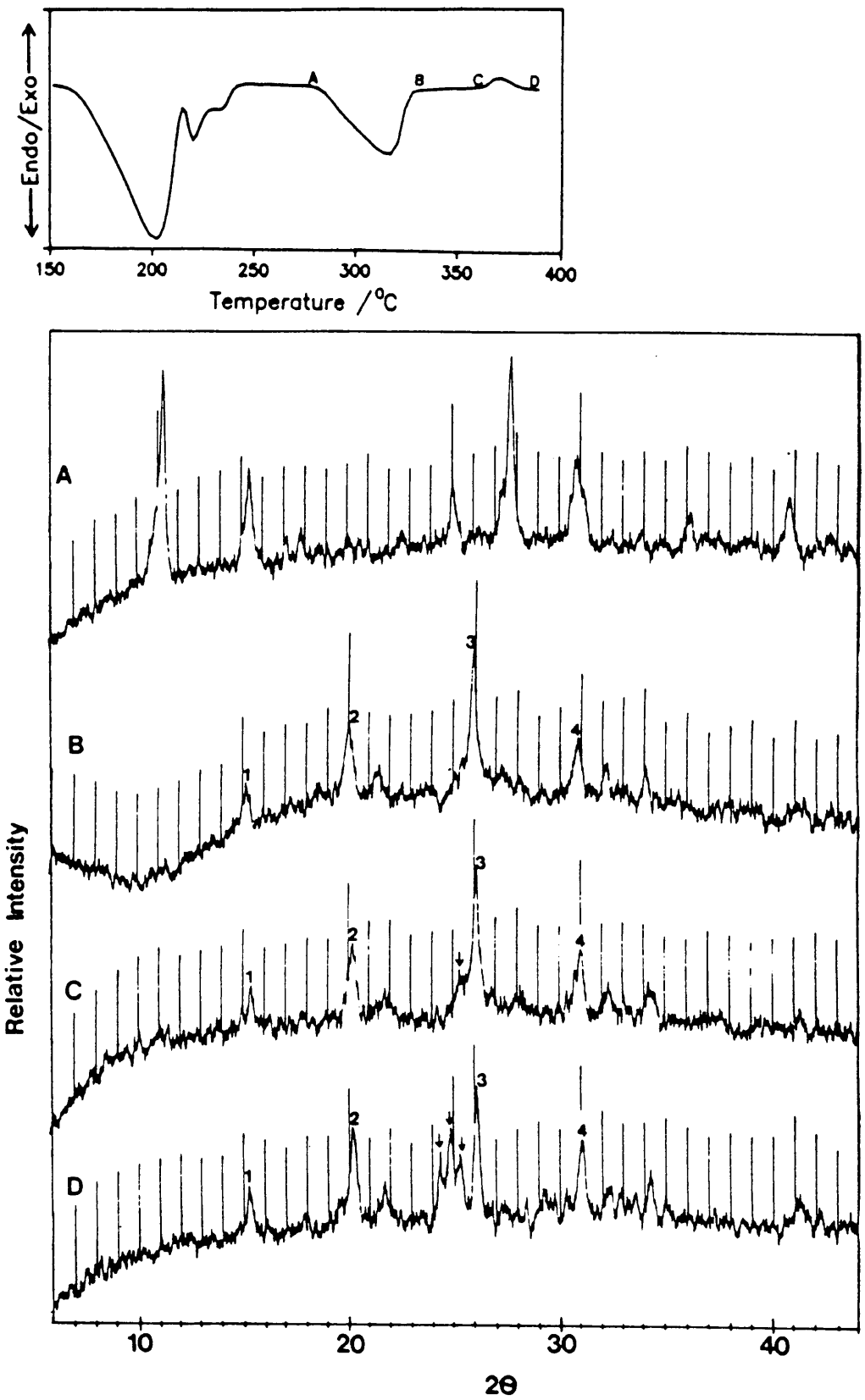

Figure 7.5. - XRPD study of the decomposition of AHV in an inert atmosphere.

Decomposition of AMV in H_2 led to complete reduction of V_2O_5 to V_2O_3 at a temperature of ±480°C (figure 7.4). This is a lower temperature than the 530°C which was needed for complete reduction by CO (figure 7.3), although similar TG and DTA-profiles are observed. This result is contradictory to the results obtained by Mintek workers [4].

7.3.2. Influence of the degree of structural order of the AHV intermediate

The three types of AHV intermediates with varying degrees of structural order (prepared by the methods described in section 7.2.2) were heated in reducing, inert and oxidizing atmospheres at a heating rate of 5 $K.min.^{-1}$. The degree of structural order is 3 < 2 < 1, with sample 1 the most ordered.

7.3.2.1. Reduceability of the V_2O_5 intermediate

From the DTA-curves (figure 7.6) it can be seen that the temperature at which total conversion to V_2O_3 is complete, is dependent on the type of AHV sample used. Conversion of sample 1 is complete at a temperature of ±600°C, while sample 2 is already converted at ±550°C. A still lower temperature of ±500°C is needed to convert sample 3 to V_2O_3.

These results indicate that a higher degree of structural disorder in the AHV intermediate leads to the formation of a more reducible V_2O_5.

7.3.2.2. Processes occurring in the absence of O_2

It was shown in sections 7.3.1.2 and 7.3.1.3 that the processes occurring in the 150 - 380°C temperature range (i.e. the decomposition processes up to the

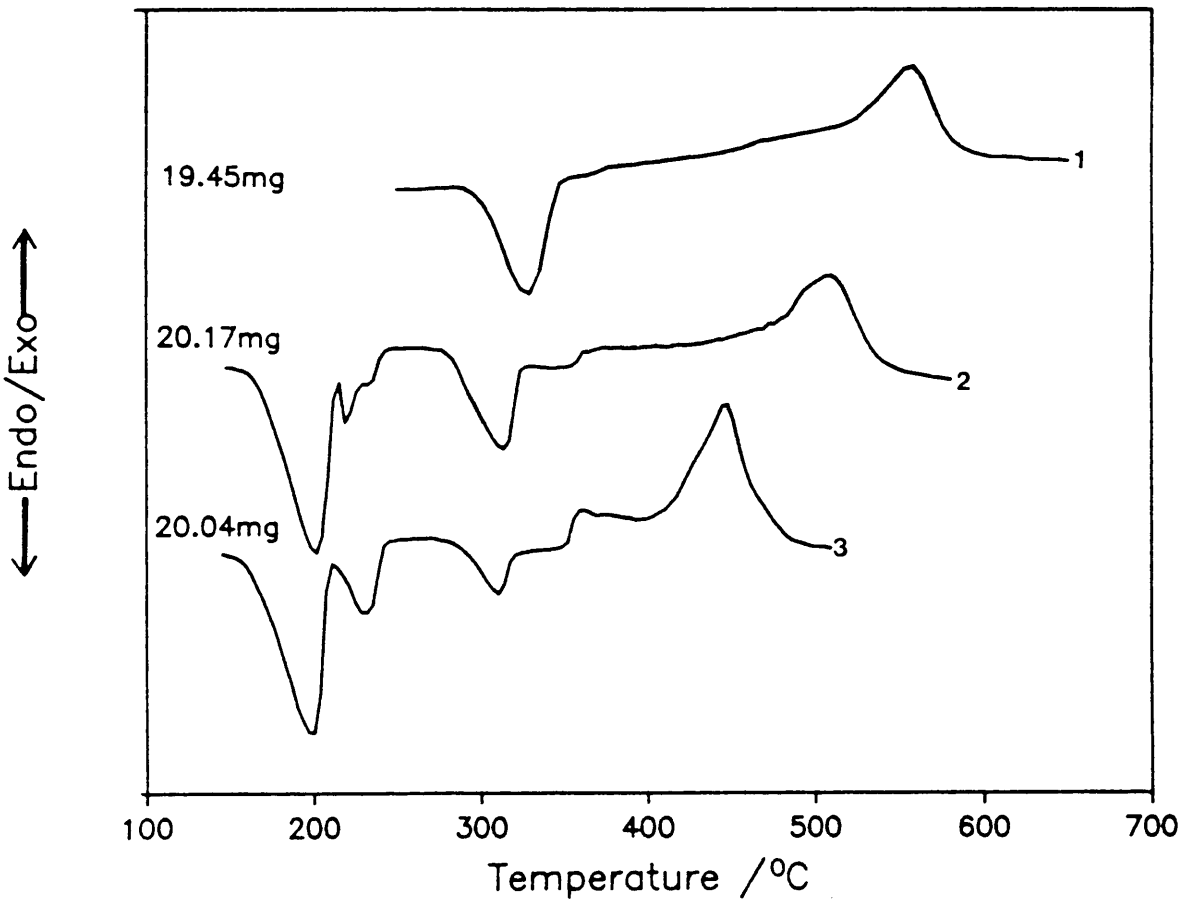

Figure 7.6. - DTA-curves for the reduction of AHV intermediates with varying degrees of structural order (1-most ordered, 3-least ordered).

formation of V_2O_5) are similar in inert and reducing atmospheres. These processes were studied more closely by decomposing samples 1 to 3 in an inert atmosphere. The DSC-curves obtained are shown in figure 7.7. The enthalpies of the various reactions were determined and are given in table 7.1, along with the corresponding mass losses obtained from the TG-experiments.

Table 7.1. - Enthalpies of the reactions occurring during decomposition of AHV in an inert atmosphere

Sample nr.[a]	Endotherm		Exotherm		Total mass loss[b] %
	Enthalpy kJ.mol^{-1} AHV	Temp. °C	Enthalpy kJ.mol^{-1} AHV	Temp. °C	
1	122.6 ± 4.4	275-325 min:302	-7.21 ± 1.4	350-380 max:364	9.1±0.2
2	83.1 ± 6.4	280-340 min:314	-20.5 ± 2.3	350-385 max:368	9.6±0.2
3	24.9 ± 0.2	305-365 min:333	-23.3 ± 0.3	390-420 max:405	11.1±0.5

a - Degree of structural order : 3 < 2 < 1 (1 most ordered).
b - Theoretical mass loss for AHV to V_2O_5 : 8.7%

The endothermic process

The fact that the transition of AHV to V_2O_5 is an endothermic process which involves the breakage of bonds and structural rearrangements implies that a certain energy barrier must be surmounted. This process probably involves the formation of an activated complex [43]. It can be understood that the decomposition of a more disordered AHV reactant must have a smaller reaction enthalpy than its more ordered counterparts. This also explains the lower reaction temperatures observed for the more disordered reactants.

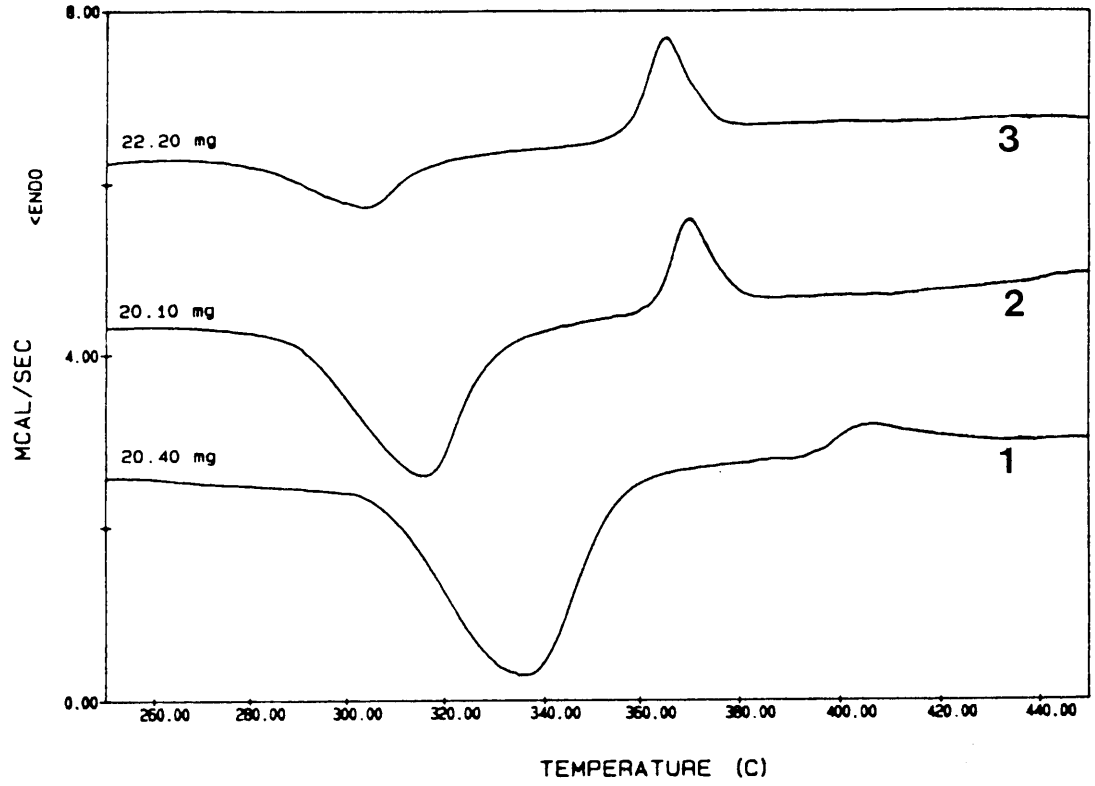

Figure 7.7. - DSC-curves for the decomposition of AHV intermediates with varying degrees of structural order in an inert atmosphere (1-most ordered, 3-least ordered).

The exothermic process

The exothermic processes observed during the decomposition reactions can probably be ascribed to the reduction of V_2O_5, due to the catalytic decomposition of ammonia by the lattice oxygen of V_2O_5. The varying reaction enthalpies of this process and the different mass losses can be ascribed to different degrees of reduction of samples 1 to 3, depending on its degree of structural order. A possible explanation for the higher degree of reduction of the more disordered sample is that the V=O bonds of V_2O_5 in the strained lattice are weakened, as was discussed in chapter 5, leading to a more reducible V_2O_5.

7.3.2.3. Processes occurring in the presence of O_2

The DTA-curves of the decomposition of AHV samples 1 to 3 in oxygen are shown in figure 7.8. It appears that two competing processes are taking place. These processes are represented by an overlapping endotherm and exotherm. For sample 1, the endotherm is dominant while for sample 3 the exotherm is dominant. It seems that on going from sample 1 to 3, the decreasing structural order results in a decrease in the endothermic reaction and a subsequent increase in the exothermic reaction.

The endothermic process

Judging from the temperatures at which the reaction peaks occur, it seems that the endotherm (figure 7.8) represents the decomposition of AHV to V_2O_5, similar to the exothermic process observed in an inert atmosphere (figure 7.7). As the disorder of the AHV intermediate increases, the enthalpy of the endotherm decreases due to the smaller amount of energy needed for the reaction to proceed.

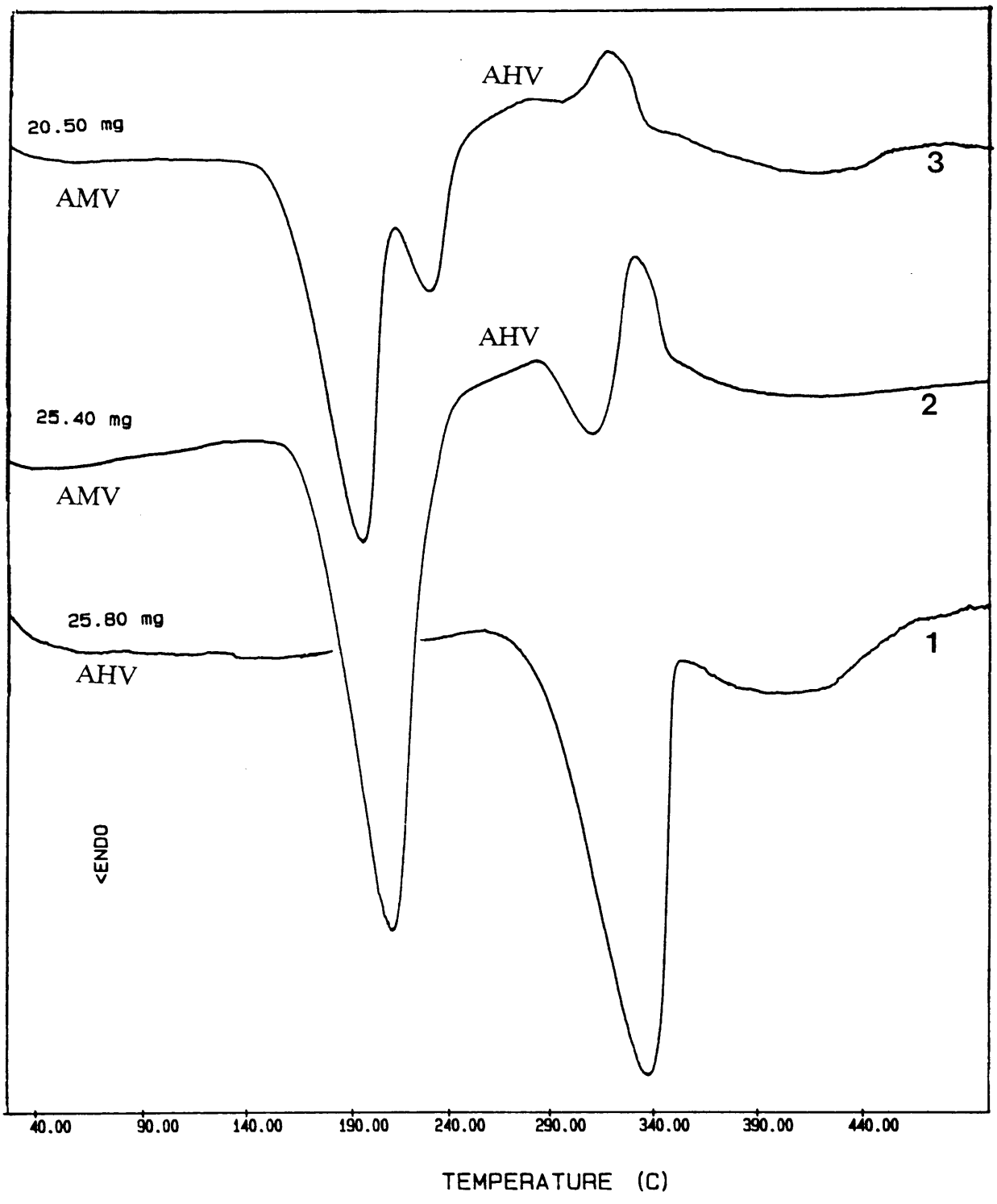

Figure 7.8. - DSC-curves for the decomposition of AHV intermediates with varying degrees of structural order in O_2. (1-most ordered, 3-least ordered)

The exothermic process

The exothermic process in figure 7.8, occurs at ±340°C which is a lower temperature (±30°C lower) than the temperature at which the exothermic process had occured in an inert atmosphere (figure 7.7). In addition to this, no simultaneous mass loss, as observed in an inert atmosphere, occurs. This is an indication that a different process is taking place other than the reduction of V_2O_5. Although the exact nature of this process is uncertian, it apparently is somehow related to the presence of oxygen in the surrounding atmosphere. It also represents the formation of an ordered V_2O_5 product from a disordered AHV intermediate.

A possible explanation could be the oxidation of ammonia and/or the oxidation of the V_2O_{5-x} system by O_2. It also could be interpreted as energy that is given off by the annealing of a disordered and oxygen deficient V_2O_5 lattice formed through the decomposition process. This would explain why the exothermic reaction enthalpy is higher for the more-defective sample and almost unnoticeable for the ordered one. This is because a higher degree of disorder and oxygen deficiency exists in the sample 3. In sample 1, a high degree of structural order exists which neccessitates an energy uptake for the breakage of bonds and rearrangements during decomposition.

7.4. DISCUSSION

The V_2O_5 formed through the thermal decomposition of AMV in the absence of O_2, was found to be reduced at lower temperatures than V_2O_5 produced in the presence of O_2. The latter type of V_2O_5 is similar to the V_2O_5 powder used in the studies on the reduction of V_2O_5. It has a similar morphology to that shown in the electron micrograph, in figure 2.2(a), and showed the same reduction behaviour.

Results obtained futher indicated that the reducibility of the V_2O_5 formed as intermediate during the thermal decomposition of AMV, is influenced by the structural order of the preceding AHV intermediate. Reduction was completed at lower temperatures when a disordered, rather than an ordered AHV intermediate, was used.

During the decomposition of AMV under all conditions, disorder and non-stoichiometry is introduced into the crystal lattice at first. In the presence of oxygen, order is apparently restored in the last stage of the decomposition when V_2O_5 is formed. This process is represented by an exothermic DTA-peak at ±350°C.

It is expected [43] that there will be considerable interaction between the V_2O_5 product of decomposition and O_2 because O_2 is readily chemisorbed on a V_2O_5 surface (100 - 480°C) [53]. The ability of oxygen atoms in the V_2O_5 lattice to exchange with adsorbed O_2 is well known.

In the absence of O_2 (in reducing and inert atmospheres), reduction of the freshly-formed V_2O_5 occurs, probably through the catalytic decomposition of ammonia which is evolved during decomposition. It could also be due to the occurence of the redox reactions 1.3 to 1.6 described by Dziembaj et al. [48].

The degree to which this reduction occurs, is apparently dependent on the structural order/disorder which exists in the intermediates of decomposition. It was shown by the DSC and TG results that a more disordered AHV intermediate leads to a higher degree of reduction of the V_2O_5 product (table 7.1).

This effect can probably be explained by the argument of Fiermans et al. [6] (section 5.4.3) and is probably partly the reason for the lower reduction

temperatures observed in figure 7.6. By considering, once again, results obtained by various workers on the nature of vanadium pentoxide catalysts, valuable information applicable to the present study was obtained.

From all studies on V_2O_5 catalysts, it emerged that these catalysts are non-stoichiometric oxides having a certain degree of anion deficiency [53]. In V_2O_5 catalysts prepared from the thermal decomposition of AMV [19] the presence of lower oxides such as V_6O_{13} has been detected. The boundaries between these lower oxides and V_2O_5 were stated to be the active part of the catalyst.

According to Andersson [19] these boundaries are regions with non-stoichiometric V_2O_5 and V_6O_{13} phases with V=O species adjacent to V^{4+} ions (which are always associated with oxygen vacancies) in the lattice. The adjacent V=O bonds are weakened because of an increased electrostatic repulsion between the vanadium and oxygen species in the bond, according to the following scheme:

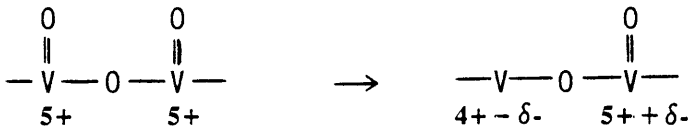

The implication that oxygen can be removed more easily from the boundary between V_2O_5 and a lower oxide such as V_6O_{13}, could explain the enhanced reduction rates observed for the V_2O_5 formed through the decompcsition of AMV in the absence of O_2. These V_2O_5 intermediates contain lower oxides, and thus active boundaries, due to the reduction by ammonia. These active boundaries contribute to a more reducible structure. In V_2O_5 samples produced in the presence of O_2, these active boundaries are absent and the sample is consequently reduced at higher temperatures owing to a less reactive structure.

CHAPTER 8
CONCLUSIONS

8.1. Reduction of V_2O_5

8.1.1. Oxide transitions

V_2O_5 can be reduced to V_2O_3 successfully by using CO or H_2 as reducing gas. The sequence of intermediate vanadium oxides that was found to form between V_2O_5 and V_2O_3 during reduction, is as follows:

$$V_2O_5 \longrightarrow V_6O_{13} \longrightarrow VO_2 \longrightarrow V_nO_{2n-1}\ (4 \leq n \leq 8) - - > V_2O_3$$

There still exists some doubt as to the formation of the homologous series of oxides V_nO_{2n-1}, but the presence of XRPD lines corresponding to those of these oxides, was detected in samples partly reduced by H_2.

The reduction can be viewed as occurring through the removal of vanadyl oxygen from the V_2O_5 lattice via the chemisorption of the reducing gas onto these sites. Shear and collapse of the vanadium-oxygen network may then occur, leading to a lower vanadium oxide structure.

8.1.2. Kinetics and mechanism of reduction

The reduction of V_2O_5 was found to be a structure sensitive process, with the reduction rate and mechanism of solid-gas interaction being dependent on the morphology of the solid as well as on the temperature of reduction. The complexity of these reduction processes encumbers a meaningful kinetic study of the reduction of V_2O_5 as is reflected in the unaccountability of the results obtained.

Notwithstanding these difficulties, the Avrami-Erofe'ev kinetic model was found to give a general description of the mechanism of reduction, describing a process of nucleation and growth. Optical microscopy studies indicated that reduction starts preferably at defects such as steps and kinks in the crystal surface. After coverage of the surface, the reaction interface advances inwards towards the centre of the crystal, resembling a contracting-volume mechanism.

8.2. The reduction of AMV

Studies conducted on the reduction of AMV have confirmed that the in situ reduction of V_2O_5 (formed as decomposition intermediate) requires lower temperatures for complete conversion to V_2O_3 than the direct reduction of V_2O_5 when used as starting material.

The higher reducibility of the intermediate V_2O_5 can be ascribed to the disorder and oxygen deficiency introduced into the V_2O_5 lattice during decomposition in the absence of oxygen. It is possible that the catalytic decomposition of ammonia evolved during decomposition causes partial reduction of the V_2O_5, leading to the formation of lower oxides (V_3O_7 and V_6O_{13}). The boundaries between V_2O_5 and these lower oxides are subjected to stress which may contribute to the higher activity because the oxygen species in these regions can be removed more easily.

8.3. CO versus H_2 as reducting gas

Throughout this study, higher reduction rates were achieved with H_2 than with CO. This applies to the reduction of both V_2O_5 and AMV. These findings are contradictory to thermodynamic predictions. However, it was shown in figure 3.3 (section 3.2.2) that there does not exist such a substantial

difference in favourability between CO and H_2 reduction in the temperature range of reduction as might at first seeem. It is possible that this existing thermodynamic favourability of CO over H_2 might be overcome if the H_2 reaction is kinetically more favourable than the CO reaction. This possibility seems likely in the light of the different mechanisms proposed for the V_2O_5-CO and V_2O_5-H_2 systems (sections 4.4.1 and 5.4.2).

8.4. Suggestions and comments concerning the industrial reduction of V_2O_5

The fact that the in situ reduction of V_2O_5 (formed as decomposition intermediate) proceeds at lower temperatures than the direct reduction of V_2O_5, can be implemented to reduce the costs of V_2O_5 reduction.

Consider the final stages of the roast-leach process (figure 1.1). Instead of converting the AMV to V_2O_5 flakes at 850°C, followed by reduction of the flakes at ±600°C by CO or H_2 to obtain V_2O_3, AMV can be reduced directly to V_2O_3 at lower temperatures.

Alternatively, decomposition of AMV to V_2O_5 at 400°C (or any temperature below the melting point of V_2O_5) instead of the 850°C used at present, would lead to a V_2O_5 product with a smaller grain size and different morphology which will be more easily reduced since the role of diffusion will be minimized.

8.4. Proposals for further study

The hypotheses formulated concerning the mechanisms of solid-gas interaction that contribute to the overall reduction mechanism and reduction behaviour observed (figures 4.4 and 4.8) for the V_2O_5-CO and V_2O_5-H_2 systems, require further investigation. Temperature-programmed reduction

(TPR) studies in which the "uptake" of the reducing gas can be monitored, may provide valuable information in this context.

A better understanding of the mechanism and the kinetics of the reduction of V_2O_5 could be obtained by preparing a V_2O_5 single crystal and studying it as such. This could facilitate the interpretation of certain kinetic parameters and would limit the influence of factors such as changes in grain size and morphology. In addition to this, the influence of contaminating substances in the lattice on the mechanism and rate of reduction could be studied.

The processes that occur during reduction of AMV, leading to the formation of a more reducible V_2O_5, could be followed by a detailed infrared spectroscopical study. Such a study could prove invaluable to the understanding of the system. Especially the role of the NH_4^+-ion could be examined in more detail. Evolved gas analysis (EGA) studies could also be implemented to clarify some of the aspects concerning the catalytic decomposition of ammonia.

Attempts were made to study the reduction of AMV with SEM, but due to the small grain sizes involved, these studies were unsuccessful.

APPENDIX A
XRPD-DATA

The following main XRPD-lines were used for identification of the compounds in this study, obtained from the ASTM powder diffraction files of the Joint Commitee on powder diffraction standards, except where otherwise indicated.

V_2O_5

d/Å	I/I_1
5.76	40
4.38	100
4.09	35
3.40	90
2.88	65
3.40	90
2.88	65
2.76	35
2.610	40
1.919	25
1.757	30

V_3O_7 from [8]

d/Å	I/I_1
4.069	m
3.638	m
3.568	vs
3.042	m
3.008	m
2.945	m
2.552	s
2.455	m
1.8398	vs
1.8251	s
1.7837	m

V_6O_{13}

d/Å	I/I_1
5.85	40
4.98	20
3.51	100
3.32	80
2.963	60
2.674	80
2.482	20
1.9920	60
1.9872	60
1.8401	80

VO_2

d/Å	I/I_1
3.31	30
3.20	100
2.680	30
2.427	60
2.268	40
2.137	50
1.657	20
1.654	30
1.601	30

V_2O_3

d/Å	I/I_1
3.65	60
2.70	80
2.47	60
2.18	20
1.83	25
1.69	100
1.47	25
1.43	30
1.33	10

NH_4VO_3

d/Å	I/I_1
5.89	55
4.90	80
4.14	100
3.769	30
3.165	85
2.914	55
2.714	18
2.629	30
2.453	25

$(NH_4)_2V_6O_{16}$ from [52]

d/Å	I/I_1
7.84	vs
5.64	s
3.91	m
3.55	s
3.26	m
3.21	m
2.92	m
2.90	m
2.87	m

APPENDIX B
THERMODYNAMIC DATA

The thermodynamic data of vanadium oxides used for the calculations in chapter 3 were obtained from Barin and Knacke [55] except for the data for V_6O_{13} which were obtained from the $H°_T$-$H°_{298}$ values published by Mah [56]. A least square, non-linear curve fitting routine developed by Stander [3] was used to evaluate the heat capacity polynomial coefficients for V_6O_{13}.

Table B1 - Gibbs free energy vs. temperature for vanadium oxides

Temp. K	G_T kcal.mol^{-1}				
	V_2O_5	V_6O_{13}	VO_2	V_2O_3	VO
298	-381.63	-1088.97	-175.17	-300.01	-105.77
300	-381.69	-1089.97	-175.19	-300.05	-105.79
400	-385.33	-1098.54	-176.82	-302.80	-106.89
500	-389.90	-1110.26	-178.99	-306.26	-108.30
600	-395.25	-1123.94	-181.50	-310.31	-109.95
700	-401.28	-1139.33	-184.31	-314.87	-111.82
800	-405.9	-1156.29	-187.38	-319.88	-113.88
900	-415.06	-1174.67	-190.68	-325.30	-116.11
1000	-423.58		-194.19	-331.09	-118.50
1100	-433.29		-197.9	-337.21	-121.03
1200	-443.42		-201.78	-343.64	-123.70
1300	-453.92		-205.82	-350.36	-126.49
1400	-464.78		-210.02	-357.36	-129.39
1500	-475.96		-214.36	-364.61	-132.42
1600	-487.45		-218.84	-372.10	-135.55

APPENDIX C
DETERMINATION OF KINETIC MODEL

The experimental, isothermal TG-curves which were obtained for the reduction of V_2O_5 by CO and H_2, were first measured by hand to obtain a set of 40 to 50 α (fraction reduced) versus t(time) data pairs for each isotherm. These data sets ($0.05 \leq \alpha \leq 0.9$) were then used as input for the computer software developed by Wagener et al. [36] in which nineteen different equations (listed in table C1), representing different kinetic models, were fitted to these data sets.

After the data had been processed, a print-out was obtained containing the following results for each $f(\alpha)$ vs. time plot:

- the slope (k),
- the correlation coefficient (R) and R^2,
- the standard deviation,
- the x and y intercepts.

After careful consideration of the correlation coefficient and the standard deviation, the kinetic model which best describes the experimental data set, was selected. The program also contains an option where a graph of the $f(\alpha)$ vs. t plot can be obtained, and this option was also used to select the best model.

Table C1 - equations for kinetic models

F1	$f(\alpha)=\alpha$	power law, n = 1
F2	$f(\alpha)=\alpha^{1/4}$	power law, n = 4
F3	$f(\alpha)=\alpha^{1/3}$	power law, n = 3
F4	$f(\alpha)=\alpha^{1/2}$	power law, n = 2
F5	$f(\alpha)=\alpha^{2}$	power law, n = ½
F6	$f(\alpha)=1-(1-\alpha)^{1/2}$	contracting area
F7	$f(\alpha)=1-(1-\alpha)^{1/3}$	contracting volume
F8	$f(\alpha)=(1-\alpha)\ln(1-\alpha)+\alpha$	two-dimensional diffusion
F9	$f(\alpha)=(1-2/3\alpha)-(1-\alpha)^{2/3}$	three dimensional diffusion
F10	$f(\alpha)=[1-(1-\alpha)^{2/3}]^{2}$	Jander
F11	$f(\alpha)=-\ln(1-\alpha)$	Avrami-Erofe'ev, n = 1
F12	$f(\alpha)=[-\ln(1-\alpha)]^{2/3}$	Avrami-Erofe'ev, n = 3/2
F13	$f(\alpha)=[-\ln(1-\alpha)]^{1/2}$	Avrami-Erofe'ev, n = 2
F14	$f(\alpha)=[-\ln(1-\alpha)]^{1/3}$	Avrami-Erofe'ev, n = 3
F15	$f(\alpha)=[-\ln(1-\alpha)]^{1/4}$	Avrami-Erofe'ev, n = 4
F16	$f(\alpha)=\ln[\alpha/(1-\alpha)]$	Prout-Tompkins
F17	$f(\alpha)=1/(1-\alpha)-1$	Second order
F18	$f(\alpha)=\ln\alpha$	Exponential law
F19	$f(\alpha)=1/(1-\alpha)^{1/2}-1$	Third order

Example

The reduction of V_2O_5 platelets by CO at 490°C led to the following α vs t data:

t/s	α
1600	.038
1800	.047
2000	.058
2200	.068
2400	.079
2600	.093
2800	.107
3000	.121
3200	.140
3400	.159
3600	.178
3800	.201
4000	.224
4400	.271
4800	.318
5200	.369
5600	.420
6000	.472
6400	.519
6800	.568
7200	.612
7600	.659
8000	.696
8400	.734
8800	.769
9200	.799
9600	.827
10000	.855
10400	.879
10800	.899
11200	.916
11600	.932

The results obtained after the data processing are contained in table C2. The functions that were considered the best candidates are indicated with *, and their corresponding f(α) vs t plots are given in figures C1(a) to (f).

After consideration of the results in table C2 as well as the f(α) vs t plots in figure, the Avrami-Erofe'ev (n=2) equation, F13, was selected as the kinetic equation that describes the experimental data the best.

Table C2 - results of kinetic fits

function	slope/s^{-1}	intercept	R	R^2	std. err.	x intercept/s
F1	1.01E-04	-.1534	.995	.9899	.0324	1525.9
F2	5.46E-05	.4387	.9641	.9295	.0482	-8024.19
F3	6.60E-05	.3139	.9707	.9422	.0523	-4753.92
F4	8.21E-05	.1259	.9811	.9625	.0518	-1533.61
F5	9.59E-05	-.2737	.9816	.9636	.0596	2857.49
* F6	7.64E-05	-.1604	.9953	.9906	.0238	2099.4
* F7	5.96E-05	-.136	.9912	.9824	.0255	2281.06
F8	7.67E-05	-.2356	.9658	.9328	.0658	3071.52
F9	2.08E-05	-.0657	.9557	.9133	.0205	3157.24
F10	3.14E-05	-.1041	.9303	.8654	.0397	3311.15
F1	2.53E-04	-.6639	.9745	.9496	.1865	-2624.03
* F12	1.81E-04	-.2876	.9952	.9905	.057	1582.81
* F13	1.45E-04	-.0673	.9996	.9993	.0126	462.86
* F14	1.06E-04	.1988	.9984	.9968	.0193	-1880.57
* F15	8.35E-05	.3577	.9953	.9905	.0261	-4283.58
F16	5.54E-04	-3.6461	.9949	.9898	.1798	6585.71
F17	9.46E-04	-3.2365	.8555	.7319	1.8315	3422.57
F18	3.01E-04	-2.9822	.9386	.881	.3536	9919.57
F19	2.31E-04	-7117	.9262	.8576	.3021	3072.02

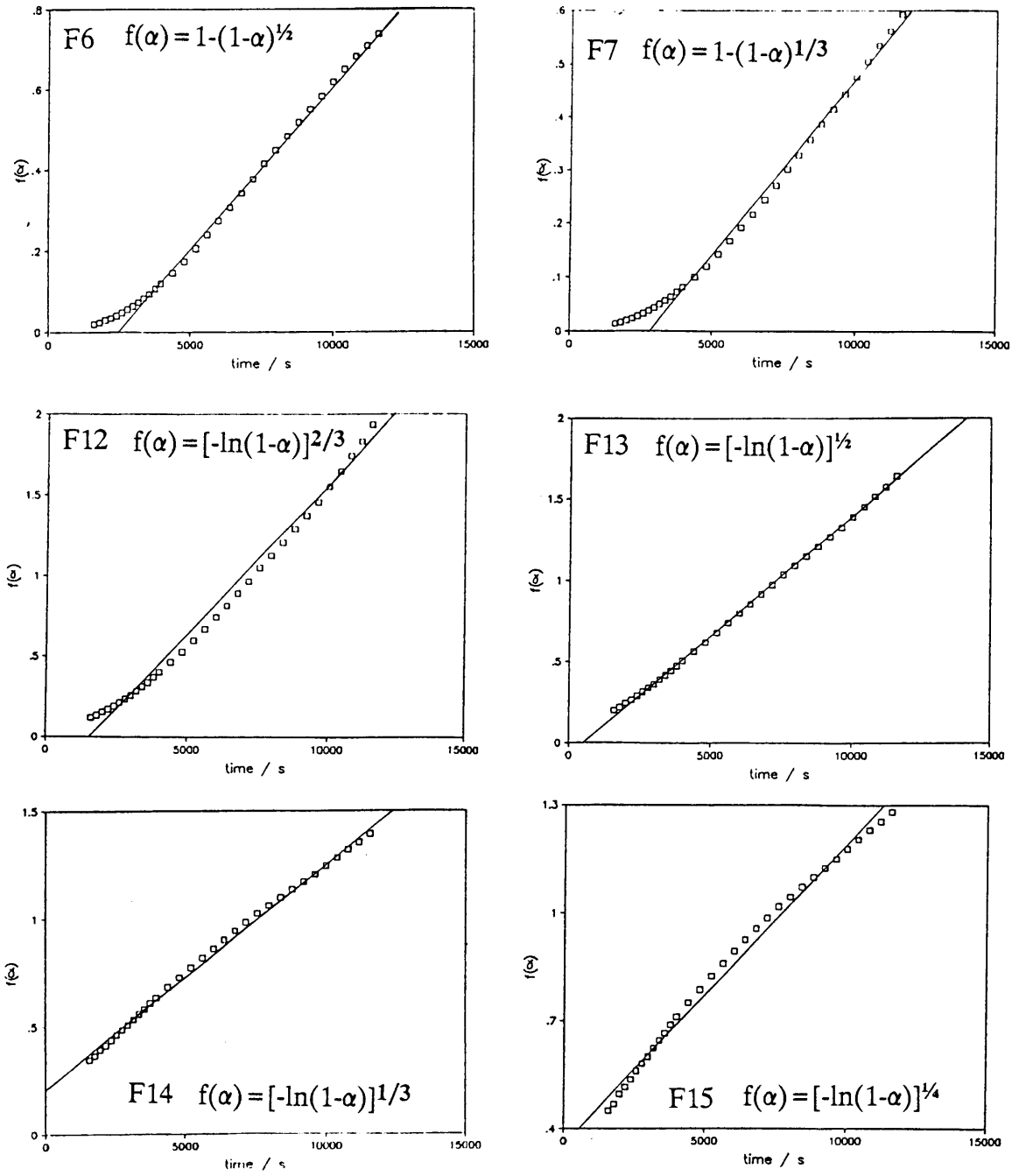

Figure C1 - f(α) vs. t plots for the six functions that gave the best fits to the the experimental data.

REFERENCES

[1] HAWKINS B.R.M., "Vanadium", **South Africa's mineral industry**, Minerals bureau of S.A., Johannesburg, (1985)127-130

[2] ROHRMANN B., "Vanadium in South Africa (metal review series no. 2)", *J. S. Afr. Inst. Min. Metall.* 85(1985)141-150

[3] STANDER P.P., "A fundamental study of the oxidation of Coulsonite (FeV_2O_4) in mixtures of Na_2CO_3 and Na_2SO_4", **M.Sc. thesis**, University of Pretoria, 1988

[4] MOOIMAN M.B., private communication, Mintek, 1987

[5] BYSTRöM A., WILHELMI K.A. and BROTZEN O., "Vanadium pentoxide - a compound with five co-ordinated vanadium atoms", *Acta Chem. Scand.* 4(1950)1119

[6] FIERMANS L., CLAUWS P., LAMPRECHT W., VAN DEN BROUCKE L. and VENNIK J., "Single crystal V_2O_5 and lower oxides. A survey of their electronic, optical, structural and surface properties." *Phys. Stat. Sol. (a)* 59(1980)485

[7] GRYMONPREZ G., FIERMANS L. and VENNIK J., "Structural properties of vanadium oxides." *Acta Cryst.* A33(1977)834

[8] WALTERSSON K., FORSLUND B. and WILHELMI K.A., "The crystal structure of V_3O_7." *Acta Cryst.* B30(1974)2644

[9] ANDERSSON G., "Studies on vanadium oxides. II. The crystal structure of vanadium dioxide." *Acta Chem. Scand.* 10(1956)623

[10] ANDERSSON G., "Studies on vanadium oxides. I. Phase analysis." *Acta Chem. Scand.* 8(1954)1599

[11] STRINGER J., "The vanadium-oxygen system - a review." *J. Less-Common Metals* 8(1965)1-14

[12] KOSUGE K., "The phase diagram and phase transitions of the V_2O_3-V_2O_5 system." *J. Phys. Chem. Sol.* 28(1967)1613

[13] WILHELMI K.A. and WALTERSSON K., "On the crystal structure of a new vanadium oxide, V_4O_9." *Acta Chem. Scand.* 24,19(1970)3409

[14] THéOBALD F., CABALA R. and BERNARD J., "Essai sur la structure de VO_2(B)." *J. Solid State Chem.* 17(1976)431-438

[15] HORIUCHI S., SAEKI M., MATSUI Y. and NAGATA F., "Transitions of V_6O_{13} to VO_2 observed with a high-resolution electron microscope." *Acta Cryst.* A31(1975)660

[16] HYDE B.G. and TILLEY R.J.D., "Deformation twinning of V_2O_5 during chemical reduction." *Phys. Stat. Sol. (a)* 2(1970)749

[17] GAI P.L., "Microstructural changes in vanadium pentoxide in controlled environments." *Phil. Mag. A* 83,3(1983)359

[18] FIERMANS L., CLAUWS P., VENNIK J. and DEKEYSTER W., "Defect structures and related properties in V_2O_5 and its lower oxides." *Meded. K. Acad. Wet., Lett. Schone Kunsten, Belg., Kl Wet.* 41,3(1979)154pp.

[19] ANDERSSON A., "Activities of V-Ti-O catalysts in the ammoxidation of 3-picoline (II) Acid-base properties." *J. Catal.* 76(1982)144

[20] INOMATA M., MIYAMOTO A. and MURAKAMI Y., "Mechanism of the reaction of NO and NH_3 on vanadium oxide catalyst in the presence of oxygen under dilute gas condition." *J. Catal.* 62(1980)140

[21] MIYAMOTO A., KOBAYASHI K., INOMATA M. and MURAKAMI Y., "Nitrogen-15 tracer investigation of the mechanism of the reaction of NO with NH_3 on vanadium oxide catalysts." *J. Phys. Chem.* 86(1982)2945

[22] POSPIšIL M., "Study of the reduction kinetics of mixed oxides NiO-V_2O_5 with hydrogen." *J. Therm. Anal.* 27(1983)77

[23] BOSCH H., KIP B.J., VAN OMMEN J.G. and GELLINGS P.J., "Factors influencing the temperature-programmed reduction profiles of vanadium pentoxide." *J. Chem. Soc. Faraday Trans. I* 80(1984)2479

[24] MACIEJEWSKI M., RELLER A. and BAIKER A., "Influence of the grain morphology of V_2O_5 on its reduction-reoxidation behaviour." *Thermochim. Acta* 96(1985)81

[25] RODER Z., MINK G. and BERTóTI I., "DSC-GC studies on the oxidation of CO over vanadia catalysts." *Thermochim. Acta* 107(1986)181

[26] ELYUTIN V.P., PAVLOV Y.A., POLYAKOV V.P. and SHEBOLDAEV S.B., "Reactions of oxides V_2O_5, MoO_3 and WO_3 with carbon and carbon monoxide." *Inorg. Mater.* 6,1(1970)30

[27] KOSAKI Y., MIYAMOTO A. and MURAKAMI Y., "The oxidation of CO on Pt/Al_2O_3 containing a metal oxide." *Bull. Chem. Soc. Jpn.* 55,9(1982)2706

[28] MORI K., MIYAMOTO A. and MURAKAMI Y., "Catalytic reaction on well characterized vanadium oxide catalysts. 1. Oxidation of CO." *J. Phys. Chem.* 88(1984)2735

[29] MARSHNEVA V.I., BORESKOV G.K. and SOKOLOVSKII V.D., "The mechanism of CO oxidation on metal oxides. II. Kinetics and mechanism of CO oxidation on V_2O_5." *Kinetics i Kataliz (transl.)* 13,5(1972)1209-1214

[30] MARSHNEVA V.I., BORESKOV G.K. and SOKOLOVSKII V.D., "The mechanism of CO oxidation on metal oxides. I. Investigation of the stepwise occurrence of CO on V_2O_5." *Kinetics i Kataliz (transl.)* 13,2(1972)351

[31] BAIKER A., DOLLENMEIER P. and HE R., "Structure sensitivity of CO oxidation on vanadium pentoxide." *J. Chem. Soc., Chem. Commun.* com. 1753(1985)413

[32] HIROTA K., KERA Y. and TARATANI S., "Carbon monoxide oxidation with an oxygen tracer over a vanadium pentoxide catalyst." *J. Phys. Chem.* 72,9(1968)3133

[33] BAIKER A., DOLLENMEIER P., HE R. and WOKAUN A., "CO oxidation on V_2O_5's of different grain morphology, structure sensitivity of the reaction." *J. Catal.* 100(1986)345-352

[34] MORI K., MIURA M., MIYAMOTO A. and MURAKAMI Y., "Catalytic reactions on well-characterized vanadium oxide catalysts. 3. Oxidation of hydrogen." *J. Phys. Chem.* 88(1984)5232-5235

[35] ELYUTIN V.P. et al., *Chern. Metall.* 12,5(1969)5-8

[36] VAN VUUREN C.P.J. and WAGENER J.B., "A microcomputer system for isothermal thermogravimetric analysis." *Intelligent instruments and computers* 5,2(1987)72-77

[37] MOORE J.W. and PEARSON R.G., **Kinetics and mechanism.** Third ed., John Wiley and sons, (1981)32

[38] BROWN M.E., DOLLIMORE D. and GALWEY A.K., **Comprehensive chemical kinetics Vol.22. Reactions in the solid state.** Bamford C.H. and

Tipper C.F.H., Elsevier Scientific publishing Co., Amsterdam/New York/Oxford, (1980)88-99

[39] BOND G.C., **Catalysis by metals.** Academic press, London/New York, (1962)149-181

[40] BATLEY G.E., EKSTROM A. and JOHNSON D.A., "Studies of topochemical heterogeneous catalysis. 3. Catalysis of the reduction of metal oxides by hydrogen." *J. Catal.* 34(1974)368-375

[41] COLPAERT M.N., FIERMANS L., CLAUWS P. and VENNIK J., "Thermal and low energy bombardment induced oxygen loss of V_2O_5 single crystals: transition to V_6O_{13}." *Surf. Sci.* 86(1973)513

[42] BROWN M.E., GLASSER L. and STEWART B.V., "The thermal decomposition of ammonium metavanadate (III) A structural view of the decomposition mechanism." *J. Therm. Anal.* 7(1975)125

[43] BROWN M.E., GLASSER L. and STEWART B.V., "The thermal decomposition of ammonium metavanadate (II) The kinetics and mechanism of decomposition." *J. Therm. Anal.* 7(1974)529

[44] BROWN M.E., GLASSER L. and STEWART B.V., "The thermal decomposition of ammonium metavanadate (I) The stoichiometry of decomposition." *J. Therm. Anal.* 2(1970)287

[45] TANIGUCHI M. and INGRAHAM T.R., "Mechanism of the thermal decomposition of ammonium metavanadate." *Can. J. Chem.* 42(1964)2467

[46] SAS T.M., NOVOZHILOV V.A., VELIKODNYI Y.A., SUVOROV V.N. and SOROKIN V.E., "Thermal decomposition of ammonium metavanadate." *Zh. Neorg. Khim. (transl.)* 23(1978)3245

[47] KHULBE K.C. and MANN R.S., "Thermal decomposition of ammonium metavanadate." *Can. J. Chem.* 53(1975)2917

[48] DZIEMBAJ L. and DZIEMBAJ R.D., "Temperature-programmed decomposition of NH_4VO_3 and NH_4VO_3-TiO_2 investigated by MS and DTA methods." *J. Therm. Anal.* 17(1979)57

[49] SELIM S.A., PHILIP Ch.A. and MIKHAIL R.Sh., "Thermal decomposition of ammonium metavanadate." *Thermochim. Acta.* 36(1980)287

[50] SELIM S.A., PHILIP Ch.A. and MIKHAIL R.Sh., "Surface properties of thermally decomposed ammonium metavanadate." *Thermochim. Acta.* 39(1982)144

[51] TRAU J., "Electrical conductivity measurements during the thermal decomposition reaction of AMV." *J. Therm. Anal.* 6(1974)355

[52] KELMERS A.D., "Ammonium, potassium, rubidium and cesium hexavanadates." *J. Inorg. Nucl. Chem.* 21(1961)45

[53] BHATTACHARYYA S.K. and MAHANTI P., "Studies on kinetics of chemisorption of oxygen and electrical conductivity changes on vanadium pentoxide catalysts." *J. Catal.* 20(1971)10

[54] HABER J., KOZLOWSKA A. and KOZLOWSKI R., "The structure and properties of vanadium oxide surface compounds." *J. Catal.* 102(1986)52

[55] BARIN I. and KNACKE O., **Thermochemical properties of inorganic substances.** Springer-Verlag, 1973.

[56] MAH A.D., **Thermodynamic properties of vanadium and its compounds.** United States Department of the Interior, Bureau of Mines, Rep. no. 6727(1966)84pp.